

**PREDICTING LOAD SETTLEMENT RESPONSE OF PILE FOUNDATION  
USING DEEP NEURAL NETWORK**

by  
MOZAHER UL KABIR

MASTER OF SCIENCE IN CIVIL AND GEOTECHNICAL ENGINEERING



DEPARTMENT OF CIVIL ENGINEERING  
BANGLADESH UNIVERSITY OF ENGINEERING AND TECHNOLOGY  
Dhaka, Bangladesh

April, 2023

**PREDICTING LOAD SETTLEMENT RESPONSE OF PILE FOUNDATION  
USING DEEP NEURAL NETWORK**

by  
MOZAHER UL KABIR

A thesis submitted to the Department of Civil Engineering,  
Bangladesh University of Engineering and Technology, Dhaka,  
in partial fulfillment of the requirements for the degree of  
Master of Science in Civil and Geotechnical Engineering



DEPARTMENT OF CIVIL ENGINEERING  
BANGLADESH UNIVERSITY OF ENGINEERING AND TECHNOLOGY  
Dhaka, Bangladesh

April, 2023

The thesis titled “Predicting Load Settlement Response of Pile Foundation Using Deep Neural Network”, submitted by Mozaher Ul Kabir (Roll No. 1018042201, Session: October, 2018) has been accepted as satisfactory in partial fulfillment of the requirement for the degree of M.Sc. Engg. (Civil & Geotechnical) on April 15, 2023.

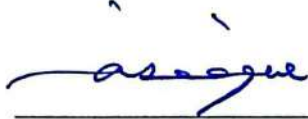
### BOARD OF EXAMINERS



---

Dr. Mohammad Shariful Islam  
Professor  
Department of Civil Engineering  
BUET, Dhaka-1000

Chairman  
(Supervisor)



---

Dr. Abu Siddique  
Professor and Head  
Department of Civil Engineering  
BUET, Dhaka

Member  
(Ex-Officio)



---

Dr. Eqramul Hoque  
Professor  
Department of Civil Engineering  
BUET, Dhaka

Member



---

Dr. Hossain Md. Shahin  
Professor and Head  
Department of Civil and Environmental Engineering  
IUT, Gazipur

Member  
(External)

## DECLARATION

It is thereby declared that except for the contents where specific references have been made to the work of others, the study contained in this thesis is the result of investigations carried out by author under the supervision of Dr. Mohammad Shariful Islam, Professor, Department of Civil Engineering, Bangladesh University of Engineering and Technology.

No part of this thesis has been submitted to any university or educational establishment for a degree, diploma or other qualification (except for publication).



---

Mozahet Ul Kabir

## ACKNOWLEDGEMENT

The author would like to express his heartfelt gratitude to Dr. Mohammad Shariful Islam, Professor in the Department of Civil Engineering at the Bangladesh University of Engineering and Technology (BUET), for his consistent supervision and guidance throughout the research work. Working with him was a great privilege and I couldn't have finished the research work without his unwavering support and inspiration. Additionally, his knowledge sharing, generosity, and support in data collection have all been of tremendous assistance to me. I will always be in debt to him for introducing me to an environment that promotes research, for his continuous encouragement, and for all the instructions and trainings he provided to advance my future career in research.

Sincere thanks should be extended to Dr. Hossain Md. Shahin, Professor, Department of Civil and Environmental Engineering, Islamic University of Technology (IUT), for his support with this research, particularly in the area of numerical analysis. The author would also like to express his heartfelt thanks to Dr. Abu Siddique, Professor and Head, Department of Civil Engineering, BUET and Dr. Eqramul Hoque, Professor, Department of Civil Engineering, BUET, for their valuable time they have provided as members of the board of examiners.

Special thanks to Mr. A H M S Aktar, Project Director, First Dhaka Elevated Expressway (FDEE), for his kind approval and support in providing data from the FDEE project. His prompt response helped me to initiate the process of data collection within a very short time. Also, thanks to Mr. Md. Maksudul Alam, Project Director (3rd Terminal), HSIA project, for his consent and support in providing data from the ongoing HSIA project. He provided required assistances to visit the project area and collect field data. Lastly, I'm also in debt to my parents for their continuous support, love and blessings.

## ABSTRACT

The primary objective of this study is to explore the capabilities of Deep Neural Network (DNN) models in predicting the load settlement behavior of pile foundations. As the safety and stability of a structure heavily rely on the performance of the piles, it is crucial to monitor their load settlement behavior. Conventionally, static load tests are conducted at construction sites to achieve this. However, static load tests come with various complexities, such as being expensive, time-consuming, and sometimes leading to destructive outcomes. The study aims to address these challenges by seeking a more efficient, accurate, and reliable technique to capture the complete response of pile load-settlement behavior. By utilizing DNN models, the research aims to provide an alternative approach that can potentially streamline the prediction process, ultimately enhancing the understanding and management of the pile foundation behavior in construction projects.

In order to predict the load settlement behavior of pile foundations, this study employed the development of various Deep Neural Network (DNN) models, including MLP, LSTM, Bi-LSTM, 1D CNN, and TabNet. A dataset of approximately 712 load-settlement data points was gathered from 42 full-scale load test data sets, encompassing relevant information about pile characteristics and soil profiles. The selected input parameters for model development included pile geometry, stiffness, applied load, settlement, loading-unloading cycles, and the SPT (Standard Penetration Test) profile of the specific location. To facilitate model training and evaluation, the dataset was initially divided into training and testing sets. Several techniques, such as batch normalization, dropout, and principal component analysis (PCA), were applied to eliminate unnecessary dimensions, reduce the impact of noise, and handle outliers effectively within the dataset. By employing these techniques, the DNN models were better equipped to process and interpret the input data accurately, aiming to improve the accuracy and reliability of load settlement behavior predictions for pile foundations.

Besides DNN models, the finite element method (FEM) has been used to carry out the simulation of static pile load tests. This method has the advantage over traditional analysis techniques as more realistic test conditions can be taken into account and displacements and stresses within the soil body and pile are coupled, thus representing more realistic pile-soil interaction behavior with more realistic assumptions. The commercial finite element program Plaxis-3D was used for this simulation purpose. The layered soil profile was modeled using the hardening soil model, while the pile was modeled as an embedded beam element using the elastic model. The selection of soil models and corresponding parameters was ensured by comparing the results with the laboratory test results and SPT correlations.

However, the obtained prediction results from both models were compared with field test results, and eventually performances were assessed using statistical performance indicators like MSE, RMSE, MAE, and correlation coefficients. The findings demonstrated quite satisfactory performances of the DNN models and FEM to forecast both of the two loading-unloading cycles that are commonly generated during field static load tests. It is also evident that Plaxis-3D shows higher accuracy except when the TabNet model is employed with PCA. TabNet with PCA was concluded to be the optimized model ( $R^2=0.92$ ) for prediction of load settlement response. Hence, it can be recommended that using the learned simple model input parameters, it is possible to predict the load-settlement behavior within a satisfactory range by applying the proposed DNN models. This will ultimately reduce time and costs by the optimization of test plans.

## LIST OF CONTENTS

|   |     |
|---|-----|
| DECLARATION   | i   |
| ACKNOWLEDGEMENT   | ii  |
| ABSTRACT  | iii |
| LIST OF CONTENTS  | iv  |
| LIST OF FIGURES   | vii |
| LIST OF TABLES  | ix  |
| LIST OF ABBREVIATIONS   | x   |
| CHAPTER 1: INTRODUCTION                                       | 1   |
| 1.1 General   | 1   |
| 1.2 Background  | 2   |
| 1.3 Objectives of the study                                   | 3   |
| 1.4 Organization of the thesis                                | 3   |
| CHAPTER 2: LITERATURE REVIEW                                  | 5   |
| 2.1 Introduction  | 5   |
| 2.2 Pile Load Test Methods                                    | 5   |
| 2.2.1 Static Load Test  | 7   |
| 2.2.2 Plastic and Elastic Deformation of Pile                 | 8   |
| 2.3 Methods for Pile Capacity Determination                   | 10  |
| 2.4 Limitations of Load Tests                                 | 12  |
| 2.5 Deep Neural Networks (DNNs)                               | 13  |
| 2.5.1 Multilayer Perception (MLP)                             | 15  |
| 2.5.2 Convolutional Neural Network (CNN)                      | 16  |
| 2.5.3 Recurrent Neural Network (RNN)                          | 17  |
| 2.5.4 TabNet  | 20  |
| 2.6 Past Researches   | 22  |
| 2.6.1 Current Status of Pile Load Test Research in Bangladesh | 23  |
| 2.6.2 Relevant Researches on FEM                              | 24  |
| 2.6.3 Relevant DNN Researches                                 | 26  |
| 2.7 Research Gaps   | 29  |
| CHAPTER 3: SUB-SOIL INVESTIGATION AND DATA COLLECTION         | 34  |
| 3.1 Introduction  | 34  |
| 3.2 Sub-soil Investigation                                    | 34  |
| 3.2.1 Site Information  | 34  |

|   |  |    |
|---|--|----|
| 3.2.3   | Field Tests                              | 35 |
| 3.2.4   | Standard Penetration Test (SPT)          | 35 |
| 3.2.5   | Sample Collection for Laboratory Testing | 36 |
| 3.3   | Laboratory Test Results                  | 37 |
| 3.3.1   | Atterberg Limit Test                     | 37 |
| 3.3.2   | Specific Gravity and Hydrometer Test     | 38 |
| 3.3.2   | Triaxial Test                            | 39 |
| 3.4   | Data Collection                          | 41 |
| 3.4.1   | Data Sets for DNN Model                  | 42 |
| CHAPTER 4: FEM ANALYSIS AND MODEL DEVELOPMENT |  | 43 |
| 4.1   | Introduction                             | 43 |
| 4.2   | Project Information                      | 44 |
| 4.3   | Constitutive Models                      | 46 |
| 4.4   | Parameters for Numerical Modeling        | 47 |
| 4.4.1   | Soil Stiffness Parameters                | 49 |
| 4.4.2   | Shear Strength Parameters                | 49 |
| 4.4.3   | Structural Parameters for Pile           | 50 |
| 4.5   | Calibration of Constitutive Model        | 51 |
| 4.6   | FEM Model Development                    | 52 |
| 4.6.1   | Model Geometry and Boundary              | 52 |
| 4.6.2   | Interfaces                               | 54 |
| 4.6.3   | Mesh                                     | 55 |
| 4.6.4   | Elements                                 | 55 |
| 4.6.5   | Modelling Staged Construction            | 56 |
| 4.6.6   | Settlement Analysis Results of Plaxis-3D | 57 |
| 4.7   | Summary                                  | 70 |
| CHAPTER 5: DNN MODEL DEVELOPMENT              |  | 72 |
| 5.1   | Introduction                             | 72 |
| 5.2   | Model inputs                             | 73 |
| 5.3   | Data Preprocessing                       | 74 |
| 5.3.1   | Data Cleaning                            | 74 |
| 5.3.2   | Data Scaling or Normalization            | 75 |



|  |            |
|--|------------|
| 5.4 Dimensionality Reduction and Feature Selection | 76         |
| 5.5 Model Training and Validation                  | 76         |
| 5.6 Performance Evaluation of the Models           | 78         |
| 5.6.1 MLP Model Development                        | 80         |
| 5.6.2 RNN Model Development                        | 83         |
| 5.6.3 1D-CNN Model Development                     | 88         |
| 5.6.4 TabNet Model Development                     | 92         |
| 5.6.5 TabNet with PCA                              | 95         |
| 5.7 Summary  | 101        |
| <b>CHAPTER 6: COMPARISON OF MODEL PERFORMANCES</b> | <b>103</b> |
| 6.1 Introduction                                   | 103        |
| 6.2 Performance Comparison                         | 103        |
| <b>CHAPTER 7: CONCLUSIONS AND RECOMMENDATIONS</b>  | <b>107</b> |
| 7.1 Introduction                                   | 107        |
| 7.2 Conclusions                                    | 107        |
| 7.3 Recommendations for Future Research            | 109        |
| <b>REFERENCES</b>                                  | <b>110</b> |
| <b>APPENDIX-A</b>                                  | <b>120</b> |
| <b>APPENDIX-B</b>                                  | <b>122</b> |
| <b>APPENDIX-C</b>                                  | <b>125</b> |

## LIST OF FIGURES

|  |    |
|--|----|
| <b>Figure 2.1:</b> Static Load Test (SLT) Setup for HSIA project   | 9  |
| <b>Figure 2.2:</b> Process of machine learning (Ahmed, 2021)   | 13 |
| <b>Figure 2.3:</b> A layered structure of nodes for MLP (Jiang et al., 2022)   | 15 |
| <b>Figure 2.4:</b> Sample pictorial process of CNN (Ihsanto et al., 2020)  | 17 |
| <b>Figure 2.5:</b> Sample RNN architecture (Zhu et al., 1998)  | 18 |
| <b>Figure 2.6:</b> Sample LSTM architecture (Yuan et al., 2019)  | 19 |
| <b>Figure 2.7:</b> Bi-LSTM Architecture (Tourille et al., 2017)  | 20 |
| <b>Figure 2.8:</b> Sample TabNet architecture (Arik and Pfister, 2021)   | 22 |
| <b>Figure 3.1:</b> Position of the soil samples from the study area in the plasticity chart                                  | 38 |
| <b>Figure 3.2:</b> Results of grain size analysis of collected samples   | 39 |
| <b>Figure 3.3:</b> Triaxial test setup   | 40 |
| <b>Figure 3.4:</b> Deviatoric Stress vs. Strain under triaxial test results at 200 kPa                                       | 41 |
| <b>Figure 3.5:</b> Failure envelopes for triaxial consolidated drained test for silty clay                                   | 41 |
| <b>Figure 4.1:</b> Flow diagram for FEM model  | 44 |
| <b>Figure 4.2:</b> Equivalent soil stratigraphy at the BH40 location of pile load test.                                      | 45 |
| <b>Figure 4.3:</b> Load-settlement curve of TP-07  | 46 |
| <b>Figure 4.4:</b> $E_{50\text{ ref}}$ determination from the Deviatoric Stress vs. Strain diagram                           | 49 |
| <b>Figure 4.5:</b> Calibration of HS model with the triaxial test data   | 52 |
| <b>Figure 4.6:</b> Geometry of FE model  | 53 |
| <b>Figure 4.7:</b> (a) Soil elements and (b) Beam elements (Plaxis 3D manual 2020)   | 56 |
| <b>Figure 4.8:</b> (a) Deformed mesh and (b) Total displacements at make ground condition                                    | 62 |
| <b>Figure 4.9:</b> (a) Deformed mesh and (b) Total displacements at 100% design load   | 63 |
| <b>Figure 4.10:</b> (a) Deformed mesh and (b) Total displacements at 200% of design load                                     | 64 |
| <b>Figure 4.11:</b> Total displacements at 0% of design load (end of final phase)  | 65 |
| <b>Figure 4.12:</b> Total cross-sectional displacements at the pile center for (a) 100% and (b) 200% of design load          | 66 |
| <b>Figure 4.13:</b> Displacement contours for (a) 100% and (b) 200% of design load   | 67 |
| <b>Figure 4.14:</b> Stress-vector diagrams at loading condition of (a) 100% and (b) 200% design load                         | 68 |
| <b>Figure 4.15:</b> Surface plots at loading condition (a) 100% and (b) 200% of design load                                  | 69 |
| <b>Figure 4.16:</b> Comparison of Plaxis-3D result with insitu pile load test data.  | 70 |
| <b>Figure 4.17:</b> Comparison of Plaxis 3D results with insitu pile load test data (a) General case and (b) Normalized case | 71 |
| <b>Figure 5.1:</b> DNN model pipeline  | 72 |

|  |     |
|--|-----|
| <b>Figure 5.2:</b> Performance of MLP model with respect field data  | 82  |
| <b>Figure 5.3:</b> Regression plot for MLP model (a) Generalized and (b) Normalized  | 83  |
| <b>Figure 5.4:</b> Adopted (a) LSTM (Hochreiter and Schmidhuber, 1997) and (b) Bi-LSTM (Graves and Schmidhuber, 1997) architectures                                | 84  |
| <b>Figure 5.6:</b> Performances of different RNN models (a) LSTM, (b) LSTM (Normalized), (c) Bi-LSTM and (d) Bi-LSTM (Normalized)                                  | 87  |
| <b>Figure 5.7:</b> 1D-CNN prediction results   | 90  |
| <b>Figure 5.8:</b> Comparison between field test data and 1D-CNN prediction results (a) General case and (b) Normalized case                                       | 91  |
| <b>Figure 5.9:</b> Residual plot for 1D-CNN prediction   | 92  |
| <b>Figure 5.10:</b> Comparison between field test data and TabNet prediction results without PCA (a) General case and (b) Normalized case                          | 94  |
| <b>Figure 5.11:</b> Comparison between field test data and TabNet prediction results with PCA (a) General case and (b) Normalized case                             | 96  |
| <b>Figure 5.12:</b> Performance comparison of TabNet model with different PCA and batch size   | 98  |
| <b>Figure 5.13:</b> Importance analysis of components  | 99  |
| <b>Figure 5.14:</b> TabNet prediction results (a) Without PCA and (b) With PCA   | 100 |
| <b>Figure 5.15:</b> Residual plot for TabNet models (a) Without PCA (b) With PCA   | 101 |
| <b>Figure 6.2:</b> Performances of different DNN models (a) MLP model, (b) 1D-CNN, (c) LSTM, (d) Bi-LSTM model, (e) TabNet (Without PCA) and (f) TabNet (With PCA) | 105 |
| <b>Figure 6.3:</b> Performance of Plaxis 3D model  | 106 |

## LIST OF TABLES

|   |     |
|---|-----|
| <b>Table 2.1:</b> Pile load test methods  | 6   |
| <b>Table 2.2:</b> Summary of previous studies on Load-Settlement behavior of pile foundation  | 30  |
| <b>Table 2.2:</b> Summary of previous studies on Load-Settlement behavior of pile foundation  | 31  |
| <b>Table 3.1:</b> Recommended SPT procedure (ASTM D1586)  | 35  |
| <b>Table 3.2:</b> List of laboratory tests  | 36  |
| <b>Table 3.3:</b> Undisturbed sample collected at different depth   | 36  |
| <b>Table 3.4:</b> Correlations between plasticity of soil and strength (Atkins, 1997)   | 37  |
| <b>Table 3.5:</b> Plasticity values for cohesive soil at different depth  | 38  |
| <b>Table 3.6:</b> Strength properties of silty clay layer   | 40  |
| <b>Table 4.1:</b> Soil model parameters and laboratory tests needed for determination of parameters for the Hardening Soil model (modified after Plaxis 2002) | 48  |
| <b>Table 4.2:</b> Input parameters for FEM model development  | 50  |
| <b>Table 4.3:</b> Structural Parameters   | 51  |
| <b>Table 4.4:</b> Soil parameters for Hardening Soil Model calibration  | 51  |
| <b>Table 4.5:</b> Calculation Phases of Plaxis-3D for Static Load Test (SLT) simulation   | 58  |
| <b>Table 5.1:</b> Criterion for layered soil profile considerations   | 73  |
| <b>Table 5.2:</b> Feature selection and annotation  | 77  |
| <b>Table 5.3:</b> Performance factors of DNN models   | 80  |
| <b>Table 5.4:</b> Variation of MLP model results within different batch sizes   | 81  |
| <b>Table 5.5:</b> Performances of RNN models  | 84  |
| <b>Table 5.6:</b> Performance on settlement behavior prediction with 1D-CNN model   | 90  |
| <b>Table 5.7:</b> Comparative experiment results  | 102 |
| <b>Table 6.1:</b> Comparison of performances of different models  | 104 |

## LIST OF ABBREVIATIONS

| <b>Abbreviation</b> | <b>Full form</b>                       |
|---------------------|--|
| AI                  | Artificial Intelligence                |
| ANN                 | Artificial Neural Network              |
| Bi-LSTM             | Bi-directional Long Short-Term Memory  |
| CD                  | Consolidated Drained                   |
| CPT                 | Cone Penetration Test                  |
| CNN                 | Convolutional Neural Network           |
| CRP                 | Constant Rate of Penetration           |
| DNN                 | Deep Neural Network                    |
| DT                  | Decision Tree                          |
| FE                  | Finite Element                         |
| FDEE                | First Dhaka Elevated Expressway        |
| FEM                 | Finite Element Model                   |
| GUI                 | Graphical User Interface               |
| HS                  | Hardening Soil                         |
| HSIA                | Hazrat Shahjalal International Airport |
| LSTM                | Long Short-Term Memory                 |
| MF                  | Membership Function                    |
| MI                  | Machine Intelligence                   |
| ML                  | Machine Learning                       |
| MLP                 | Multi-Layer Perceptron                 |
| MAE                 | Mean Absolute Error                    |
| MSE                 | Mean Squared Error                     |
| RMSE                | Root Mean Squared Error                |
| NN                  | Neural Network                         |
| PCA                 | Principal Component Analysis           |
| RNN                 | Recurrent Neural Network               |
| SLT                 | Static Load Test                       |
| SPT                 | Standard Penetration Test              |

# CHAPTER 1

## INTRODUCTION

### 1.1 General

Foundation plays the most vital role in transferring loads to the ground. It ensures the safety and stability of every construction. Depending on the soil condition and its challenges, deep foundations are used to transfer the loads to the deeper and more compatible soil layers. Hence, as a deep foundation, it is required to assess the performances of pile foundation. To ensure the optimized design of a pile foundation, the load-settlement behavior, measurement of capacity and the verification of static calculations or the calibration of other tests at identical soil conditions can all be accomplished through the application of static load testing.

Load-settlement behavior of pile foundations, in accordance with ASTM D1143-81, is preferably developed and described on the basis of results from static load tests (SLT). Throughout the course of these tests, increasing loads are applied at particular time intervals in a progressive manner; the settlement is measured after each stage. The load settlement curve that was obtained is then analyzed in greater detail. In this method, the load should be increased until the pile reaches the maximum load, which leads to the identification of the pile's ultimate capacity. The limit state is defined as the situation in which the increment in settlements is unrestrained without the need to increase the load applied. From that the settlement behavior and probable ultimate capacity of the pile is being reported. But it requires huge time and is less efficient in many cases due to its operational costs. Also, in some cases it is a destructive test.

As a result, numerous studies have been carried out to illustrate the load-settlement behavior without performing field load tests. Numerical analysis has been shown to be highly beneficial in predicting the behavior of piles under different loading conditions (Sellountou and Roberts, 2007; Wehnert and Vermeer, 2004). By comparing the measured deformation of the pile to the predicted deformation from the numerical analysis, research has shown that numerical analysis can be used to validate the results of a static load test (El-Mossallamy, 2020; Unsever et al., 2014; Reul, 2004; Kimura and Zhang, 2000 Franke et al., 1994) and even for providing additional information about the pile's behavior that is not available from a static load test (Ahmed and

Neelima, 2009; Johnson et al., 2006; Karthigeyan et al.,2007). Also, many recent research uses Artificial Intelligence (AI) to forecast pile-load settlement behavior (Unsever et al., 2015; Momeni et al., 2014; Nejad et al., 2009; Shahin et al., 2002). However, the use of neural networks in predicting the pile capacity started in the 1990's (Goh, 1995; Boscardin and Cording, 1989;), when used in a form of a model to predict an estimate of the friction capacity of driven piles in clay soils. Explicit understanding of the settlement components is required in this case. Traditional pile load-settlement assessment methods use pile geometry, material qualities, applied load, and soil properties. To increase prediction accuracy, the updated Deep Neural Network (DNN) models were also introduced (Alzo'Ubi and Ibrahim, 2021; Schmüdderich et al., 2020; Mohanty et al., 2018). However, the best model to accurately simulate behavior remains unclear. Latest DNN model like TabNet and principal component analysis techniques were missing in the previous literatures. On the other hand, the previous research works on FEM of pile load test lacks the details on proper soil model selection and layered soil profile consideration. Hence, this study aims to develop preferable methods in terms of efficiency and higher accuracy in predicting the load-settlement behavior considered variations in soil type, layered profile, loading-unloading cases and developed models.

## **1.2 Background**

Pile load test is an essential part of pile foundation design. It provides the most precise assessment of ultimate load capacity obtained by carrying out full-scale in-situ load tests and displaying the actual load settlement response of pile (Kee, 1978). A variety of test methods are to be found in the industry. Static load test is the most basic and widely used test through which actual bearing capacity of the pile as installed in the field can be verified (Coduto, 2014; Fellenius, 1980). Therefore, most design codes require Static Load Test (SLT) to be performed at construction sites, illustrating the discrepancy in settlement. Nevertheless, while essential, the aforementioned approach comes with its own difficulties in that it is expensive, tedious and time-consuming, presents complications for the construction process and is not environmentally friendly (Nejad et al., 2009). Hence, searching for an efficient, accurate and reliable technique to capture the full response of pile load settlement curve is inevitable. In this research, initially, the finite element method (FEM) will be used to carry out the simulation of

static pile load test. This method has the advantage over traditional analysis techniques as more realistic test conditions can be taken into account. Furthermore, displacements and stresses are coupled within the soil body and pile (Momeni et al., 2014; Unsever et al., 2015). The commercial finite element programs PLAXIS 3D will be used for this simulation purpose. In addition to this numerical approach, this study aims at further extension by establishing an evolutionary Deep Neural Network (DNN) model using input parameters that can easily be determined without the need for expensive and time-consuming in-situ testing. This study will be devoted to filling the gaps and to differentiating from the previous studies (Alzo'Ubi and Ibrahim, 2021; Schmüdderich et al., 2020; Jebur et al., 2018; Mohanty et al., 2018; Krasinski and Wiszniewski, 2017; Unsever et al., 2015) in terms of incorporating both the numerical simulation and implementation of the DNN model with a view to figuring out the most reliable and optimized model for prediction of load settlement response under varying load and soil conditions.

### **1.3 Objectives of the Study**

The present study aims to achieve the following objectives:

- (i) To conduct numerical simulation of static pile load test using the finite element method.
- (ii) Perform sensitivity analysis to identify model parameters and construct Deep Neural Network (DNN) models using experimental datasets for predicting pile settlement.
- (iii) To determine model performances and accuracies comparing with field test data.

### **1.4 Organization of the Thesis**

To exemplify the process for reaching the aforementioned aims while coping with the study's scope, the overall thesis has been assembled with a total of six chapters. The order of these six chapters will be as follows:

Chapter One concisely portrays an overview of the context of entire research work including introduction, objective of the research, background of the study and organization of the thesis.

Chapter Two documented the literature reviews. Reviewing available relevant literatures on static load test, finite element modeling, DNN models such as MLP,



LSTM, Ni-LSTM, TabNet and their applications in the field of geotechnical engineering. It also incorporates programs used for those applications; finally concluded the literature gaps and necessity of detailed study.

Soil sample collection, interpretation of test reports and data handling have been outlined in Chapter Three. It also contains detail of the methodology used for data collection, site information, data handling, and data sorting, as well as the field investigation and lab tests that were carried out in order to achieve the research work's objectives.

Chapter Four contains the brief discussion on the FEM model development using compatible soil models, required parametric considerations for different soil layers, calculation steps and settlement analysis results. Details of the selected project for numerical modeling and project geometry has also been illustrated here.

Chapter Five contains the brief description on architecture of the Deep Neural Network (DNN) models used in this study. It also outlines the procedure of DNN model development and validation results comparing with filed load test results.

Finally, Chapter Six outlines the major conclusions drawn from this study and also based on the comparison of both the DNN and numerical models. In addition to that, some recommendations have also been provided focusing on the limitations of this research.

## **CHAPTER 2 LITERATURE REVIEW**

### **2.1 Introduction**

Subsurface conditions, site location and topography including the structural and geometric aspects of the structure to be supported, all play a role in determining the necessity of pile foundation and its uses (Yamashita et al., 2011; Vesic, 1977). The maximum load on a pile is the maximum load at which the soil or the pile could fail. Where pile points embedded in deep sand, rock or even clayey soil, the pile failure condition may control design, but in most cases, the soil failure determines the ultimate load (Yamashita, 2012). The soil usually fails in the same way: by direct-shear failure along the shaft, followed or preceded by punching shear under the point. Several empirical ultimate load criteria must be utilized because the ultimate load is frequently not clearly specified. The majority of the time, these have been determined by taking into account total settlements of the pile under a test load (Yamashita, 2012). Hence, it can be concluded that static load test is popular and almost an obvious requirement to simulate the load-settlement behavior (Farquhar, 1990).

Yet, despite being necessary, the aforementioned method has its own drawbacks, including the fact that it is expensive, laborious, and time-consuming, complicates the construction process, and is not ecologically friendly. This chapter has been enhanced with available researches on the FEM and DNN evolution over time (Alkhafaji and Imani, 2022). In addition, useful critique will be offered in regards to Bangladesh's implementation of FEM and DNN. By doing so, the overview will once again legitimize the importance of this study.

### **2.2 Pile Load Test Methods**

According to their purposes, load tests on foundation pile can be divided into design load tests and proof load tests (Al-Homoud et al., 2004; Fellenius, 1980). The design load test is usually kept to failure or at least to a maximum load not less than three times the intended service load. It is a destructive test, and has to be carried out on a purposely installed test pile, which doesn't belong to the foundation. The aim of a design load test is to determine, at the design stage, the bearing capacity of the pile and its load

settlement relationship. Also, it has been tried to show that, if the pile shaft is properly instrumented, it allows the determination of fraction of the bearing capacity taken by the base and the shaft of the pile (Viggiani et al., 2014). Load tests that are conducted

**Table 2.1:** Pile load test methods

| Name of the Test  | Type  | Standard/Methods | Output  |
|---|---|------------------|---|
| Static Load Test (SLT)                                    | a) Quick test<br>b) Maintained load test<br>c) Constant rate penetration test | ASTM D1143       | Pile deflections and load-settlement                              |
| Pile Driving Analyze (PDA Test)                           | Dynamic Test, Quick test  | ASTM D4945       | Pile capacity and integrity                                       |
| Statnamic Load Test                                       | Quick test  | ASTM D7383       | Detailed load-deflection behavior in complex soil conditions      |
| Osterberg Load Test (O-Cell Test)                         | Quick test  | ASTM D4719       | Capacity of high-capacity foundation systems                      |
| Bi-Directional Load Test (BDMT)                           | Quick test  | ASTM D8169       | Estimation of both axial and lateral pile capacities and behavior |
| High Strain Dynamic Load Test (Pile Integrity Test - PIT) | Dynamic test, Quick test  | ASTM D4945       | Pile integrity and detection of potential defects                 |

mostly has been depicted in Table 2.1. Proof load tests, on the contrary are carried out on piles selected among the piles of the foundation, after they have been all installed. This test cannot be destructive, and hence the maximum test load is usually limited to 2 times the intended service load. The total test load shall be applied in increments amounting to 25, 50, 75, 100, 125, 150, 175, and 200 percent of the anticipated working load (ASTM D1143-81). Proof load test is aimed at verifying the correct installation of piles and also load settlement behavior and determination of bearing capacity may also be obtained. The piles to be proof tested are selected only after all piles have been installed in order to prevent a particular careful installation of the intended test pile and to obtain an equal care for all the piles. Usually, a SPT is carried out in the vicinity of

the test pile, in order to know the exact sub surface profile at the test site. This can be helpful to obtain soil parameters as inputs for the finite element analysis (Albusoda et al., 2020; Elsherbiny and El Naggar, 2013).

### **2.2.1 Static Load Test**

Static load tests relied upon an accurate measure of a pile's ultimate resistance. Ultimate resistance is the maximum resistance mobilized by the positive shaft resistance and toe bearing in the soil. Static load testing involves loading the pile statically by placing increments of load and recording settlements as the load is applied following ASTM D1143 (Fakharian et al., 2014; Fellenius et al., 2004; Rajagopal et al., 2012). As the pile resistance may set up (resistance increased with time) or relax (resistance decrease with time), static load tests are often performed after some wait period so that equilibrium conditions are re-established. Two principal types of test may be used for compression loading on piles - the constant rate of penetration (CRP) test and the maintained load test. Maintained load test will be used in this study.

In the maintained load test, the load is increased in stages to 1.5 times or twice the working load with time settlement curve recorded at each stage of loading and unloading. The general procedure is to apply static loads in increments of 25% of the anticipated design load (Fakharian et al., 2014). In the Machine Learning technique, the load test arrangements as specified in ASTM D1143 shall be followed. According to ASTM D1143 each load increment is maintained until the rate of settlement is not greater than 0.25 mm/hr or 2 hours is elapsed, whichever occurs first. All the load tests were conducted with the application of load equal to two times the allowable load. The loads were applied in eight equal increments. Two strain dial gauges were placed each on either side of the pile to measure the vertical settlement of the collar firmly attached to the pile top concerning the reference beams. The reference beams were finely supported in the ground at enough distance away from both the pile and supports of the loading platform. After applying the load on pile head through hydraulic jack, the settlements of the pile were recorded at 30 sec, 1, 2, 5, 10, 15, 30, 60 and 90 minutes intervals on strain gauges rested on reference beams and attached with the pile head. Each load increment was maintained until the rate of the settlement was not greater than 0.25 mm/hr. or until 2 (two) hours had elapsed, whichever occurred first. After that the next load increment is applied. This procedure is followed for all increments of load.

After the completion of loading if the test pile has not failed the total test load is removed any time after twelve hours if the butt settlement over one hour period is not greater than 0.25 mm otherwise the total test load is kept on the pile for 24 hours. After the required holding time, the test load is removed in decrement of 25% of the total test load with 1 hour between decrement. If failure occurs, jacking the pile is continued until the settlement equals 15% of the pile diameter or diagonal dimension. In general, static load applying equipment are set up first. The load test set up of this study were similar to that pictured in Figure 2.1.

It was determined how much movement there was at the top of the pile by employing four displacement transducers that were positioned on a reference beam. Two telltales were set up along the perimeter of the pile and came to an end close to the foot of the H-Pile. The measurements of the backup pile head as well as the measurements of the movements of the reaction pile were taken utilizing survey methods. Figure 2.1 depicts the setup that were utilized in order to measure the movement of the top of the pile. The top of pile movement was measured using four displacement transducers mounted on a reference beam.

### **2.2.2 Plastic and Elastic Deformation of Pile**

Elastic and plastic soil deformation associated with pile deformation are reasons behind the movement of pile head. This ultimately results in the settlement of the structure. The conclusions to be drawn on deformation from load tests is the plastic deformation, not the overall downward movement of the pile head under the test load. The load-settlement curve of the plastic deformation is the most significant and this is the one from which the working load and factor of safety should be determined (Smith, 1960). The plastic deformation curve can be obtained by repeatedly increasing a decreasing the applied load while conducting a static pile load test. Here, loads are incrementally and detrimentally applied following the "ASTM guideline" D1143-81 for individual piles under vertical axial load.

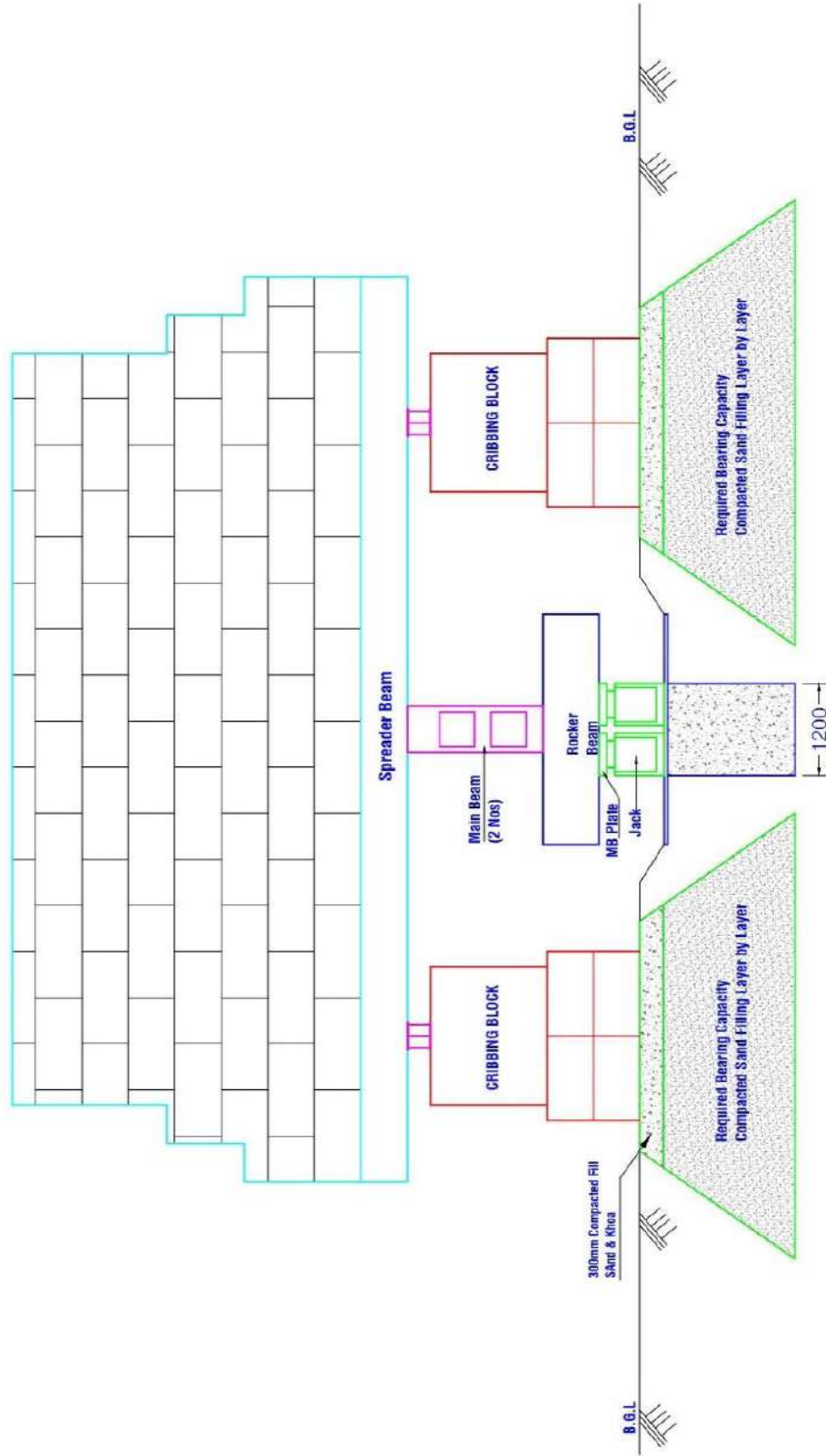


**Figure 2.1:** Static Load Test (SLT) Setup for HSI A project

### 2.3 Methods for Pile Capacity Determination

The bearing capacity of pile can also get determined from the load-settlement behavior of the pile. Researchers and codes suggested various methods for determining the limiting load capacity of a pile, among which some are listed below.

- (i) **Davisson Offset Method:** Davisson (1972) proposed a very useful method of computing the ultimate load capacity of a pile. This method is probably the best known and widely used all over the world. This has also been recommended by BNBC 2020 for determining the capacity of pile. It is also known as offset method as it defines the failure load. The elastic shortening of the pile, considered as point bearing, free standing column, is computed and plotted on the load-settlement curve, with the elastic shortening line passing through the origin. An offset line is drawn parallel to the elastic line. The offset is usually 0.15 inch plus a quake factor, which is a function of pile tip diameter. For normal size piles, this factor is usually taken as 0.1D inch, where D is the diameter of pile in foot. The intersection of offset line with gross load-settlement curve determines the arbitrary ultimate failure load. Davisson method is too restrictive for drilled piles, unless the resistance is primarily friction. This method is recommended for driven precast piles. The methodology is based on the assumption at a specific small toe movement of the tested pile. This method is popularly used all over the world because it provides the lowest estimate of axial compression capacity from the actual load-settlement curve without any requirement of extrapolation. However, Davisson's method requires the pile to be loaded near failure to be applicable.
- (ii) **Chin-Kondner Extrapolation:** Chin (1970) proposed an application to piles on the general work by kondner (1963) based on the assumption that the relationship between load and settlement is hyperbolic. Chin-Kondner Extrapolation is another widely used method for estimating the ultimate bearing capacity of a pile based on the results of a static pile load test. The method involves plotting the load-settlement curve obtained from the load test and extrapolating the curve to estimate the ultimate capacity of the pile. Each settlement is divided with its corresponding load and the resulting values are plotted against the settlement. Each settlement is divided with its corresponding load and the resulting values are plotted against the settlement.

- (iii) Decourt Method: Decourt (1999) proposed a method similar to Chin-Konder where each load is divided with its corresponding movement and the resulting values are plotted against the applied load. The Decourt extrapolation limit is equal to the ratio between the y-intercept and the slope of the line which is also the value of load at intersection.
- (iv) Mazurkiewicz's Method: This method is based on the assumption that the load-settlement curve is approximately parabolic. The load-settlement curve is a series of equal pile head settlement lines drawn on an abscissa. 45-degree line is drawn to intersect the next vertical line running through the next load point and the ultimate failure load is defined by the intersection of the straight line with the load axis.
- (v) British Standard Institution Criterion: Terzaghi (1942) reported that the ultimate load capacity of a pile may be considered as that load which causes a settlement equal to 10% of the pile diameter. However, this criterion is limited to a case where no definite failure point or trend is indicated by the load-settlement curves. This criterion has been incorporated in BS 8004 "Code of Practice for Foundations" which recommends that the ultimate load capacity of pile should be that which causes the pile to settle a depth of 10% of pile width or diameter. The allowable load capacity of pile should be 50% of the final load, which causes the pile to settle a depth of 10% of pile width or diameter (BS 8004). It was also recommended to be used for load capacity determination by BNBC 2020.
- (vi) Indian Standard Criteria: BNBC 2020 recommended this standard for capacity determination of pile foundation from static load test results. According to IS: 2911 Part-4, ultimate load capacity of pile is smaller of the following criterion (a) and (b). On the other hand, Allowable load capacity of pile is smaller of the criterion (c) and (d).
  - (a) Load corresponding to a settlement equal to 10% of the pile diameter in the case of normal uniform diameter pile or 7.5% of base diameter in case of underreamed or large diameter cast in-situ pile.
  - (b) Load corresponding to a settlement of 12 mm.
  - (c) Two thirds of the final load at which the total settlement attains a value of 12 mm.



- (d) Half of the final load at which total settlement equal to 10% of the pile diameter in the case of normal uniform diameter pile or 7.5% of base diameter in case of under-reamed pile.
- (vi) Butler-Hoy Criterion: This is also a BNBC 2020 recommended guideline. Butler and Hoy (1977) states that the intersection of tangent at initial straight portion of the load-settlement curve and the tangent at a slope point of 1.27 mm/ton determines the arbitrary ultimate failure load.
- (vii) Brinch-Hansen 90% Criterion: The Brinch Hansen (1963) proposed a definition for ultimate load capacity as that load for which the settlement is twice the settlement under 90 percent of the full test load. The ultimate load may be taken to calculate the allowable load using a factor of safety of 2.0 to 2.5, where failure occurs. This has also been recommended by BNBC 2020 to be used for determination of pile capacity.

#### **2.4 Limitations of Load Tests**

The static load test using ASTM D1143-81 can also be limited in terms of time and money consumption. These limitations include:

- (i) Time consumption: The test can be time-consuming to set up and perform, especially if the pile is located in a remote or hard-to-reach location. In addition, the test can take several hours to complete, during which time the pile must be loaded and the deformation measured.
- (ii) Cost: The cost of the test can be high due to the need for specialized equipment, such as load frames, load cells, and measuring devices, as well as the need for trained personnel to perform the test. A study (Rybak and Król, 2018) found that the cost of performing a static load test on a pile can be several times higher than the cost of performing a dynamic load test using a hammer. Also, it was showed that the time and cost associated with performing a static load test can be significantly reduced by using innovative testing methods, such as using wireless sensors and data acquisition systems (Middendrop et al., 2022). Moreover, a study (Sellountou and Roberts, 2007) found that the cost and time consumption of performing a static load test can be reduced by using a rapid load test method, which involves applying the load to the pile quickly and measuring the deformation in real-time.

Hence, several research was conducted till now to supplement the static-load test of pile foundation which aims to demonstrate the accurate load-settlement behavior. There are several literature studies that suggest that numerical analysis can be used to supplement the results of a static pile load test. A study by (Sellountou and Roberts, 2007; Wehnert and Vermeer, 2004) found that numerical analysis can be used to predict the behavior of piles under different loading conditions, such as those that occur during earthquakes, and to provide additional information about the pile's behavior that is not available from a static load test. Study showed that numerical analysis can be used to validate the results of a static load test by comparing the measured deformation of the pile to the predicted deformation from the numerical analysis (El-Mossallamy, 2020; ÜNSEVER et al., 2014; Reul, 2004; Kimura and Zhang, 2000; Franke et al., 1994). It was also found that numerical analysis can be used to determine the load-displacement behavior of piles under different loading conditions, such as those that occur during earthquakes (Mazzoni et al., 2006), and to provide additional information about the pile's behavior that is not available from a static load test (Ahmed and Neelima, 2009; Johnson et al., 2006). These studies suggest that numerical analysis can be a useful supplement to a static pile load test, providing additional information about the pile's behavior and helping to validate the test results.

## 2.5 Deep Neural Networks (DNNs)

The total method can be reduced even further by beginning with the training data, then proceeding to apply machine learning, and finally generating a model (Figure 2.6). After the model has been created, one can obtain output by providing this model with some value for the corresponding input.

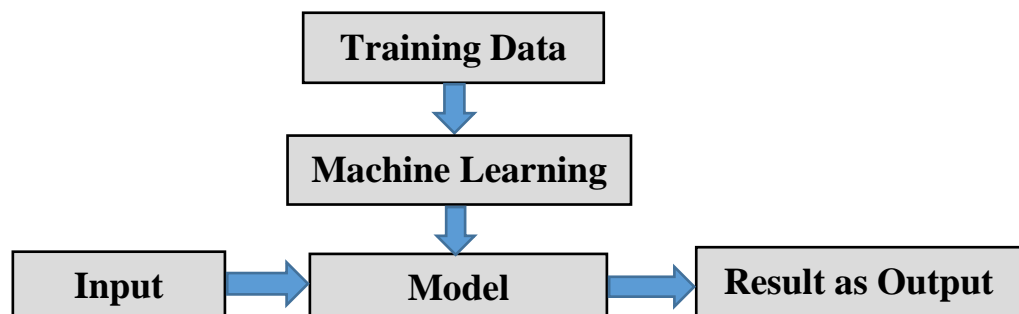


**Figure 2.2:** Process of machine learning (Ahmed, 2021)

Recently, deep learning techniques have been developed as a paradigm change for the automatic extraction of useful feature representation from data using deep neural

networks. These techniques have been established as deep learning methodologies. Learning strategies for Machine Learning (ML) can be further segmented into three primary categories: supervised learning, unsupervised learning, and reinforcement learning. Each of these categories has its own unique set of characteristics. The first category, known as the supervised learning process, bears some resemblance to the way in which humans acquire knowledge. In this scenario, the train machine receives proper input consistently in addition to accurate output. On the other hand, in the case of unsupervised learning, there is no mention of an output. In addition to that, there is another category known as reinforcement learning, which describes situations in which grades and certain outputs are given with inputs. Relating to the fact that the algorithm will need to be able to recognize the characters in order to complete the research, which eliminates any possibility of unsupervised or reinforcement learning being used. The procedure that each ML technique use to learn from the training data and produce a model is where the techniques differ from one another. As a result, Neural Networks (NN) are frequently utilized as the model for Machine Learning, which will be covered in further detail below.

The back-propagational training technique for feed-forward Artificial Neural Network (ANN) was established in 1986, despite the fact that the concept of neural networks was first described in 1943. Since then, research on applications of neural networks has advanced significantly (Das, 2013), They now have a higher rate of application success in the areas of business model prediction, speech recognition, biomedical engineering, control issues, as well as many other engineering disciplines, including geotechnical engineering (Javadi and Rezania, 2009; Das, 2013).

A number of deep learning-based approaches have been successfully applied in the field of geotechnical engineering (Das, 2013; Javadi and Rezania, 2009). They have variations in their architecture and mostly contemplates the structure of human brain, Deep Neural Network models (DNN) have ability to model the non-linear relationship between a set of input and the corresponding outputs. In the literature, there are numerous DNN model types, such as convolutional neural network (CNN), recurrent neural network (RNN), tabular neural network (TabNet), etc. The current success of DNN models is attributable to the availability of large datasets for training DNN models, the rapid development of DNN algorithms, and the accessibility of powerful

computers for modeling and training complex neural networks to achieve accelerated performance and results (Goodfellow et al., 2016). The model architectures are being discussed in the following sub-sections:

### 2.5.1 Multilayer Perception (MLP)

It is composed of multiple layers of connected "neurons," also known as "Nodes." An input layer, one or more hidden layers, and an output layer are the three separate layers that make up this network of neurons. The raw data that we intend to analyze is received by the input layer, and each subsequent layer processes this data using a set of learnt weights and biases. On the basis of the input data that has been processed, the output layer then generates the anticipated output. It means MLP can estimate values for non-linear correlations at a greater extent (Fath et al., 2020; Esfe et al., 2015). The theory is that by processing the data via several layers, the MLP can learn to identify intricate patterns and connections in the data that a single-layer network might find challenging to spot (Montazer et al., 2018). To reduce the difference between the expected output and the actual output, MLPs work by varying the weights of the connections between the neurons in the network. This procedure, referred to as network training. After the network has been trained, predictions can be made using fresh input data. In order to accomplish this, the input data is propagated across the network using a technique called forward propagation, and the output layer then generates the anticipated result (Gouda et al., 2022; Jiang et al., 2022).

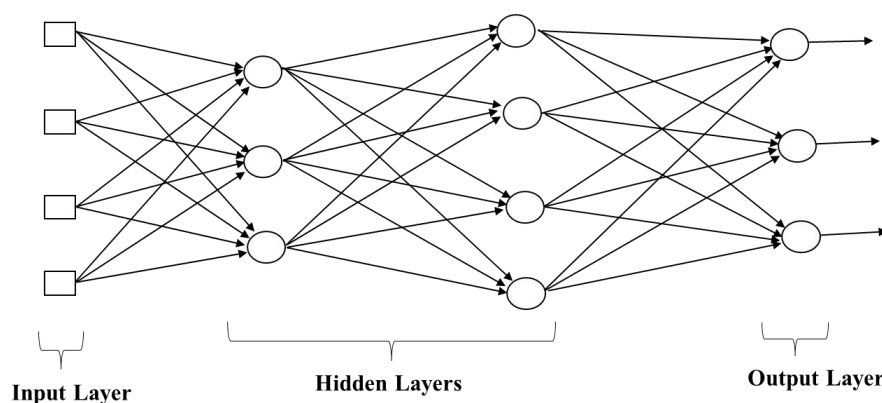


**Figure 2.3:** A layered structure of nodes for MLP (Jiang et al., 2022)

The advantages of MLPs include their ability to be trained on a variety of data types, including both structured and unstructured data, and their versatility in application, including classification, regression, and dimensionality reduction. Additionally, MLPs

have the advantage of being relatively simple to train when compared to some other kinds of neural networks. This is because to how easy and straightforward the learning process is with an MLP.

Given that the number of weights and biases in the network increases exponentially with the number of layers and neurons, MLP is not particularly well-suited to handling exceedingly large or complicated datasets. Additionally, time series data frequently contains long-term dependencies, which MLPs may find challenging to master.

### **2.5.2 Convolutional Neural Network (CNN)**

Input, convolutional, pooling, fully connected, and output layers comprise convolutional neural networks' basic network structures, often cascading architectures (Hannun et al., 2019). The input layer is in charge of feeding the matrix to be processed into the network; the convolutional and pooling layers are interconnected in pairs and are in charge of feature mining and extraction; the amount of connectivity between these layers can be adjusted depending on the model's complexity (Ihsanto et al., 2020). The output and fully connected layers carry out the final categorization.

The convolutional layer is the core component of the CNN, which is in charge of the recursive convolution of the input matrix to extract the associated features. CNNs are designed to automatically learn and extract features from images through a process known as convolution. A small portion of the preceding layer is used as input by the convolutional layer, which then chooses a convolutional kernel to be placed there and multiplies it by the value of the corresponding neuron in the convolutional layer to produce the convolutional result (Acharya et al., 2017). The convolutional layer has to have the stride hyper-parameter configured for improved training outcomes. The first convolutional layer, with a kernel size of 6, several 12, and a stride of 1, is used in this paper. The second and third convolutional layers (kernel size is 2, the number is 12, and the stride is 1). During training, the network learns the filters that produce the most useful features for the given task by adjusting the weights of the filters using back propagation. The loss function used during training is typically cross-entropy, which measures the difference between the predicted and actual class probabilities.

The pooling layer, the down sampling layer, samples the convolutional layer's output data by down sampling the features while maintaining the depth dimension. This

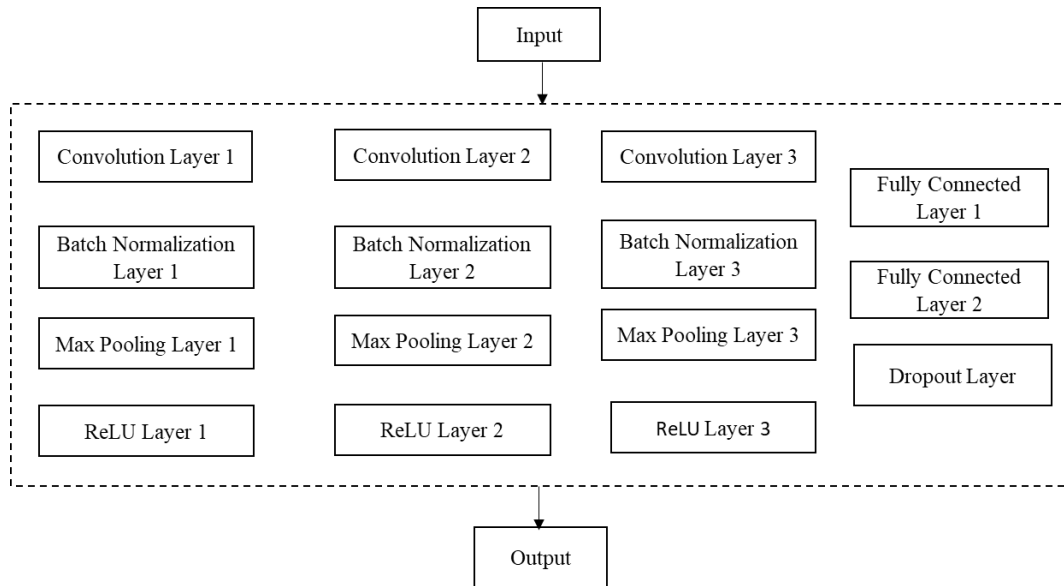


**Figure 2.4:** Sample pictorial process of CNN (Ihsanto et al., 2020)

increases the generalizability of the model and curbs the overfitting phenomenon while using fewer parameters and computations in the network. Maximum pooling and average pooling are the two most popular pooling operations (Acharya et al., 2017; Kiranyaz et al., 2015). Average pooling indicates that the average value within the local window data is selected for calculation, and maximum pooling indicates that the maximum value of the data within the local window is selected.

### 2.5.3 Recurrent Neural Network (RNN)

A recurrent neural network is a neural network that is specialized for processing a sequence of data with the time step index. Another way to think about RNNs is that they have a “memory” which captures information about what has been calculated so far. In the traditional neural network ANN, nodes in different layers (input layer, hidden layer, and output layer) are connected to each other, and the nodes between each layer are independent (Mousavi and Afghah, 2019). However, in RNN, it is identical that adjacent nodes in one hidden layer are connected to each other.

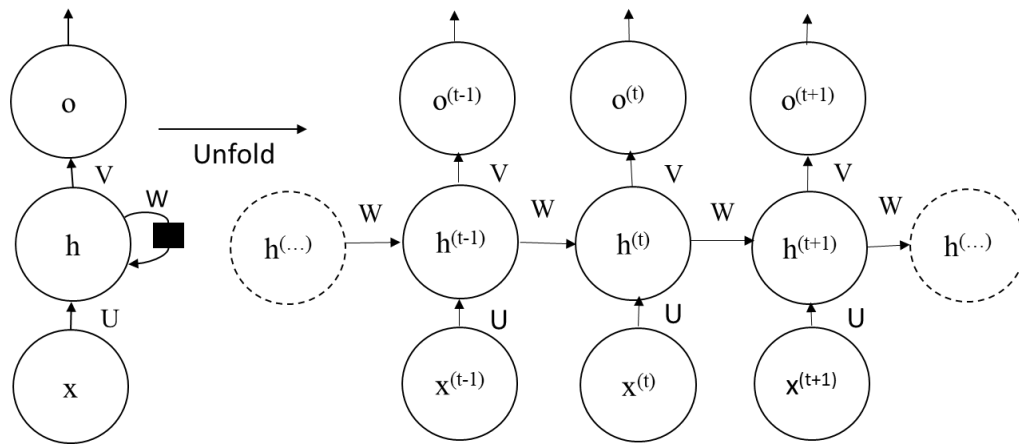


**Figure 2.5:** Sample RNN architecture (Zhu et al., 1998)

A notation of an RNN may be seen on the left side of the preceding picture, and an RNN that has been unrolled (or unfolded) into a full network can be seen on the right side of the same diagram. When we talk about unrolling, what we really mean is writing down the network for the entire sequence. For instance, if the sequence that we are interested in is a three-word sentence, the neural network would be unrolled into a three-layer structure, with one layer devoted to each word in the sentence. (Übeyli, 2009; Zhu et al., 1998).

Due to the unique structure, RNN is characterized by a superior ability in time series prediction and can theoretically handle arbitrary long sequences (Kumar et al., 2021; Zhu et al., 1998). However, its shortage lies in processing long distance information. The learning ability will be weakened owing to the gradient vanishing or exploding problem, which makes it difficult to capture long-term time dependences (Pascanu et al., 2013). To remedy this problem of conventional RNN, long short-term memory network (LSTM) was proposed (Gers et al., 2000; Hochreiter and Schmidhuber, 1997), which is an upgrade of original standard RNN. The thorough formation of an LSTM unit can be assessed in Fig. 2.10. A LSTM unit includes three gate controllers, known as the input, forget, and output gates individually. Every information going through this unit has to be decided whether to be remembered or forgotten, then assigned to corresponding gate. To avoiding the gradient vanishing problem, the LSTM network implements temporal memory through switching those gates (Yuan et al., 2019).

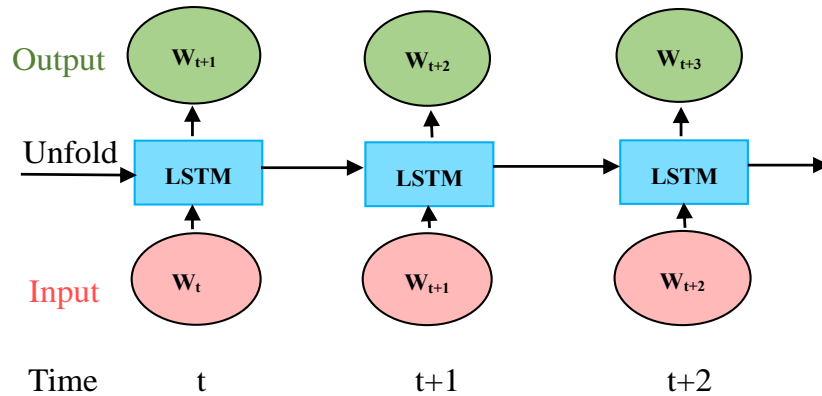


**Figure 2.6:** Sample LSTM architecture (Yuan et al., 2019)

Hence, LSTM is one type of Recurrent Neural Network that deals mostly with sequential data. In LSTM to retain memory cell state is used. The cell state is similar to production chain, the parameter flows straight forward, but some linear processes, such as addition and multiplication, will interact. The state of the cell depends on the interactions, and if there are no interactions, it will flow along without changes. LSTM will add or remove information to the cell state through gates which are structures that allow optional information to cross. Gates are implemented using sigmoid functions which produces two decisions either 0 or 1 assuming that 0 will block information flow and 1 will allow it. Three of these gates are available in LSTM, which determines the final cell state.

On the other hand, Bidirectional recurrent neural networks (RNN) are really just putting two independent RNNs together, known as Bi-LSTM (Huang et al., 2022; Ye et al., 2019). This structure allows the networks to have both backward and forward information about the sequence at every time step. Using bidirectional will run your inputs in two ways, one from past to future and one from future to past and what differs this approach from unidirectional is that in the LSTM that runs backward you preserve information from the future and using the two hidden states combined you are able in any point in time to preserve information from both past and future (Tourille et al., 2017). Bi-LSTM has also a successful history of its application in the field of geotechnical engineering (Liu et al., 2021; Shen et al., 2021; Zhang et al., 2021).



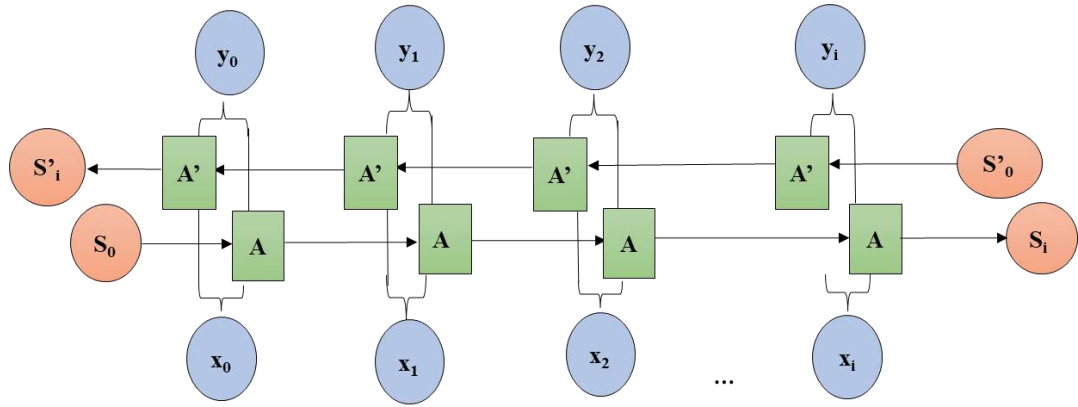


**Figure 2.7:** Bi-LSTM Architecture (Tourille et al., 2017)

### 2.5.4 TabNet

TabNet is a deep learning algorithm for tabular data, introduced by Google AI in 2020. It is designed to improve the performance and interpretability of machine learning models on structured data such as spreadsheets and databases. Despite being the most prevalent data type in the realm of AI (Chui et al., 2018), deep learning for tabular data is largely underdeveloped and most applications still rely mostly on variations of ensemble decision trees (DTs). It is because DT-based approaches have certain advantages:

- (i) They are representationally efficient for decision manifolds with roughly hyperplane boundaries, which are common in tabular data.
- (ii) They are highly interpretable in their basic form (for example, by tracking decision nodes), and there are well-liked post-hoc explain ability methods for their ensemble form, for example (Lundberg et al., 2018).
- (iii) They are highly interpretable in their basic Second, because previously-proposed DNN architectures, such as stacked convolutional layers or multi-layer perceptrons (MLPs), are not well-suited for tabular data, the absence of suitable inductive bias frequently prevents them from finding the best solutions for tabular decision manifolds (L. Xu et al., 2019; Shavitt and Segal, 2018; Goodfellow et al., 2016).

TabNet uses a combination of attention mechanisms, sparse regularization, and other techniques to achieve a high level of accuracy while also providing interpretable models that can be easily understood by domain experts (L. Xu et al., 2019). It is a deep tabular

data learning architecture that uses sequential attention to choose which features to reason from at each decision step. The TabNet encoder is composed of a feature transformer, an attentive transformer and feature masking. A split block divides the processed representation to be used by the attentive transformer of the subsequent step as well as for the overall output. For each step, the feature selection mask provides interpretable information about the model's functionality, and the masks can be aggregated to obtain global feature important attribution. The TabNet decoder is composed of a feature transformer block at each step. Though, TabNet is the latest addition in DNN models but it has achieved great success in images (Arik and Pfister, 2021), text (Nishida et al., 2017), rainfall forecast (Yan et al., 2021) etc. However, there has been no significant application of TabNet in the field of geotechnical engineering yet. In general, for tabular data sets, ensemble tree models are still mainly used. In many data-mining competitions. These rely on the following:

- (i) The tree model has a decision manifold, which approximates the boundary of the hyper plane. The boundary of the hyper plane can effectively divide the data so that the tree model has an efficient representation of tabular data.
- (ii) Good interpretability.
- (iii) Fast training speed.

Secondly, the previously proposed DNN structure is not suitable for tabular data. Traditional DNN based on convolutional layers or multi-layer perceptron (MLP) often have too many parameters for tabular data and lack proper inductive bias, which makes them unable to find the decision manifold for tabular data. The main disadvantage of the decision tree and its variant model is the dependency of feature engineering. A very important reason why deep learning methods can achieve great success in images, natural language, and audio is that deep learning can encode raw data into meaningful representations (Yan et al., 2021). End-to-end training based on the back propagation algorithm can effectively encode tabular data, thereby reducing or even eliminating the need for feature engineering (Arik and Pfister, 2021).

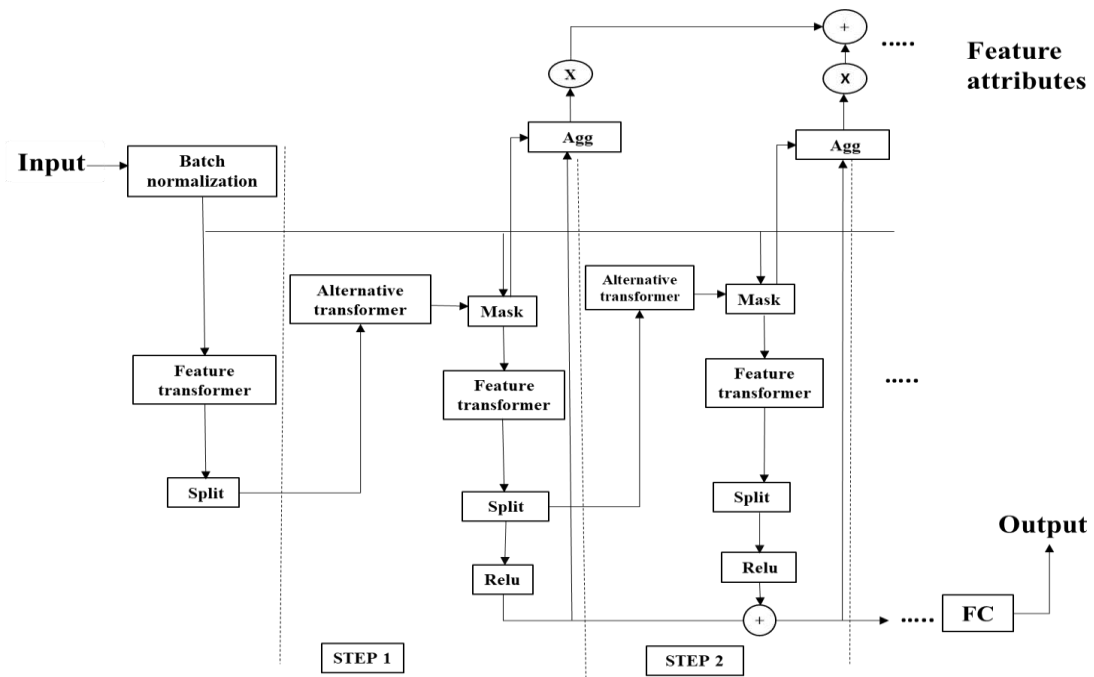


**Figure 2.8:** Sample TabNet architecture (Arik and Pfister, 2021)

Figure 2.12 shows that the TabNet encoder architecture is mainly composed of a feature transformer, an attentive transformer, and feature masking at each decision step. The tabular data includes category data and numeric data. TabNet uses original numerical data and uses trainable embedding to map categorical features to numerical features. Each decision step inputs the same  $B \times D$  feature matrix;  $B$  is the batch size, and  $D$  is the dimension of the feature. TabNet's encoding is based on the processing of multiple decision steps. The characteristics of each decision step are determined by the output of the previous decision step through the Attentive transformer. This outputs the processed feature representation and integrates it into the overall decision-making.

## 2.6 Past Researches

Finite element method has been employed extensively for the analysis of geotechnical issues (Brinkgreve and Engin, 2013; Potts et al., 2001; Schweiger et al., 2001). This is most likely a result of the numerous intricate problems unique to geotechnical engineering that have been overcome by the introduction of finite element modeling. This may help to explain why they are popular now a days in the field of geotechnical engineering (Brinkgreve and Engin, 2013).

### **2.6.1 Current Status of Pile Load Test Research in Bangladesh**

Very few research has been conducted in Bangladesh to analyze the load-settlement behavior of pile foundation. Sadeque (1989) studied pile load tests on the bored pile at three different sites of Dhaka city and compared them with the existing theoretical results. The variables considered are critical depth, loosening effect of soil, and groundwater level. But due to a lack of sufficient data, the study could not draw any correlation between theoretical results and the actual results from the pile load tests.

Morshed (1991) developed a simple analytical method based on 1D finite element technique with empirical method to predict the non-linear pile resistance in embedded sand. It eventually developed the analytical methods based on laboratory test results, to predict the load-deformation behavior of piles and to use them as an alternative method of analysis. Little parametric study was performed and there were no verification comparing with filed data.

However, there are quite a handsome amount of research on capacity prediction from Static Load Test. PWD (Public Works Department, Bangladesh) has conducted multiple projects in Bangladesh to estimate the ultimate load capacity of large diameter cast-in-situ piles and small and large precast piles. Several initiatives have also been executed on a small-scale prestressed pile. Test and service piles were subjected to load evaluations. The majority of tests were conducted under the supervision of BUET (Bangladesh University of Engineering and Technology) consultants on a full-time basis. Several researchers have published the outcomes of pile load experiments.

Ansary et al. (1999) summarized the pile load test performed by BUET in different sites of Bangladesh as consultants of PWD between 1996 to 1999 and presented a summary of their pile load test data collection.

Yasin et. al. (2009) established correlation between the ultimate load capacity prediction from both the Static Pile Load Test and SPT-N value. Cast-in-situ bored pile and driven pile load capacities in the same soil were compared in the same study.

Khan (1997) investigated small prestressed piles. Pile load tests were compared to static and dynamic pile capacities. The lambda-method can accurately predict pile capacities driven through and resting on Dhaka Clay. The alpha-method predicts Dhaka Clay skin

friction only. Lamda and alpha techniques can predict pile capacities driven through Dhaka clay but resting on medium dense sand.

Rahaman (2008) proposed a design method of such piles in more efficient and effective way with the help of proper field investigations and laboratory test results. Also, extrapolated load-settlement curves from were used to determine the ultimate carrying capacities of piles of different diameter by methods proposed by Mazurkiewicz, Van Weele and Davisson and concluded to have good agreement with those determined by theoretical method.

Rahman (2016) established an analytical method to separate skin frictional resistance and end bearing components for a given load on a pile based on static load-settlement data and direct shear test data.

Halder (2016) also studied the capacity of two test piles using soil investigation data applying BNBC-2015 (draft) and AASHTO 2002 method. The relationship among capacity of static load test and predicted capacities (using BNBC-2020, SPT, AASHTO-2002, driving equations) were compared and correlation values were obtained (Halder, 2016). Also, the SPT method was justified as an effective approach to be used for pile capacity estimation (Islam, 2018).

### **2.6.2 Relevant Researches on FEM**

Finite element method has been employed extensively for the analysis of geotechnical issues (Potts et al., 2001). This is most likely a result of the numerous complex problems unique to geotechnical engineering that have been overcome by the introduction of finite element modeling and also due to their high accuracy. Specifically, the successful application of FEM in the field of geotechnical engineering is for slope stability analysis (Zheng et al., 2005; Griffiths and Fenton, 2004), tunnel engineering (Kabir et al., 2017; Franzius and Potts, 2005), foundation engineering (Jimenez and Sitar, 2009; Nour et al., 2002) and so on. This may help to explain why they are popular now a days in the field of geotechnical engineering.

The bearing capacity of a single pile is most usually determined by pile load test or by empirical methods. Several scholars continue to study the complicated issue of pile behavior in soil, particularly in the case of its settlement due to vertical loads. Its installation is more disruptive to the surrounding soil than drilling for piles, and it

has a substantial impact on changes in soil parameters and, as a result, on the behavior and capacity of the pile under load. Because of this, it is occasionally impossible to estimate the pile-bearing capacity with an accuracy of more than 30% (Krasin'skin, 2014). With the current rapid development of numerical analysis, the use of finite element method is attracting engineer's attention towards using this method as one option (Elsherbiny and El Naggar, 2013; Naveen et al., 2011; Said et al., 2009; Reul, 2004). Different constitutive models are used to simulate the soil pile interaction following the development of more and more comprehensive constitutive models to describe the complex behavior of geomaterial under different loading conditions (Y. Wu et al., 2013; Ti et al., 2009; Hejazi et al., 2008). In many of the previous studies pile load-settlement behavior was assessed for a uniform soil type. For clayey soil the pile-load settlement behavior assessed (Chung and Yang, 2017) using finite element method which concluded with a recommendation for further analysis in a stratified soil condition. In other literatures, study on non-cohesive soil was also conducted (Unsever et al., 2015; Krasin'skin, 2014). Elasto-perfectly plastic model with Mohr- Coulomb failure criterion, usually named as Mohr Coulomb model, is widely used in finite element analysis of geotechnical engineering, due to its simplicity (Naveen et al., 2011; Said et al., 2009). The failure envelope, being dependent on the major and minor principal stresses is defined by cohesion,  $c$  and internal frictional angle,  $\phi$ . In the MC model a constant stiffness is used (Baziar et al., 2009; Li et al., 2009). Whereas in an advanced model for replicating the behavior of many soil types, including both soft and stiff soils, is the Hardening Soil model (Obrzud, 2010; Schanz et al., 2019; Ti et al., 2009). Numerical analyses for simulation of soil-pile interaction can be done in two ways: The first is a continuum-based method like boundary element method or finite element method (FEM), in which continuity of the soil domain is inherent in formulations; while the second method is a load transfer method which models the soil through a set of independent springs attached to the piles. In the first method, the use of Mindlin's solution was used in a linear boundary element formulation (Lee, 1993; Randolph and Wroth, 1978; Poulos, 1968). Subsequently, linear solutions were developed for piles and pile groups (Banerjee and Davies, 1978) in non-homogenous soils. FEM approaches were attempted by Desai (Randolph and Wroth, 1978; Desai et al., 1974), Besides them, Pressley and Poulos (Pressley and Poulos, 1986) used an elastic perfectly plastic soil model in an axisymmetric FEM to approximately analyze pile groups. Three-dimensional analysis of vertically loaded pile groups was studied by

Ottaviani (Ottaviani, 1975). Also, Muqtadir and Desai et al. (1986) analyzed three-dimensional pile groups under vertical loads. After that, significant improvement in the study was ensured for a single pile by using the commercial finite element programs with better predictions and simulation results (Naveen et al., 2014). However, when soil is subjected to initial deviatoric stress, its stiffness decreases and irreversible plastic strains appear at the same time. The observed relationship between the axial strain and the deviatoric stress in the exceptional case of a drained triaxial test can be well approximated by a hyperbola. The well-known hyperbolic model (Duncan & Duncan, 1955) utilizes the relationship was also then first proposed for pile-load test. But the Hardening Soil model vastly outperforms the hyperbolic and other available models (Cardoso Bernardes et al., 2022; Gowthaman and Nasvi, 2017) which has been considered in this study to assess the load-settlement behavior of pile foundation.

This research proposes the authors' new numerical model for assessing pile behavior. A Finite Element Method (FEM) model can simulate soil changes caused by pile installation. Real-world static pile load testing validated the concept. The numerical simulations with and without pile placement were compared to in situ pile load tests. Krasinski et al. (2014) used a similar approach to numerically model the screw pile installation process; however, field tests showed that the soil parameters need proper investigation. Here, in this study, the in-depth investigations required for developing the HS model were clarified, including its validation with soil model calibration. Moreover, this research incorporates the infield installation impacts that correspond to its layered soil profile. The computational stability of the current study was further ensured in numerical simulation using the Plaxis-3D finite element program by introducing time intervals between loading increments or decrements during field testing.

### **2.6.3 Relevant DNN Researches**

Machine Learning/Deep Learning algorithms are a burgeoning entity that has been effectively used for practically every problem in geotechnical engineering over the last decade. Applications of DNNs in geotechnical engineering include the prediction of liquefaction (Hanna et al., 2007, Javadi et al., 2006, Kim and Kim, 2006; Baziar and Ghorbani, 2005; Eldin Ali and Najjar, 1998; Agrawal et al., 1997), the estimation of several soil properties such as shear strength and stress history (Kurup and Dudani,

2002, Lee et al., 2003, Penumadu and Chameau, 1997) and soil settlement predictions (Chen et al., 2006; Shahin and Jaksa, 2005; Shahin et al., 2004; Shahin et al., 2003)

The discipline of geotechnical engineering has made use of a wide variety of Artificial Intelligence (AI) techniques, such as Deep Neural Networks (DNN). That is why, it has been demonstrated that DNN is a useful modeling technique in geotechnical engineering. Yet, it has been noted that ANN is a useful modeling technique in geotechnical engineering, as such a model may be trained on input-output data without complex inputs or outputs. (Shahin et al., 2002). The primary goal of DNNs is for a computer program to learn patterns in data in order to infer the target values from the feature values. This makes DNN use appealing since it allows us to avoid the need for certain assumptions that are inherent to conventional methods of prediction. Both Ghaboussi (1992) and Ghaboussi et al. (1991) provide support for this idea in their respective published works. Some potential applications of neural networks in geotechnical engineering were identified through research on the constitutive modeling of material behavior with neural networks, including the modeling of soil behavior, the evaluation of liquefaction potential, the seismic ground response, and the response of geotechnical structures (Chan et al., 1995). The ability of a feed-forward backpropagation artificial neural network (ANN) to find complex non-linear relationships among different parameters has attracted a lot of attention in recent years, and this has been a driving factor in its adoption for use in solving geotechnical problems, as reported earlier (Momeni et al., 2015). Prediction of pile capacity (Mohanty et al., 2018), foundation settlement, soil qualities and behavior, and liquefaction (Hanna et al., 2007) are only few of the areas where DNNs have been put to use in geotechnical engineering, as stated by (Hazewinkel, 2022; Sarkar et al., 2015; Shahin et al., 2002).

However, the use of neural networks in predicting the pile capacity started in the 1990's (Goh, 1995; Boscardin and Cording, 1989), when used in a form of a model to predict an estimate of the friction capacity of driven piles in clay soils. The results were promising when compared to the actual data and some empirical methods. Lee et al. (Lee and Lee, 1996) tried to predict the driven pile capacity by using an artificial neural network model. The error between the predicted and the actual pile test was around 20%. However, they did not attempt to predict the entire static load test. In fact, developed three artificial neural network models to forecast driven piles capacity



(Kiefa, 1998). He compared the results with four empirical formulas, and found that the model that was devoted to forecast the total pile capacity was more accurate than others with 0.95 coefficients of determination. Furthermore, Goh et al. (1995) presented a new neural network model to predict pile capacity in sandy soils. The model's pile capacity was satisfactory when compared to other empirical formulas. Shahin et al. (2016) discussed different applications of artificial neural network in Geotechnical Engineering and mentioned different applications including predicting the pile capacity. Artificial neural network also used to estimate the pile capacity from databases of 80 cases collected from the literature and corresponding to different sites distributed all over the world (Benali and Nechnech, 2011). They reported that the networks are feasible for these kinds of problems but they did not attempt to predict the entire static load test. Moreover, artificial neural networks were used for predicting the axial capacity of a driven pile (Maizir and Kassim, 2013). Artificial neural network (ANN) and random forest (RF) algorithms were utilized to predict the ultimate axial bearing capacity of driven piles (Pham et al., 2020). Optimized machine learning methods had also shown great potential to estimate bearing capacity of piles using swarm optimisation algorithm (Kardani et al., 2020). In another study, the pile setup was predicted using a deep neural network model considering SPT value (Nejad et al., 2009) where concluded with RMSE= 14.2, R= 0.72. The predicted values were compared with those produced by some empirical formulas. It showed that the model produced satisfactory results. But all those studies were very specific in regards of soil condition which represents uniformity (either cohesive or cohesionless). Also, pile settlement was predicted as a function of load, pile geometry, and CPT test data. Accordingly, the load, pile characteristics, and CPT test parameters will be presented in the input layer and the determined settlement in the output layer with an RMSE of 0.44, MAPE =0.234 (Ofrikhter and Ponomarev, 2021). Prediction of pile settlement using artificial neural networks based on standard penetration test data. DNN model is developed for predicting pile behavior based on the results of average cone penetration test (CPT) results for different layers (Nejad and Jaksa, 2017) RMSE 3.68, R= 0.94. RNN model has the ability to reliably predict the load–settlement response of axially loaded steel driven piles (Shahin, 2014). As we can see in the above-mentioned studies, no serious attempt was made to predict the entire static load test; in this research we demonstrate that static load test can be reasonably predicted by deep neural networks with enough training data.

Moreover, while predicting the load settlement behavior, interrelated high-dimensional data are one of the challenges that still has to be solved. The usage of these raw data could increase computing costs and cause the deep learning model to overfit. The quality of the raw data collected is typically also impacted by measurement sensor failure and ambient noise. To increase prediction accuracy, the noise from the working time data needs to be efficiently removed. This noise's elimination is still difficult. Additionally, there are still a relatively small number of studies in existence that use the DNN approach to predict the load-settlement behavior of pile foundations. Incorporating PCA to minimize the input datasets dimensionality by reserving principal components, this study offers the best fitted DNN model to forecast the behavior of pile foundations. Additionally, it launches the model with noise-filtered data by eliminating any minor components that are impacted by the noise.

## **2.7 Research Gaps**

Handsome number of studies are available on cast-in-situ bored pile and driven pile load capacity predictions in the perspective of Bangladesh. Most of the cases, extrapolated load-settlement curves were used to determine the ultimate bearing capacities of piles of different diameter by established method or BNBC 2020 or even any other established methods to predict the capacity of pile. Also, analytical methods were developed to separate skin frictional resistance and end bearing components for a given load on a pile based on static load-settlement data and direct shear test data. Correlations are even available between the ultimate load capacity prediction from both the Static Pile Load Test and SPT-N value. However, very limited studies are available to predict the load-settlement behavior of pile which can capture the insights of an entire static load test. A summary of the available research has been detailed in Table 2.2. This may help to trim of the project cost and time by reducing the number of static load test from the ongoing projects in Bangladesh.

From the available literatures, it was clear that different constitutive models are used to simulate the soil pile interaction following the development of more and more comprehensive constitutive models to describe the complex behavior of geomaterial under different loading conditions.

**Table 2.2:** Summary of previous studies on Load-Settlement behavior of pile foundation

| Authors                       | Soil Type<br>(Pile Tip/<br>Toe) | Layered<br>Soil Profile | Soil Parameter |   |        | Pile Configuration |   |    |              | Applied<br>Load | Methods Adopted to Capture Load-Settlement<br>Behavior |           |           |              | Performance<br>Comparison | Sensitivity<br>Analysis |
|-------------------------------|---------------------------------|-------------------------|----------------|---|--------|--------------------|---|----|--------------|-----------------|--|-----------|-----------|--------------|---------------------------|-------------------------|
|                               |                                 |                         |                |   |        | L                  | D | EA | Pile<br>Type |                 | Analytical   | Empirical | Numerical | AI           |                           |                         |
|                               |                                 |                         | N              | c | $\phi$ |                    |   |    |              |                 |  |           |           |              |                           |                         |
| Vesic<br>(1977)               | Sand                            | ×                       | ×              | × | √      | √                  | √ | √  | ×            | √               | ×  | √         | ×         | ×            | ×                         | √                       |
| Desai<br>(1974)               | Sand                            | ×                       | ×              | √ | √      | √                  | √ | √  | ×            | √               | ×  | ×         | √         | ×            | √                         | ×                       |
| Lee (1993)                    | Sand                            | √                       | ×              | × | ×      | √                  | √ | √  | ×            | √               | Logarithmic  | ×         | ×         | ×            | ×                         | ×                       |
| Guo and<br>Randolph<br>(1999) | Clay                            | √                       | ×              | × | ×      | √                  | √ | ×  | Group Pile   | √               | Logarithmic  | ×         | ×         | ×            | ×                         | ×                       |
| Kiefa<br>(1998)               | Sand                            | ×                       | ×              | × | ×      | √                  | √ | ×  | Driven Pile  | √               | ×  | ×         | ×         | GRNN         | √                         | ×                       |
| Pooya nejad<br>et.al (2009)   | ×                               | √                       | √              | × | ×      | √                  | × | ×  | ×            | √               | ×  | ×         | ×         | ANN-<br>BPNN | √                         | √                       |
| Ismail and<br>Jeng (2011)     | ×                               | ×                       | √              | × | ×      | √                  | √ | √  | ×            | √               | ×  | ×         | ×         | HON          | √                         | ×                       |
| Shahin et.al<br>(2013)        | ×                               | ×                       | ×              | × | ×      | √                  | √ | √  | Steel        | √               | ×  | ×         | ×         | RNN          | ×                         | √                       |
| Ismail et<br>al. (2013)       | ×                               | ×                       | √              | × | ×      | √                  | √ | ×  | ×            | √               | ×  | ×         | ×         | PSO-<br>BPNN | √                         | ×                       |

**Table 2.2:** Summary of previous studies on Load-Settlement behavior of pile foundation

| Authors                       | Soil Type<br>(Pile Tip/<br>Toe) | Layered<br>Soil<br>Profile | Soil Parameter |   |        | Pile Configuration |   |    |              | Applied<br>Load | Methods Adopted to Capture Load-Settlement Behavior |           |           |          | Performance<br>Comparison | Sensitivity<br>Analysis |
|-------------------------------|---------------------------------|----------------------------|----------------|---|--------|--------------------|---|----|--------------|-----------------|---|-----------|-----------|----------|---------------------------|-------------------------|
|                               |                                 |                            |                |   |        | L                  | D | EA | Pile<br>Type |                 | Analytical  | Empirical | Numerical | AI       |                           |                         |
|                               |                                 |                            | N              | c | $\phi$ |                    |   |    |              |                 |   |           |           |          |                           |                         |
| Jian-lin et al.<br>(2014)     | Deep<br>Clay                    | ×                          | ×              | × | ×      | ×                  | × | ×  | ×            | √               | ×   | ×         | Plaxis-3D | ×        | √                         | ×                       |
| Gowthaman<br>et. al (2016)    | Soft soil                       | ×                          | ×              | × | ×      | ×                  | × | ×  | ×            | √               | ×   | ×         | Plaxis-2D | ×        | √                         | ×                       |
| Jebur et. Al.<br>(2018)       | Sand                            | ×                          | ×              | × | √      | √                  | √ | √  | ×            | √               | ×   | ×         | ×         | √        | ×                         | √                       |
| Schmüdderich<br>et al. (2020) | ×                               | √                          | √              | √ | √      | √                  | √ | ×  | ×            | √               | ×   | ×         | √         | ×        | √                         | √                       |
| Armaghani et<br>al. (2020)    | Gravel                          | ×                          | ×              | × | ×      | ×                  | × | ×  | ×            | √               | ×   | ×         | ×         | PSO-BPNN | √                         | √                       |
| Ofrikhter et.<br>Al. (2021)   | ×                               | ×                          | ×              | × | ×      | √                  | × | ×  | ×            | √               | ×   | ×         | ×         | ×        | ×                         | ×                       |
| Zhang (2021)                  | ×                               | √                          | ×              | × | ×      | ×                  | × | ×  | ×            | √               | ×   | ×         | √         | ×        | ×                         | ×                       |

In many of the previous studies pile load-settlement behavior was assessed for a uniform soil type using finite element method which concluded with a recommendation for further analysis in a stratified soil condition. In other literatures, study on non-cohesive soil was also conducted elastic-perfectly plastic model with Mohr- Coulomb failure criterion, usually named as Mohr Coulomb model, is widely used in finite element analysis of geotechnical engineering for its simplicity and uniform stiffness consideration. Question remains regarding the proper selection of soil model which is adequate to simulate the behavior with higher accuracy. However, when soil is subjected to initial deviatoric stress, its stiffness decreases and irreversible plastic strains appear at the same time. The observed relationship between the axial strain and the deviatoric stress in the exceptional case of a drained triaxial test can be well approximated by a hyperbola. Though hyperbolic model utilizes the relationship was previously proposed for pile-load test modeling. But the Hardening Soil model vastly outperforms the hyperbolic and other available models. It was found that there is barely any research available with proper guideline for representing soil behavior based on plasticity theory. Focusing on these limitations, in this research FEM model was developed using Plaxis-3D incorporating the sophisticated Hardening Soil Model (HS) that was developed within the context of the traditional theory of plasticity with a complete guideline of parameter determination and model calibration.

Though many recent studies are available on pile-load settlement behavior prediction using AI techniques, clear concepts are required regarding the factors affecting the settlement. Most traditional pile settlement assessment methods include the following fundamental parameters: pile geometry, pile material properties, applied load and soil properties. There are some additional factors, such as the loading/ unloading phase consideration, layered soil profile, load test method and the depth to the water table. The depth of water table is not included in this study, as it is believed that its effect is already accounted for in the measured SPT blow count. However, the effect of these missing consideration from previous literatures were considered in this study and in this research, we demonstrate that static load test can be reasonably predicted by deep neural networks with enough training data.

Moreover, while prediction with AI techniques, the load settlement behavior, interrelated high-dimensional data are one of the challenges that still has to be solved. The usage of these raw data could increase computing costs and cause the deep learning

model to overfit. The quality of the raw data collected is typically also impacted by measurement sensor failure and ambient noise. To increase prediction accuracy, the noise from the working time data needs to be efficiently removed. This noise's elimination is still difficult. Additionally, there are still a relatively small number of studies in existence that use the DNN approach to predict the load-settlement behavior of pile foundations. Incorporating PCA to minimize the input datasets dimensionality by reserving principal components, this study offers the best fitted DNN model to forecast the behavior of pile foundations. Additionally, it launches the model with noise-filtered data by eliminating any minor components that are impacted by the noise.

## **CHAPTER 3**

### **SUB-SOIL INVESTIGATION AND DATA COLLECTION**

#### **3.1 Introduction**

For the development of a finite model according to the objectives of the research and availing the scope of the study, collection of soil sample was done from the bore log adjacent to HSIA expansion project. In this particular section, the procedure of sample collection and both the in-situ and lab tests will be discussed. In addition to that, preparation of the collected data sets required to create Deep Neural Network (DNN) model will be discussed.

#### **3.2 Sub-soil Investigation**

Sub-soil investigation or geotechnical investigation is very crucial to understand the condition of any construction site. It includes soil sample collection and its techniques, conducting study on soil composition, soil properties and other parameters. In the following sub-sections, the field tests and soil sample collection techniques have been presented in detail:

##### **3.2.1 Site Information**

A pile load test also determines a pile foundation's strength and integrity. The test measures a pile's load-bearing capacity by applying a controlled load. The collected pile load test report of the selected project presents the information, test data and results of static pile load test conducted on bored pile having ID: BH40-TP-07 for terminal-3 building area of proposed Airport Expansion Project of Hazrat Shahjalal International Airport (HSIA), Dhaka. On behalf of Aviation Dhaka Consortium (ADC), Sinohydro Corporation Limited installed the pile and pile load testing work conducted by Geo-Drill BD. Static axial compressive pile load test started on 16th September 2020 and finished on 17th September 2020. The effective strength characteristics of the granular soils for Test Pile location were determined using corrected SPT N-value data from test borings and published correlations. Bore log data and soil samples were later collected including undisturbed samples for testing of the upper silty clay soil layers from different depth.

### 3.2.3 Field Tests

The most popular field tests are the standard penetration test (SPT). The following discusses the conducted field tests and the details on undisturbed soil sample collection.

### 3.2.4 Standard Penetration Test (SPT)

The most common type of field test, the standard penetration test (SPT), has been performed at the selected location. Up to a depth of around 50 m from the existing ground level, samples were taken and the SPT N-value was recorded at every 1.5 m depth interval (EGL). ASTM D 1586 outlines the testing procedure (ASTM,1989).

The general soil profile of this area is filling sand overlying silty clay layer. The depth of soft clay varies from 3 to 6 m from existing ground level (EGL). The silty clay layer exists from 12 to 23.5 m from EGL. Also, there is a presence of stiff clay after 25 m. The SPT N-value of soft clay from 7 to 13. For medium stiff clay it is 15 to 20 and for very stiff 22 to 29. SPT report is attached in the Appendix. SPT was conducted to identify the soil stratification, recording SPT-N value, ground water table recording and both disturbed and undisturbed soil sample collection.

The 115-millimeter diameter pipe (split spoon) used in the Standard Penetration Test is driven at a drop of 750 millimeters with a 63.5-kilogram hammer. The undisturbed sample was obtained in this case using a large dia sampler. The ASTM D1586 standard specifies the test. In the following Table 3.1, a short SPT N-value test procedure is presented.

**Table 3.1:** Recommended SPT procedure (ASTM D1586)

| Equipment        | Short procedure   |
|------------------|---|
| Borehole size    | 65 mm < Diameter < 115 mm   |
| Borehole support | Casing for 3m length and drilling mud   |
| Drilling         | a) Wash boring<br>b) Side discharge rotary boring<br>c) Side or upward discharge bit clean bottom of borehole |
| Drill rods       | A or AW for depths of less than 15 m N or NW for greater depths   |
| Sampler          | Standard 0.0. 51 mm +/- 1 mm, 1.D. 35 mm +/- 1 mm and length > 457 mm   |



|                        |   |
|------------------------|---|
| Equipment              | Short procedure   |
| Penetration resistance | Record number of blows for each 150 mm;<br>N = number of blows from 150 to 450 mm penetration |
| Blow count rate        | 30 to 40 blows per minute   |

### 3.2.5 Sample Collection for Laboratory Testing

During SPT, both disturbed and undisturbed samples were collected in order to conduct the laboratory tests referred in Table 3.2. They were performed to determine the overall characteristics of the soil. According to the Unified Soil Classification System, the soil has been categorized (USCS).

**Table 3.2:** List of laboratory tests

| Type of test                   | Sample Type        | No of Tests | Test Method   |
|--------------------------------|--------------------|-------------|---------------|
| Liquid Limit and Plastic Limit | Disturbed Sample   | 5           | ASTM D 4318   |
| Shrinkage Limit                | Disturbed Sample   | 5           | ASTM D 427    |
| Specific Gravity               | Disturbed Sample   | 5           | ASTM D 854    |
| Hydrometer                     | Disturbed Sample   | 5           | ASTM D 422    |
| Triaxial                       | Undisturbed Sample | 1           | ASTM D7181-20 |

As the site of Silty Clay for conducting triaxial test was selected nearby HSIA expansion project, the northern part of Dhaka city. Soil sample was collected at different depths from Existing Ground Level (EGL) at selected site mentioned in Table 3.3.

**Table 3.3:** Undisturbed sample collected at different depth

| Undisturbed Sample (UD) | Depth of Collection (m) | Sample Recovery (mm) |
|-------------------------|-------------------------|----------------------|
| UD-1                    | 2-3                     | 650                  |
| UD-2                    | 3.5-4.5                 | 600                  |
| UD-3                    | 5-6                     | 600                  |
| UD-4                    | 9-10                    | 60                   |

Metal tubes for taking undisturbed samples used were 75 mm in diameter or 750 mm long. They were driven by using a hammer. On ejection and trimming, the samples are suitable sizes for triaxial testing. The larger sample tubes are fitted with detachable cutting shoes and are generally driven using mechanized equipment. Considerable care was required to maintain the verticality of the tube when driving it.

### 3.3 Laboratory Test Results

In order to conduct the FEM analysis several laboratory tests were conducted. Also, triaxial test was conducted for undisturbed soil samples. In this section the test results have been detailed.

#### 3.3.1 Atterberg Limit Test

The objective of these tests was to determine the boundaries of different states that is liquid limit and plastic limit and thereby use them for soil classification. It is defined as the water content at which the soil has such small shear strength that it flows to close a groove of standard width when jarred in a specified manner. Plastic limit (PL) is the minimum moisture content at which the soil can be deformed plastically. It can be taken as the smallest water content at which the soil began to crumble when rolled into a thread of 3 mm in diameter. The shrinkage limit test was carried out according to ASTM D 427. To identify the engineering properties of soil, the criteria are described in Table 3.4.

**Table 3.4:** Correlations between plasticity of soil and strength (Atkins, 1997)

| Plasticity Index (%) | Description        | Dry Strength   |
|----------------------|--------------------|----------------|
| 0-3                  | Non plastic        | Very low       |
| 4-6                  | Slightly Plastic   | Low            |
| 7-12                 | Moderately plastic | Low to Medium  |
| 16-35                | Plastic            | Medium to High |
| Over 35              | High Plastic       | High           |

Initially soil samples were sorted varying on type and SPT value. Also, oven dried to get the initial/field moisture content at the very beginning of the test. From the Atterberg limit test it was observed from the test data that the full profile up to 35 m depth, majority of soil have more than 80% of material passing through #200 sieve (0.075 mm opening). The results of the Atterberg limit tests re represented in Table 3.5. From

Figure 3.1, it is clear that the soil up to 12 m depth is predominantly fine-grained soil falling mainly in the Unified Soil Classification System as CL and ML, which are grouped as low plastic clay and low plastic silt.

**Table 3.5:** Plasticity values for cohesive soil at different depth

| Depth (m) | Liquid Limit (%) | Plastic Limit (%) | Plasticity Index (%) | Specific Gravity ( $G_s$ ) |
|-----------|------------------|-------------------|----------------------|----------------------------|
| 1.5-1.95  | 48               | 24                | 25                   | 2.65                       |
| 6-6.5     | 44               | 23                | 21                   | 2.77                       |
| 7.5-7.95  | 44               | 30                | 14                   | 2.71                       |
| 9-9.45    | 46               | 26                | 20                   | 2.65                       |
| 33-33.45  | 39               | 24                | 15                   | 2.71                       |

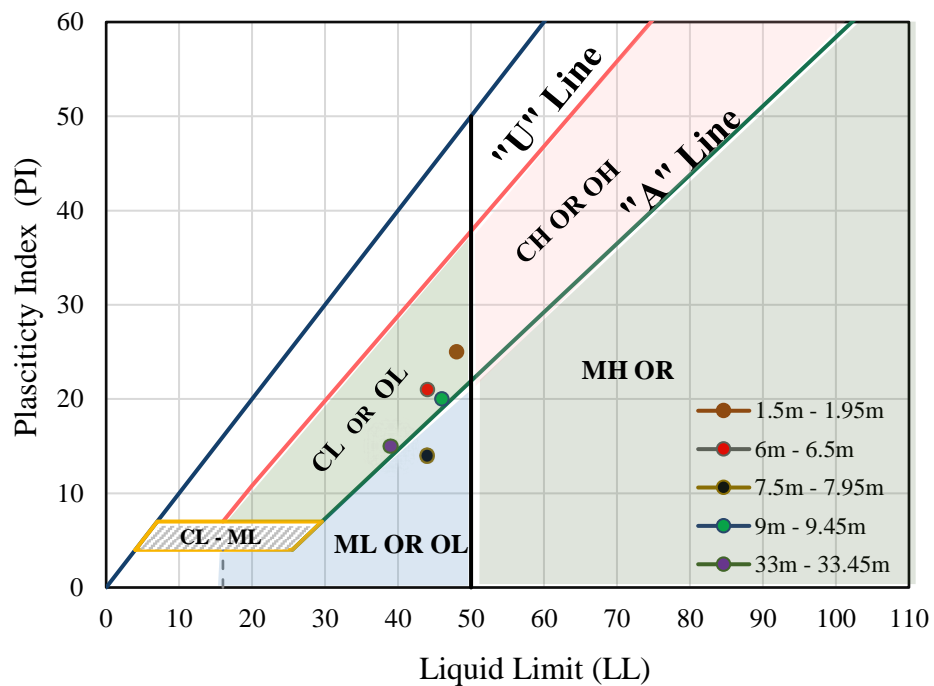


**Figure 3.1:** Position of the soil samples from the study area in the plasticity chart

### 3.3.2 Specific Gravity and Grain Size Analysis

In general, the specific gravity  $G_s$  of a material represents the ratio of the mass of a given volume of that material at a temperature to the mass of an equal volume of distilled water at the same temperature. Calculating soil properties like the degree of saturation and void ratio requires knowledge of specific gravity. ASTM D854 were

used to measure the specific gravity of soil particles. Hydrometer test and grain size analysis results are represented in Figure 3.2.

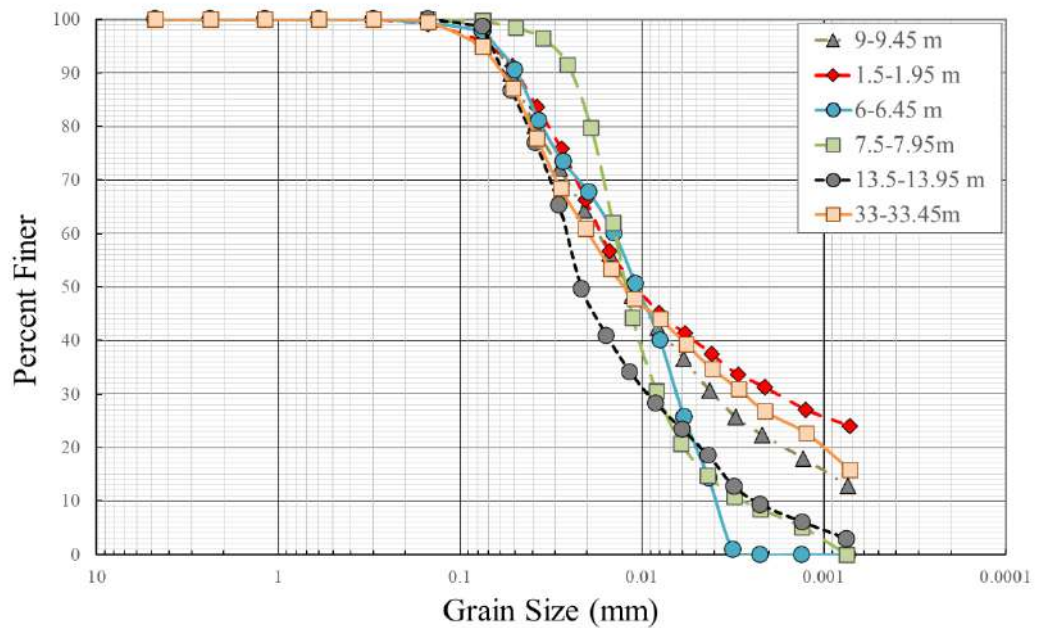


**Figure 3.2:** Results of grain size analysis of collected samples

In this investigation, a significant parameter was obtained by the specific gravity test, and the outcome was used to perform hydrometer test. Figure 3.2 represents the overall findings and observations. From the range of  $D_{50}$  it was clearly evident that silt and clay percentages were predominant in the soil samples of that particular layers

### 3.3.2 Triaxial Test

The tri-axial test is indeed a crucial test for obtaining highly accurate soil strength parameters that are essential for finite element modeling. During the Consolidated Drained (CD) triaxial test, the specimen is first consolidated under a confining pressure until the excess pore water pressure is dissipated. The axial stress is then applied to cause shear failure in the specimen, while the confining pressure is maintained. The axial strain is measured during the application of the deviator stress. The test is called "consolidated drained" because the specimen is consolidated before the application of the deviator stress, and the pore pressure is allowed to dissipate during the test. The CD test allows for the measurement of both cohesion and angle of internal friction, which are important soil strength parameters that are required for finite element modeling. In this study, the CD triaxial tests were carried out in accordance with the requirements of

test procedure ASTM D 4767 and instrumental setup presented in Figure 3.3, which is a standard test method for determining the strength and stress-strain relationships of a soil specimen. The tests were conducted on a silty clay type of undisturbed soil sample that was collected from a depth of 9-9.5 meters at the selected site of the HSIA expansion project. The results of the CD triaxial tests provided important data for the finite element modeling of the soil behavior at the project site. The test method covered the determination of strength and stress-strain relationships represented in Figure 3.4 of a cylindrical undisturbed and saturated cohesive soil specimen. There were two phases, consolidation and shear. Specimens were isotopically consolidated and sheared in compression without drainage at a constant rate of axial deformation. However, 100 kPa and 200 kPa effective confining stress were applied for the soil specimens. The test was continued till failure or 11% axial strain of the specimen whichever occurred first. For this research consolidated drained test results in Figure 3.5 were used to determine the strength parameters. The strength properties from triaxial test results are demonstrated in Table 3.6.

**Table 3.6.** Strength properties of silty clay layer

| Soil Parameters                             | Sample Condition     | Value |
|---|----------------------|-------|
| Angle of Internal friction, $\phi^\circ$    | Reconstituted Sample | 23    |
| Cohesion, $c$ (kN/m <sup>2</sup> )          | Reconstituted Sample | 18    |
| Unit Weight, $\gamma$ (kN/ m <sup>3</sup> ) | Reconstituted Sample | 16.5  |



**Figure 3.3:** Triaxial test setup

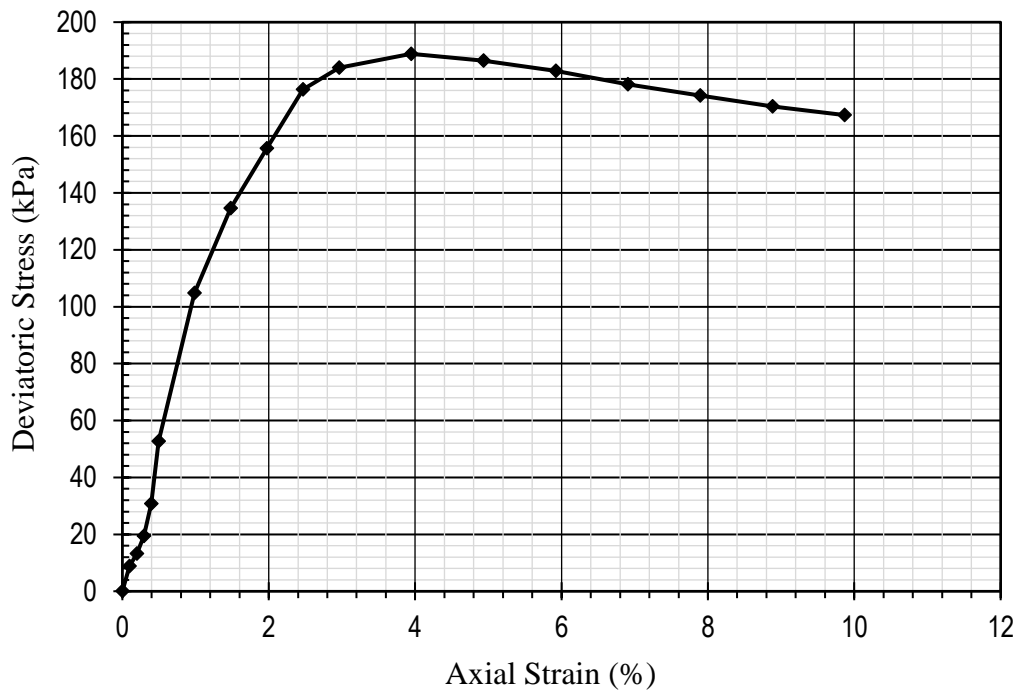


**Figure 3.4:** Deviatoric Stress vs. Strain under triaxial test results at 200 kPa

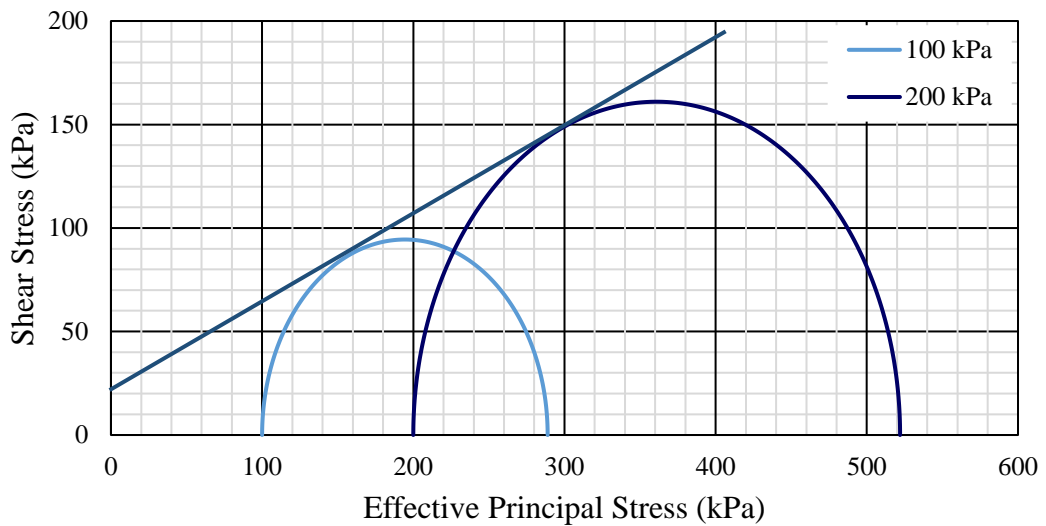


**Figure 3.5:** Failure envelopes for triaxial consolidated drained test for silty clay

### 3.4 Data Collection

This research also studies the applicability of machine learning to predict settlement behavior of pile due to static loading. As such, a data set is required that contains vibratory pile driving data. As mentioned earlier, the settlement pile is affected by

parameters relating to three major categories of different factors: pile related factors, soil related factors and loading rate. Therefore, in this research the variations in soil profile based on the SPT-N value was considered apart from the variations of pile's diameter, pile length, effective area, modulus of elasticity of pile material, loading rate and even loading/unloading cases and cycles were considered as input features for the machine learning model to predict. The approach to predict the settlement of pile with respect to the variations in load applied and other considered parameters. This portion presents the data sets used for this research and gives a detailed explanation of the data handling process.

#### **3.4.1 Data Sets for DNN Model**

The First Dhaka Elevated Expressway (FDEE) Project, the Hazrat Shahjalal International Airport (HSIA) Expansion Project, and the Padma Bridge Rail Link Project pile construction data were collected for the proposed investigation. Around 712 load-test data points captured from the 42 load test data sets of nominated projects and their basic soil profile additionally DNN model was developed to predict the load-settlement behavior of pile foundation. According to the methodology, data sets were sorted and prepared for DNN model developments. For this particular study, only RCC piles were selected of specific types. The obtained load test data sets and their relevant soil profiles from several places within the Dhaka region were used further for training, testing and validation purposes. Appendix-B shows the lithology, or soil structure, of the various locations. It should be noted that the differences within a soil layer (for example, coarse or fine-grained sand) are not depicted, making this an overview of the soil structure. This also includes the equivalent soil profile and Static Load Test data sets that are attached in the Appendix-B and Appendix-C and offer a written record of the samples. This makes it possible to characterize soil strata in greater detail.

## **CHAPTER 4**

### **FEM ANALYSIS AND MODEL DEVELOPMENT**

#### **4.1 Introduction**

In order to analyze pile foundation and determine the ultimate load capacity, one of the key concerns is the load-settlement behavior and of the pile for which static load test is conducted. More complex analytical techniques have been created to forecast the settlement and load distribution inside a single pile since the invention of computers. In this chapter, the detailed discussion will be made on soil model selection, calibration and detailed modeling steps of a pile subjected to static load. Here, the simulation of load settlement behavior of bored pile will be demonstrated considering the on-field conditions using Plaxis 3D V21. Detail modeling steps are mentioned in Figure 4.1.

When it comes to geotechnical engineering, the finite element analysis of deformation, stability and water flow, Plaxis is the computer program of choice. Because of the input techniques, the improved output capabilities can provide computational results in finer detail. In this chapter, detailed calculation procedure and input parameter selection will be demonstrated.

The two parts of Plaxis 3D V21 are the input program and the output program. The input program is used to define the model and set the properties of the analysis. At the start of the input program, the user is asked for project properties. In this part, the boundaries of the model in the two horizontal directions (x and y) and the unit system used in the analyses are set.



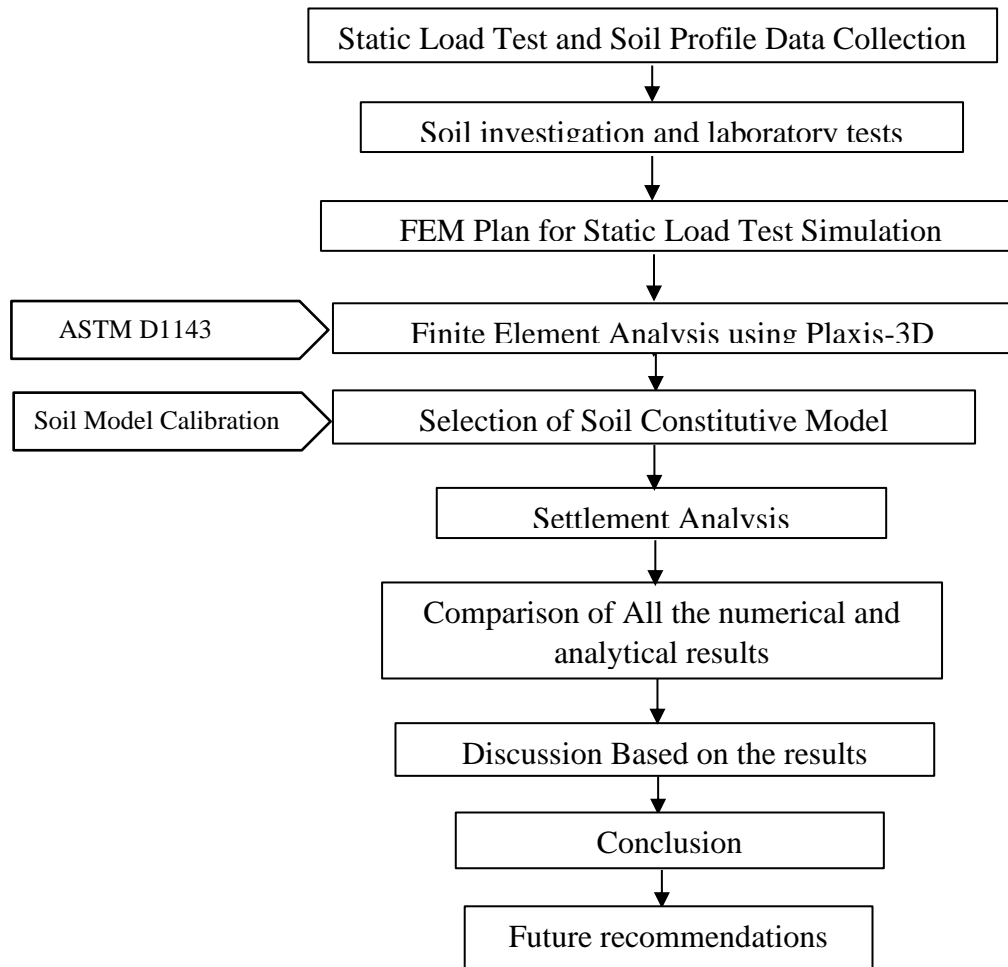


**Figure 4.1:** Flow diagram for FEM model

## 4.2 Project Information

The ongoing Hazrat Shahjalal International Airport (HSIA) Expansion Project was considered as the corresponding project location of which the static pile load test was simulated. Based on the report which presents the information, test data and results of static pile load test conducted on pilot bored pile having ID: BH40-TP-07 for terminal-3 building area of proposed Airport Expansion Project of Hazrat Shahjalal International Airport Dhaka. On behalf of Aviation Dhaka Consortium (ADC), Sinohydro Corporation Limited installed the pile and pile load testing work conducted by Geo-Drill BD. Static axial compressive pile load test started on 16th September 2020 and finished on 17th September 2020. Cyclic Load method with standard loading procedure was followed under the compliance of the contract documents and load applied by hydraulic ram against kentledge.

The pile in this case history was a reinforced concrete bored cast-in-situ pile, with a diameter of 1.2 m and a length of 44 m. It was installed adopting Hydraulic rotary

method under polymer slurry. The load vs settlement curve of the pile is shown in Figure 4.3. The reference on loading test data and borehole log sheets are attached in Appendices A and B, respectively. The soil around the pile at the test site was dominantly of silty clay with other clay and sand layers found at different depths. Percentages of the soft clay, silty clay, silty sand, fine sand were presented in Figure 4.2 as the equivalent soil stratigraphy of that particular borehole. A fine sand layer was present around at 30 m below the surface.

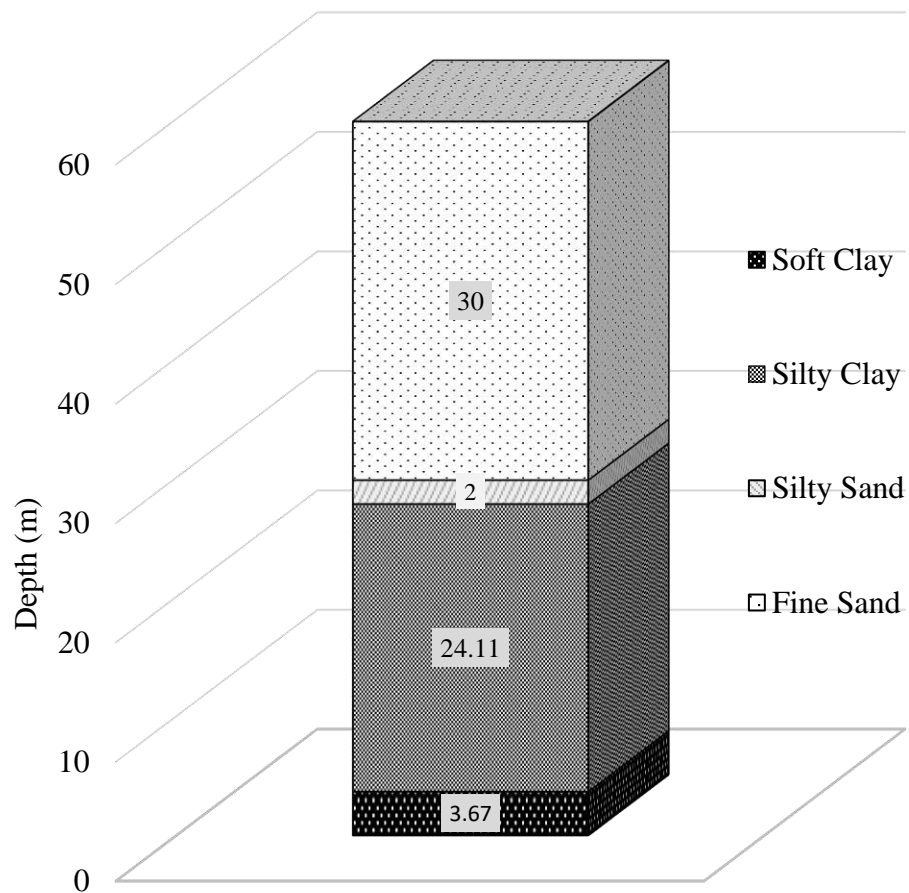


**Figure 4.2:** Equivalent soil stratigraphy at the BH40 location of pile load test

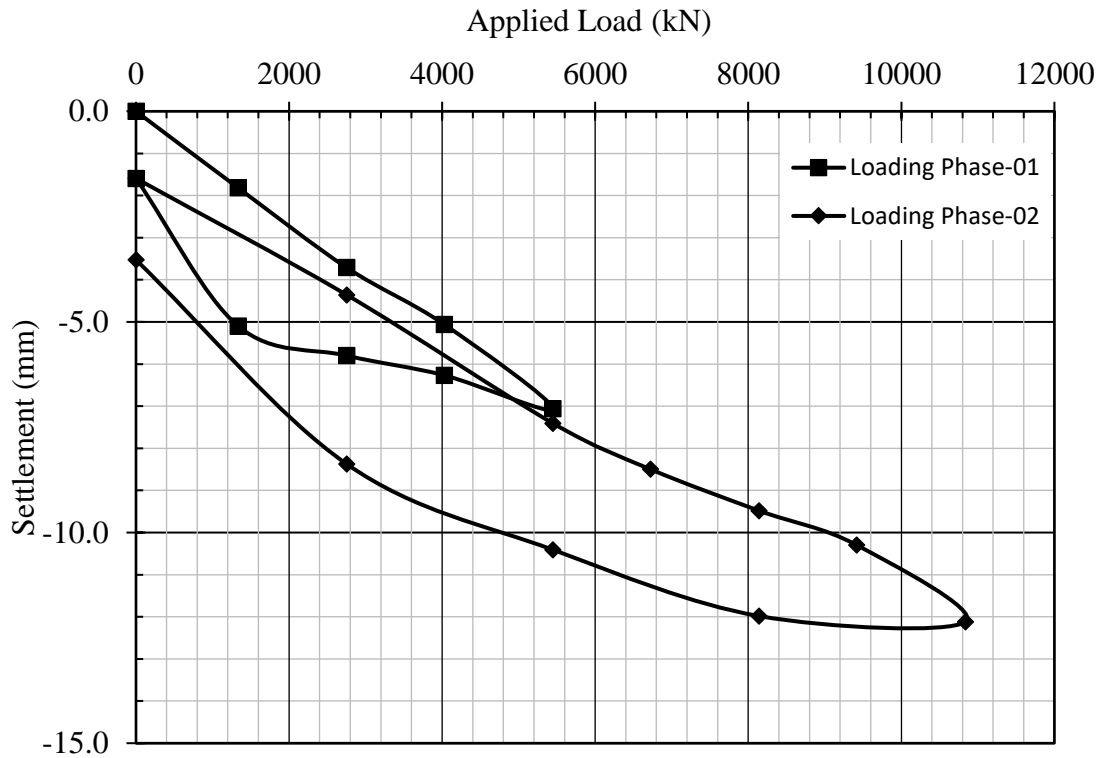


**Figure 4.3:** Load-settlement curve of TP-07

### 4.3 Constitutive Models

Constitutive models established correlations between stress and strain that detailed how materials responded to various load circumstances. Different degrees of precision are used to model the mechanical behavior of soils. Mohr-Coulomb model, Hardening Soil (HS) model, HS small model, and Soft Soil model are the four widely adopted constitutive models for numerical modeling using Plaxis 2D and Plaxis 3D. The choice of soil models is influenced by the soil profile (clay or sand), working conditions (taking into account pore pressure and loading conditions), and desired results (capacity, settlement, and stiffness).

An advanced model for replicating the behavior of many soil types, including both soft and stiff soils, is the Hardening Soil model in this instance for settlement analysis (Schanz et al., 2019; Wu et al., 2018). When soil is subjected to initial deviatoric stress, its stiffness decreases and irreversible plastic strains appear at the same time. The observed relationship between the axial strain and the deviatoric stress in the exceptional case of a drained triaxial test can be well approximated by a hyperbola. The well-known hyperbolic model (Likitlersuang et al., 2013) utilizes a relationship previously proposed by (Kondner, 1963). But the Hardening Soil model vastly

outperforms the hyperbolic and other available models (Wu et al., 2018) for the following reasons:

- (i) Substituting the theory of plasticity for the theory of elasticity.
- (ii) Taking into account the dilatancy of the soil and adding a yield cap.
- (iii) The model has a few fundamental features, including:
  - (a) Stress dependent stiffness according to a power law: Input parameter  $m$
  - (b) Plastic straining due to primary deviatoric loading: Input parameter  $E_{50}^{ref}$
  - (c) Plastic straining due to primary compression: Input parameter  $E_{oed}^{ref}$
  - (d) Elastic unloading / reloading: Input parameters  $E_{ur}^{ref}$ ,  $\nu_{ur}$
  - (e) Failure according to the Mohr-Coulomb failure criterion: Parameters cohesion  $c$ , angle of friction  $\phi$  and shearing angle  $\psi$

#### **4.4 Parameters for Numerical Modeling**

An overview of the soil behavior of this site is essential for further calibration. In this section, an interpretation of soil stiffness properties is provided base on the soil report. Also, the mechanical properties of soil layer are summarized in Table 4.2. As we have selected the Hardening soil model, being an advanced constitutive model, it needs to be calibrated. When considering the undrained calculations, there are two types of undrained behavior in Plaxis-3D, which are Undrained (A) and Undrained (B). Finite element analysis employing the Hardening Soil model in Plaxis has been proven to successfully simulate five field-scale experiments of soil-geosynthetic composites (Wu et al., 2018). The Turner-Fairbank Highway Research Center of the Federal Highway Administration provided a stable environment for the tests (J. T. Wu et al., 2013). This technical remark uses the angular gravelly soil utilized in the studies as an illustration. Figure 4.4 shows the stress-strain and volume change relationships used to determine the model parameters for the Hardening Soil model. These relationships were obtained through consolidated drained triaxial tests. These Hardening soil model parameters are discussed shortly in the following Table 4.1.

**Table 4.1:** Soil model parameters and laboratory tests needed for determination of parameters for the Hardening Soil model (modified after Plaxis 2002)

| Parameters                                     | Description and test needed to determine the parameter  |
|--|---|
| Secant stiffness, $E_{50}^{ref}$               | Secant stiffness to describe plastic straining due to primary deviatoric loading at a selected reference pressure Test needed to determine the parameter: Drained triaxial compression tests  |
| Oedometer stiffness, $E_{oed}^{ref}$           | Oedometer stiffness to describe plastic straining due to primary compression at a selected reference pressure needed to determine the parameter: Primary loading in oedometer tests (default value suggested by Plaxis: $E_{oed}^{ref} \approx E_{50}^{ref}$ )  |
| Unloading /reloading stiffness, $E_{ur}^{ref}$ | Unloading/reloading Stiffness describes elastic unloading/reloading behavior at a selected reference pressure Test needed to determine the parameter: Unloading/reloading in triaxial compression tests (default value suggested by Plaxis: $E_{ur}^{ref} \approx 3E_{50}^{ref}$ )                            |
| Elastic Poisson's ratio, $\nu_{ur}$            | Poisson's ratio is a property that describes the volume change of a material in a direction perpendicular to the application of a load. Test needed to determine the parameter: Unloading/reloading in triaxial compression tests (default: $\nu_{ur}=0.2$ )  |
| Cohesion, $c$                                  | Test needed to determine the parameter: Drained triaxial compression tests loaded to failure  |
| Angle of friction, $\phi$                      | Test needed to determine the parameter: Drained triaxial compression tests loaded to failure  |
| Shearing angle, $\psi$                         | Test needed to determine the parameter: Drained triaxial compression tests with measurement of volume change.   |
| Power of a power law, $m$                      | Power of a power law used to describe the level of stress dependency of soil stiffness Test needed to determine the parameter: Typical range: $0.5 \leq m \leq 1$ ; default value suggested by Plaxis: $m = 0.5$ ( $m = 1$ for logarithmic stress dependency (as in soft clay); $m = 0.5$ in sands and silts) |
| Reference pressure, $p^{ref}$                  | No test is required to determine this parameter. Default value of $P^{ref}$ is considered 100 kPa.  |
| Failure ratio, $R_f$                           | Default value of $R_f$ is considered 0.9  |

#### 4.4.1 Soil Stiffness Parameters

To simulate the plastic behavior of soil, the plastic soil stiffness parameters  $E_{50}^{ref}$  and  $E_{ur}^{ref}$  were used. Generally, soil loading conditions are appropriate for the secant modulus at 50% strength and that is why abbreviated as  $E_{50}^{ref}$ . Hence, in Figure 4.4, the slope at 50% strength was referred to be  $E_{50}^{ref}$ .

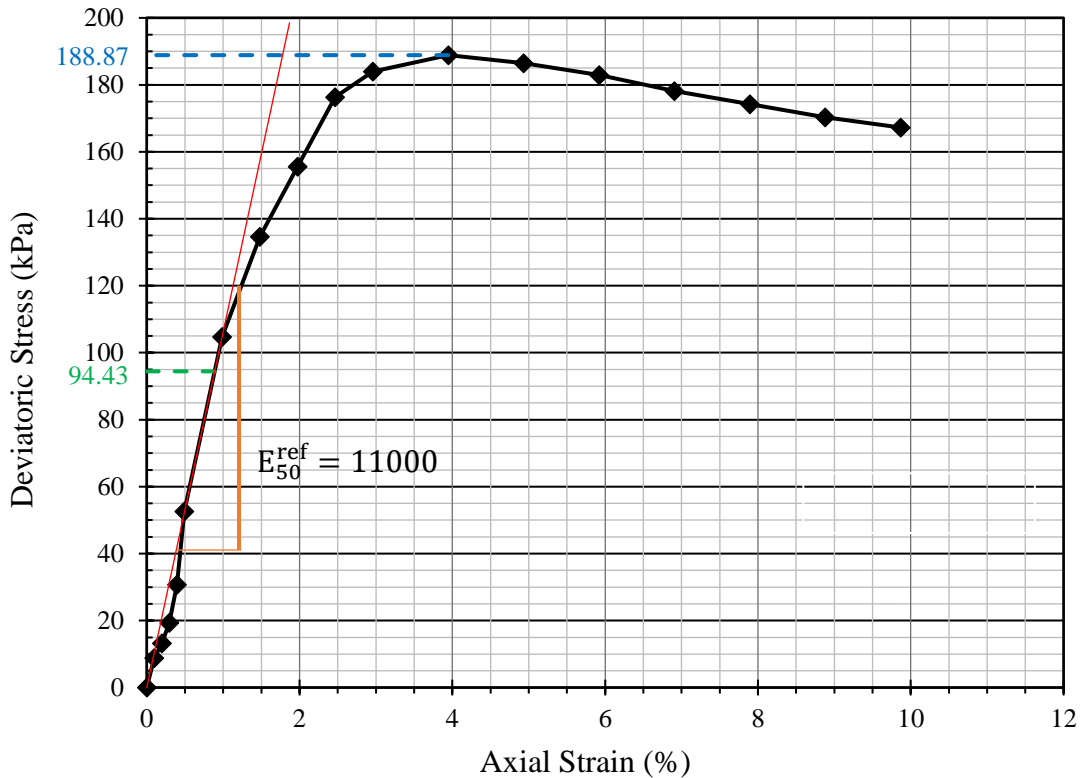


**Figure 4.4:**  $E_{50}^{ref}$  determination from the Deviatoric Stress vs. Strain diagram

#### 4.4.2 Shear Strength Parameters

Shear strength parameters, namely, angle of internal friction ( $\varphi$ ) and cohesion ( $c$ ) are generally determined from drained triaxial tests. Also, another common practice is from the direct shear test result that are taken from samples obtained from shallow depth. But for deeper layers, where laboratory test results are not available, correlation method provided by Bowles (1996) were used. Shioi and Fukui (1982) Japanese standard, has been used to determining angle of internal friction. For dominant silty clay layer of our selected site, we have conducted drained triaxial test and determined the strength parameters demonstrated from Figure 4.4. For other soil layers, respective soil

investigation reports collected from the project office, other guidelines (Uddin, 2015; Islam et al., 2013) and correlations were used to determine the required soil parameters mentioned in Table 4.2.

**Table 4.2:** Input parameters for FEM model development

| Soil Type<br>Parameters                | Unit               | Soft Clay          | Silty Clay | Silty Sand         | Fine Sand          |
|--|--------------------|--------------------|------------|--------------------|--------------------|
| Dry Unit Weight, $\gamma_d$            | kN/ m <sup>3</sup> | 15.5               | 16.5       | 17                 | 17                 |
| Moist Unit Weight, $\gamma_{sat}$      | kN/ m <sup>3</sup> | 16                 | 17         | 18                 | 18                 |
| Triaxial Stiffness, $E_{50}^{ref}$     | kN/m <sup>2</sup>  | 8000               | 11000      | 15000              | 30000              |
| Oedometer Stiffness, $E_{oed}^{ref}$   | kN/m <sup>2</sup>  | 8000               | 11000      | 15000              | 30000              |
| Un/reloading Stiffness, $E_{ur}^{ref}$ | kN/m <sup>2</sup>  | 24000              | 33000      | 45000              | 90000              |
| Frictional angle, $\phi^\circ$         | -                  | 5                  | 23         | 30                 | 33                 |
| Cohesion, $c$                          | kN/m <sup>2</sup>  | 18                 | 18         | 1                  | 1                  |
| Sources                                | -                  | Islam et al., 2013 | This study | Islam et al., 2013 | Islam et al., 2013 |

#### 4.4.3 Structural Parameters of Pile

From the discussions made above, it can be understood that a major portion of the significance of this study depends on the structural parameter that was use while developing the Plaxis-3D model. In this case, the pile foundation was modeled as embedded beam elements with  $\nu = 0.2$  and  $E = 29.73$  GPa. For the RCC pile, respective diameter was considered to be 1.2 m based on the pile details report from field data collection from the consultant office of HSIA project. Table 4.3 provides a summary of the beam element properties that were used.

**Table 4.3: Structural Parameters**

| Parameters of piles      | Unit              | Value                   |
|--------------------------|-------------------|-------------------------|
| Pile Diameter, D         | m                 | 1.2                     |
| Pile Length, L           | m                 | 44                      |
| Modulus of Elasticity, E | kN/m <sup>2</sup> | 29.73 x 10 <sup>6</sup> |
| Poisson's Ratio, $\nu$   | kN/m <sup>3</sup> | 0.20                    |
| Unit Weight, $\gamma$    | kN/m <sup>3</sup> | 25                      |

#### 4.5 Calibration of Constitutive Model

As per ASTM D 4767, the CD triaxial compression test was used to measure the shear strength parameters. The undisturbed sample was also used to prepare the cylindrical specimens. For silty clay, however, effective confining stresses of 100 kPa and 200 kPa were used. The test was carried out until the specimen failed or experienced an axial strain of 11%, which ever came first. An overview of the parameters determined from the Tri-axial test is shown in Table 4.4. Using Plaxis 3D software, the values were plugged into the HS model and stress–strain curves from the CD triaxial compression tests were obtained. This was performed using the ‘Soil Test’ feature in Plaxis-3D.

**Table 4.4: Soil parameters for Hardening Soil Model calibration**

| Soil Parameters                        | Unit               | Value |
|--|--------------------|-------|
| Dry Unit Weight, $\gamma_d$            | kN/ m <sup>3</sup> | 16.5  |
| Void ratio, e                          | -                  | 0.586 |
| Triaxial Stiffness, $E_{50}^{ref}$     | kN/ m <sup>2</sup> | 11000 |
| Oedometer Stiffness, $E_{oed}^{ref}$   | kN/ m <sup>2</sup> | 11000 |
| Un/reloading Stiffness, $E_{ur}^{ref}$ | kN/ m <sup>2</sup> | 33000 |
| Frictional angle, $\varphi^\circ$      | -                  | 23    |
| Cohesion, c                            | kN/ m <sup>2</sup> | 18    |

Figure 4.5 shows the comparison of the numerical and experimental results of the CD triaxial compression test for 200 kPa confining pressure. The comparison demonstrates



that the HS model can simulate the stress and strain behavior of the collected undisturbed silty clay soil sample with a marginal fluctuation from the conducted triaxial test result.

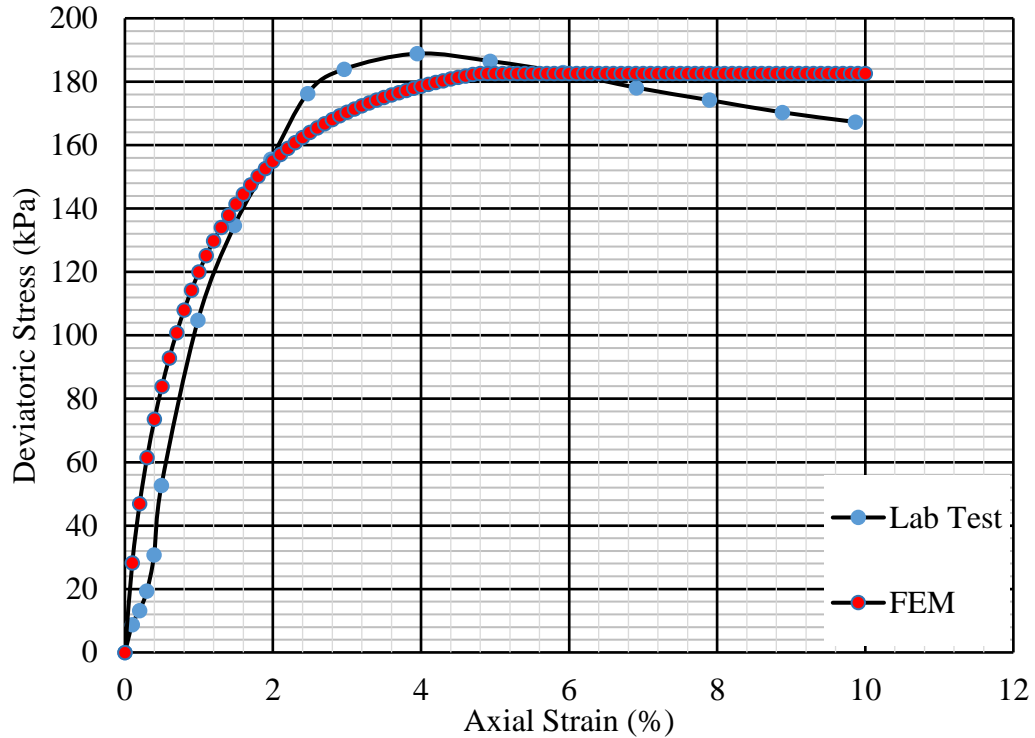


**Figure 4.5:** Calibration of HS model with the triaxial test data

## 4.6 FEM Model Development

Numerical analysis was used to study the load-settlement behavior and failure load for large diameter bored pile under vertical loads is applied at the pile head using the commercial software (Plaxis 3D-V21). The detailed procedure is mentioned in the following sections.

### 4.6.1 Model Geometry and Boundary

In PLAXIS 3D Foundation, the generation of a 3D finite element model begins with the creation of model geometry. A geometry model is a composition of bore holes and work planes. The work planes are used to define geometry lines and structures contour lines along the elevation level. The bore holes are used to define the local soil stratigraphy, ground surface level and pore pressure distribution. The boundary surfaces and their influence on the result are important factors to consider in every Plaxis model.

If the space between the expected event and the boundaries during a phase is large, the boundary influence will become small. The disadvantage with a large model is the greater number of elements required, which will lead to longer calculation times. A suitable compromise must be found for effective modeling, where the calculation time is held as short as possible without significant influences from the model boundaries.

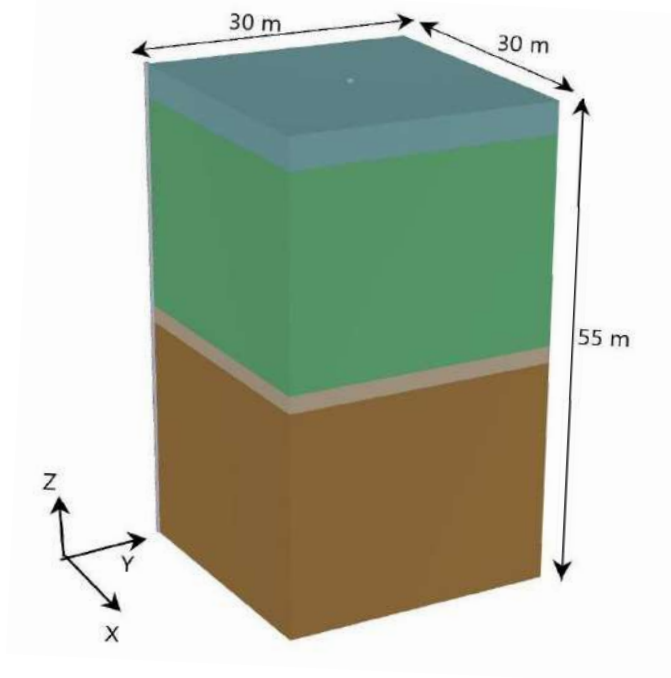


**Figure 4.6:** Geometry of FE model

To analyze the problem of pile, the full geometric model was selected, which results in a three-dimensional finite element model with three degrees of freedom at each node (i.e. x- direction, y- direction and z-direction).

The model dimensions considered for the pile load test simulation was 30 m along both X & Y direction and 55 m along Z-direction, as shown in Figure 4.6. The circular 1.2 m diameter and 44 m long pile was installed right at the mid of the geometry with as embedded beam element. An embedded beam is a structural object (such as a pile, rock bolt or grout body) composed of beam elements that can be placed in arbitrary direction in the sub-soil and that interacts with the sub-soil by means of special interface elements. The interaction may involve a skin resistance as well as a tip resistance. The skin friction and the tip resistance are determined by the relative displacement between the soil and the pile. Although an embedded beam does not occupy volume, a particular volume around the pile (elastic zone) is assumed in which plastic soil behavior is excluded. The size of this zone is based on the (equivalent) pile diameter according to

the corresponding embedded beam material data set. This makes the pile behave almost like a volume pile. However, installation effects of piles are not taken into account and the pile-soil interaction is modelled at the center rather than at the circumference.

The behavior of the elements can be prescribed with the boundary conditions. It can be manually adjusted for every surface with five different settings, free, normally fixed, horizontally fixed, vertically fixed or fully fixed. The free setting gives the surface the ability to move freely in all cartesian directions, while the fixed alternative means that they are locked in all directions. The normally fixed alternative locks the elements at the boundary from moving in the normal direction. The external boundary conditions of the model were generated according to the following rules:

- (i) The right and left edge were fixed in horizontal direction and free to move in the vertical ( $U_x = 0$ ).
- (ii) The bottom boundary was fixed in all three directions, ( $U_x = U_y = U_z = 0$ ).
- (iii) The top boundary was free in all directions
- (iv) For ground water flow drainage boundary was closed in all directions except the  $Z_{min}$ .

Here, the modern material models of the code could be used to directly enter the characteristics of the soil. For this study, the Hardening Soil material model was used. For granular soils, the undrained A type was used, and for cohesive soils, the undrained B type was used. In the model, the pile was modeled by "embedded pile elements."

#### **4.6.2 Interfaces**

Interfaces are used when modeling soil structure interaction. Interfaces will be required to simulate the finite frictional resistance between the structure such as pile and adjacent soil. It allows relative displacement and separation between the structure and soil mass. The basic property of an interface element is the associated material data set for soil and interfaces. Interface element models the interaction between a pile and the soil which is intermediate between smooth and fully rough. The roughness of the interaction is modeled by choosing a suitable value for the strength reduction factor in the interface ( $R_{inter}$ ). This factor relates the interface strength (structure surface friction and adhesion) to the soil strength (friction angle and cohesion) to model the soil-structure interaction accurately. The interface strength for these elements was assumed in the order of 1

( $R_{inter} = 1$ ) since no detailed information could be obtained and as also recommended earlier (Vilhar et al., 2018).

### 4.6.3 Mesh

Plaxis allows for a fully automatic generation of finite element mesh. The generation of the mesh is based on a robust triangulation procedure, which results in “unstructured” meshes. These meshes may look disorderly, but the numerical performance of such meshes may yield better results than for regular structure meshes. The mesh generator requires a general meshing parameter which represents the average element size,  $l_e$ , computed based on the outer geometry dimensions  $x_{max}$ ,  $x_{min}$ ,  $y_{max}$ ,  $y_{min}$ ,  $z_{max}$  and  $z_{min}$  using the following relationship:

$$l_e = \frac{r_e}{20} \sqrt{(x_{max} - x_{min})^2 + (y_{max} - y_{min})^2 + (z_{max} - z_{min})^2}$$

Where,  $r_e = 2.0$  (very coarse mesh)

= 1.5 (coarse mesh)

= 1.0 (medium mesh)

= 0.7 (fine mesh)

= 0.5 (very fine mesh)

The target element dimension or average element size, ( $l_e$ ) is based on the parameter called relative element size factor ( $r_e$ ). Regarding the element distribution, distinction is made between the above mentioned five global levels. More displacement and bending moment can be induced by a finer mesh. When the mesh goes from very fine to very coarse, the sizes can change by up to 20% (Dao, 2011). Also, the time it takes to do calculations goes up a lot as the mesh size gets smaller.

### 4.6.4 Elements

The elements contain Gauss points (stress points), where the constitutive relation is applied to define the relation between stresses and strains. In PLAXIS 3D, the basic soil elements of the 3D finite element mesh are the 10-node tetrahedral elements. The element stiffness matrix is evaluated by numerical integration using four Gauss points (Stress points) in Plaxis 3D (Figure 4.7). These elements are generated from the mesh.

The accuracy of the 10-node tetrahedral element and the compatible structural elements depend on the sufficient fineness of the mesh.

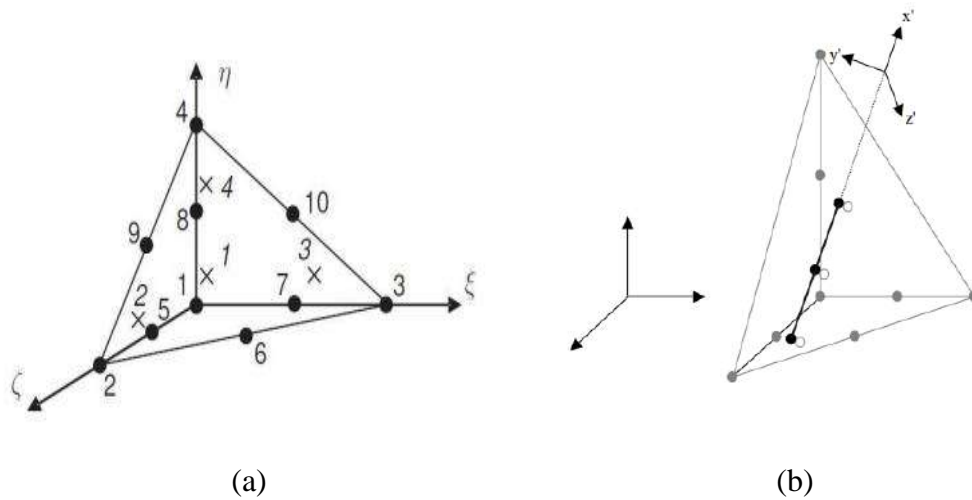


**Figure 4.7:** (a) Soil elements and (b) Beam elements (Plaxis 3D manual 2020)

Here, the pile was modeled as embedded beam. Properties and model parameters for embedded beams were entered in separate material data sets. Embedded beams can be used to model different types of slender structures that interact with the surrounding soil/rocks such as piles, ground anchors or rock bolts. A data set for embedded beams generally represents a certain type of embedded beam, including the pile/rock bolt material and geometric properties, as well as the interaction properties with the surrounding soil or rock (bearing capacity).

#### 4.6.5 Modelling Staged Construction

In Plaxis 3D, the calculation process was broken up into stages called "calculation phases". The defined calculation phases for FEM modeling are mentioned in the Table 4.5. As was already said, the first phase is always the initial conditions. After the first phase, a good number of other phases could be added based on how the construction process was planned. Starting from this phase, it's also possible to change the soil and structural parameter data and the water condition, as well as turn on or off loadings, soil clusters, and structural objects. The water table was considered at ground level in this case referring to borehole data for the selected site.

Here in Plaxis 3D, this initial phase was defined selecting the calculation type  $K_0$  procedure which indicates the initial ground condition considering the earth pressure at rest. Mainly, two calculation types that were used are:

- (i) Plastic: To apply the loading conditions.
- (ii) Consolidation: To allow the required time interval for settlement.

Next, the calculation phases are set up in a staged construction mode based on the objectives of the study once all the geometric entries have been finalized. Calculation is divided into several phases to simulate the entire load test process based on ASTM D1143, as it will be in the actual case. Table 4.4 lists the steps and required adjustments of significant features in each calculation phase and the associated settlement results. Each geometric element for each stage can be turned on or off depending on the conditions and steps of the calculation phases. The characteristics of each stage of the analysis, such as the type of calculation, the maximum time interval for each phase, and the allowable level of error, can be set independently. Analysis can be done once every stage has been set up.

#### **4.6.6 Settlement Analysis Results of Plaxis-3D**

There are several ways to monitor the outcomes of an analysis in Plaxis 3D. Curves, graphs, and tables are just a few of the numerous ways the Plaxis 3D Output program displays the outcomes of the numerical analysis. It is mostly composed of the alterations caused by stresses and deformations that are shown in a distorted mesh. An analysis of the field test condition was carried out after mesh generation and defined calculation phases with loading steps. At the very beginning the model offered a settlement of 0.69 mm for make ground condition (Figure 4.8) or earth pressure at rest. It has been observed basically due to the construction of pile and its self-weight. Hence, before applying load, the displacement was set to zero. At this no or 0% loading condition the settlement was initially monitored to be 0. Gradually, after increasing the load the settlement was monitored to be 7.9 mm (Figure 4.9) at the 100% design load of kN for the selected test pile TP-07. Figure 4.10 provides the finite element mesh for the overall model at maximum loading condition.

**Table 4.5:** Calculation Phases of Plaxis-3D for Static Load Test (SLT) simulation

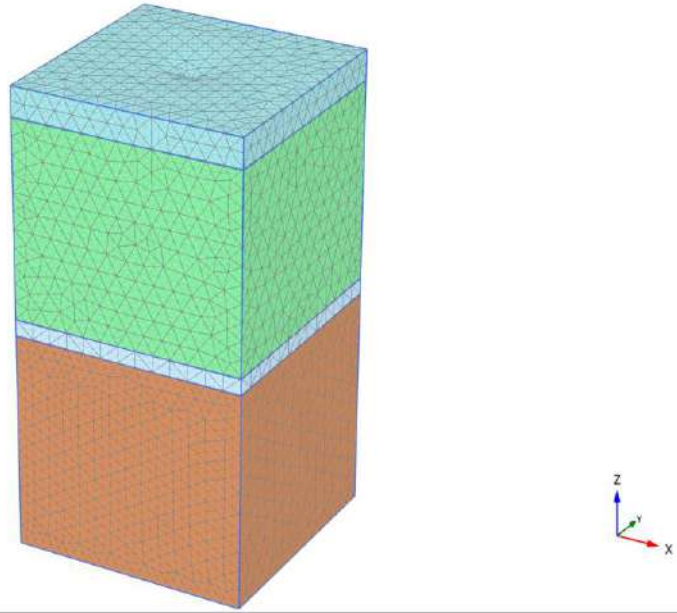
| Phases                          | Analysis type   | Elements Activated                      | Load (%) | Time (day) | Settlement (mm) |
|---------------------------------|-----------------|---|----------|------------|-----------------|
| Initial                         | K <sub>0</sub>  | (1) Surrounding soil                    | -        | -          | -               |
|                                 |                 | (2) Top/bottom boundary surface         |          |            |                 |
|                                 |                 | (3) Top/bottom prescribed displacements |          |            |                 |
| Phase 1<br>(Construction Phase) | Plastic drained | (1) Surrounding soil                    | -        | -          | 0.69            |
|                                 |                 | (2) Top/bottom boundary surface         |          |            |                 |
|                                 |                 | (3) Top/bottom prescribed displacements |          |            |                 |
|                                 |                 | (4) Embedded pile                       |          |            |                 |
| Phase 2<br>L0                   | Plastic drained | (1) Surrounding soil                    | 0        | 0          | 0               |
|                                 |                 | (2) Top/bottom boundary surface         |          |            |                 |
|                                 |                 | (3) Top/bottom prescribed displacements |          |            |                 |
|                                 |                 | (4) Embedded pile                       |          |            |                 |
| Phase 3<br>L25                  | Plastic drained | (1) Surrounding soil                    | 25       | 0          | 2.107           |
|                                 |                 | (2) Top/bottom boundary surface         |          |            |                 |
|                                 |                 | (3) Top/bottom prescribed displacements |          |            |                 |
|                                 |                 | (4) Embedded pile                       |          |            |                 |
| Phase 4                         | Consolidation   | (1) Surrounding soil                    | 25       | 0.083      | 3.465           |
|                                 |                 | (2) Top/bottom boundary surface         |          |            |                 |
|                                 |                 | (3) Top/bottom prescribed displacements |          |            |                 |
|                                 |                 | (4) Embedded pile                       |          |            |                 |
| Phase 5<br>L50                  | Plastic drained | (1) Surrounding soil                    | 50       | 0          | 4.991           |
|                                 |                 | (2) Top/bottom boundary surface         |          |            |                 |
|                                 |                 | (3) Top/bottom prescribed displacements |          |            |                 |
|                                 |                 | (4) Embedded pile                       |          |            |                 |
| Phase 6                         | Consolidation   | (1) Surrounding soil                    | 50       | 0.083      | 5.582           |
|                                 |                 | (2) Top/bottom boundary surface         |          |            |                 |
|                                 |                 | (3) Top/bottom prescribed displacements |          |            |                 |
|                                 |                 | (4) Embedded pile                       |          |            |                 |
| Phase 7<br>L75                  | Plastic drained | (1) Surrounding soil                    | 75       | 0          | 6.209           |
|                                 |                 | (2) Top/bottom boundary surface         |          |            |                 |
|                                 |                 | (3) Top/bottom prescribed displacements |          |            |                 |
|                                 |                 | (4) Embedded pile                       |          |            |                 |
| Phase 8                         | Consolidation   | (1) Surrounding soil                    | 75       | 0.083      | 6.483           |
|                                 |                 | (2) Top/bottom boundary surface         |          |            |                 |
|                                 |                 | (3) Top/bottom prescribed displacements |          |            |                 |
|                                 |                 | (4) Embedded pile                       |          |            |                 |
| Phase 9<br>L100                 | Plastic drained | (1) Surrounding soil                    | 100      | 0          | 7.254           |
|                                 |                 | (2) Top/bottom boundary surface         |          |            |                 |
|                                 |                 | (3) Top/bottom prescribed displacements |          |            |                 |
|                                 |                 | (4) Embedded pile                       |          |            |                 |

| Phases           | Analysis type   | Elements Activated                      | Load (%) | Time (day) | Settlement (mm) |
|------------------|-----------------|---|----------|------------|-----------------|
| Phase 10         | Consolidation   | (1) Surrounding soil                    | 100      | 0.25       | 7.911           |
|                  |                 | (2) Top/bottom boundary surface         |          |            |                 |
|                  |                 | (3) Top/bottom prescribed displacements |          |            |                 |
|                  |                 | (4) Embedded pile                       |          |            |                 |
| Phase 11<br>UL75 | Plastic drained | (1) Surrounding soil                    | 75       | 0          | 7.194           |
|                  |                 | (2) Top/bottom boundary surface         |          |            |                 |
|                  |                 | (3) Top/bottom prescribed displacements |          |            |                 |
|                  |                 | (4) Embedded pile                       |          |            |                 |
| Phase 12         | Consolidation   | (1) Surrounding soil                    | 75       | 0.083      | 6.965           |
|                  |                 | (2) Top/bottom boundary surface         |          |            |                 |
|                  |                 | (3) Top/bottom prescribed displacements |          |            |                 |
|                  |                 | (4) Embedded pile                       |          |            |                 |
| Phase 13<br>UL50 | Plastic drained | (1) Surrounding soil                    | 50       | 0          | 6.387           |
|                  |                 | (2) Top/bottom boundary surface         |          |            |                 |
|                  |                 | (3) Top/bottom prescribed displacements |          |            |                 |
|                  |                 | (4) Embedded pile                       |          |            |                 |
| Phase 24         | Consolidation   | (1) Surrounding soil                    | 50       | 0.083      | 6.268           |
|                  |                 | (2) Top/bottom boundary surface         |          |            |                 |
|                  |                 | (3) Top/bottom prescribed displacements |          |            |                 |
|                  |                 | (4) Embedded pile                       |          |            |                 |
| Phase 15<br>UL25 | Plastic drained | (1) Surrounding soil                    | 25       | 0          | 5.842           |
|                  |                 | (2) Top/bottom boundary surface         |          |            |                 |
|                  |                 | (3) Top/bottom prescribed displacements |          |            |                 |
|                  |                 | (4) Embedded pile                       |          |            |                 |
| Phase 16         | Consolidation   | (1) Surrounding soil                    | 25       | 0.083      | 5.509           |
|                  |                 | (2) Top/bottom boundary surface         |          |            |                 |
|                  |                 | (3) Top/bottom prescribed displacements |          |            |                 |
|                  |                 | (4) Embedded pile                       |          |            |                 |
| Phase 17<br>UL0  | Plastic drained | (1) Surrounding soil                    | 0        | 0          | 4.467           |
|                  |                 | (2) Top/bottom boundary surface         |          |            |                 |
|                  |                 | (3) Top/bottom prescribed displacements |          |            |                 |
|                  |                 | (4) Embedded pile                       |          |            |                 |
| Phase 18         | Consolidation   | (1) Surrounding soil                    | 0        | 0.083      | 4.235           |
|                  |                 | (2) Top/bottom boundary surface         |          |            |                 |
|                  |                 | (3) Top/bottom prescribed displacements |          |            |                 |
|                  |                 | (4) Embedded pile                       |          |            |                 |
| Phase 19<br>L50  | Plastic drained | (1) Surrounding soil                    | 50       | 0          | 5.766           |
|                  |                 | (2) Top/bottom boundary surface         |          |            |                 |
|                  |                 | (3) Top/bottom prescribed displacements |          |            |                 |
|                  |                 | (4) Embedded pile                       |          |            |                 |
| Phase 20         | Consolidation   | (1) Surrounding soil                    | 50       | 0.083      | 6.275           |
|                  |                 | (2) Top/bottom boundary surface         |          |            |                 |
|                  |                 | (3) Top/bottom prescribed displacements |          |            |                 |
|                  |                 | (4) Embedded pile                       |          |            |                 |



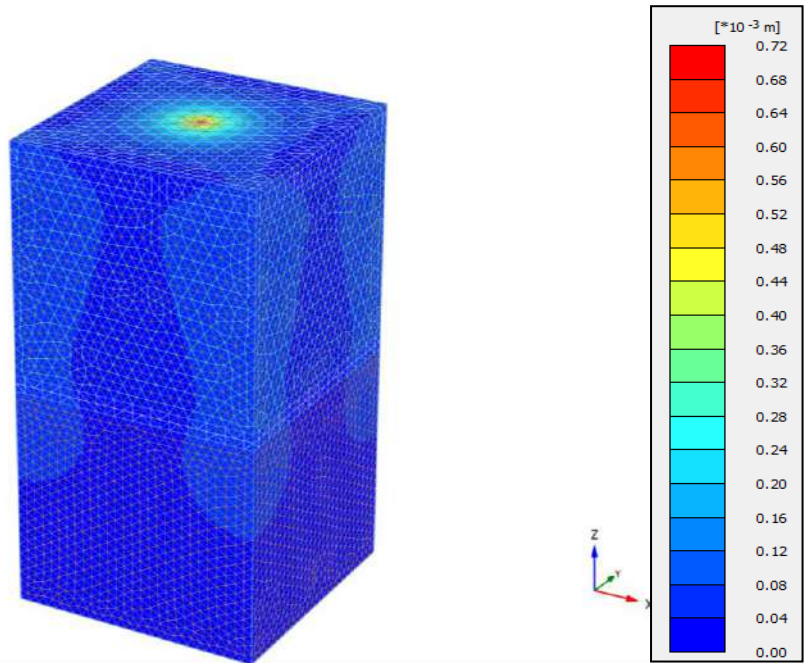
| Phases           | Analysis type   | Elements Activated                      | Load (%) | Time (day) | Settlement (mm) |
|------------------|-----------------|---|----------|------------|-----------------|
| Phase 21<br>L100 | Plastic drained | (1) Surrounding soil                    | 100      | 0          | 8.008           |
|                  |                 | (2) Top/bottom boundary surface         |          |            |                 |
|                  |                 | (3) Top/bottom prescribed displacements |          |            |                 |
|                  |                 | (4) Embedded pile                       |          |            |                 |
| Phase 22         | Consolidation   | (1) Surrounding soil                    | 100      | 0.083      | 8.405           |
|                  |                 | (2) Top/bottom boundary surface         |          |            |                 |
|                  |                 | (3) Top/bottom prescribed displacements |          |            |                 |
|                  |                 | (4) Embedded pile                       |          |            |                 |
| Phase 23<br>L125 | Plastic drained | (1) Surrounding soil                    | 125      | 0          | 9.901           |
|                  |                 | (2) Top/bottom boundary surface         |          |            |                 |
|                  |                 | (3) Top/bottom prescribed displacements |          |            |                 |
|                  |                 | (4) Embedded pile                       |          |            |                 |
| Phase 24         | Consolidation   | (1) Surrounding soil                    | 125      | 0.083      | 10.3            |
|                  |                 | (2) Top/bottom boundary surface         |          |            |                 |
|                  |                 | (3) Top/bottom prescribed displacements |          |            |                 |
|                  |                 | (4) Embedded pile                       |          |            |                 |
| Phase 25<br>L150 | Plastic drained | (1) Surrounding soil                    | 150      | 0          | 10.91           |
|                  |                 | (2) Top/bottom boundary surface         |          |            |                 |
|                  |                 | (3) Top/bottom prescribed displacements |          |            |                 |
|                  |                 | (4) Embedded pile                       |          |            |                 |
| Phase 26         | Consolidation   | (1) Surrounding soil                    | 150      | 0.083      | 11.04           |
|                  |                 | (2) Top/bottom boundary surface         |          |            |                 |
|                  |                 | (3) Top/bottom prescribed displacements |          |            |                 |
|                  |                 | (4) Embedded pile                       |          |            |                 |
| Phase 27<br>L175 | Plastic drained | (1) Surrounding soil                    | 175      | 0          | 12.76           |
|                  |                 | (2) Top/bottom boundary surface         |          |            |                 |
|                  |                 | (3) Top/bottom prescribed displacements |          |            |                 |
|                  |                 | (4) Embedded pile                       |          |            |                 |
| Phase 28         | Consolidation   | (1) Surrounding soil                    | 175      | 0.083      | 13.78           |
|                  |                 | (2) Top/bottom boundary surface         |          |            |                 |
|                  |                 | (3) Top/bottom prescribed displacements |          |            |                 |
|                  |                 | (4) Embedded pile                       |          |            |                 |
| Phase 29<br>L200 | Plastic drained | (1) Surrounding soil                    | 200      | 0          | 15.54           |
|                  |                 | (2) Top/bottom boundary surface         |          |            |                 |
|                  |                 | (3) Top/bottom prescribed displacements |          |            |                 |
|                  |                 | (4) Embedded pile                       |          |            |                 |
| Phase 30         | Consolidation   | (1) Surrounding soil                    | 200      | 0.5        | 15.65           |
|                  |                 | (2) Top/bottom boundary surface         |          |            |                 |
|                  |                 | (3) Top/bottom prescribed displacements |          |            |                 |
|                  |                 | (4) Embedded pile                       |          |            |                 |

| Phases            | Analysis type   | Elements Activated                      | Load (%) | Time (day) | Settlement (mm) |
|-------------------|-----------------|---|----------|------------|-----------------|
| Phase 31<br>UL150 | Plastic drained | (1) Surrounding soil                    | 150      | 0          | 13.37           |
|                   |                 | (2) Top/bottom boundary surface         |          |            |                 |
|                   |                 | (3) Top/bottom prescribed displacements |          |            |                 |
|                   |                 | (4) Embedded pile                       |          |            |                 |
| Phase 32          | Consolidation   | (1) Surrounding soil                    | 150      | 0.0417     | 12.90           |
|                   |                 | (2) Top/bottom boundary surface         |          |            |                 |
|                   |                 | (3) Top/bottom prescribed displacements |          |            |                 |
|                   |                 | (4) Embedded pile                       |          |            |                 |
| Phase 33<br>UL100 | Plastic drained | (1) Surrounding soil                    | 100      | 0          | 11.14           |
|                   |                 | (2) Top/bottom boundary surface         |          |            |                 |
|                   |                 | (3) Top/bottom prescribed displacements |          |            |                 |
|                   |                 | (4) Embedded pile                       |          |            |                 |
| Phase 34          | Consolidation   | (1) Surrounding soil                    | 100      | 0.0417     | 10.68           |
|                   |                 | (2) Top/bottom boundary surface         |          |            |                 |
|                   |                 | (3) Top/bottom prescribed displacements |          |            |                 |
|                   |                 | (4) Embedded pile                       |          |            |                 |
| Phase 35<br>UL50  | Plastic drained | (1) Surrounding soil                    | 50       | 0          | 9.29            |
|                   |                 | (2) Top/bottom boundary surface         |          |            |                 |
|                   |                 | (3) Top/bottom prescribed displacements |          |            |                 |
|                   |                 | (4) Embedded pile                       |          |            |                 |
| Phase 36          | Consolidation   | (1) Surrounding soil                    | 50       | 0.0417     | 8.869           |
|                   |                 | (2) Top/bottom boundary surface         |          |            |                 |
|                   |                 | (3) Top/bottom prescribed displacements |          |            |                 |
|                   |                 | (4) Embedded pile                       |          |            |                 |
| Phase 37<br>UL0   | Plastic drained | (1) Surrounding soil                    | 0        | 0          | 7.498           |
|                   |                 | (2) Top/bottom boundary surface         |          |            |                 |
|                   |                 | (3) Top/bottom prescribed displacements |          |            |                 |
|                   |                 | (4) Embedded pile                       |          |            |                 |
| Phase 38          | Consolidation   | (1) Surrounding soil                    | 0        | 0.125      | 7.042           |
|                   |                 | (2) Top/bottom boundary surface         |          |            |                 |
|                   |                 | (3) Top/bottom prescribed displacements |          |            |                 |
|                   |                 | (4) Embedded pile                       |          |            |                 |



**Deformed mesh  $|u|$  (scaled up  $2.00 \cdot 10^3$  times)**  
 Maximum value =  $0.6914 \cdot 10^{-3}$  m (at Node 24171)

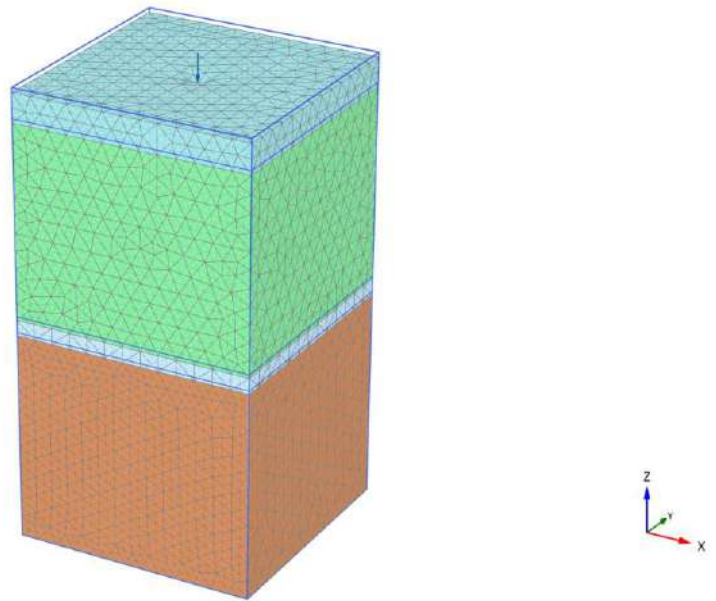
(a)



**Total displacements  $|u|$  (scaled up  $2.00 \cdot 10^3$  times)**  
 Maximum value =  $0.6914 \cdot 10^{-3}$  m (Element 1390 at Node 24171)

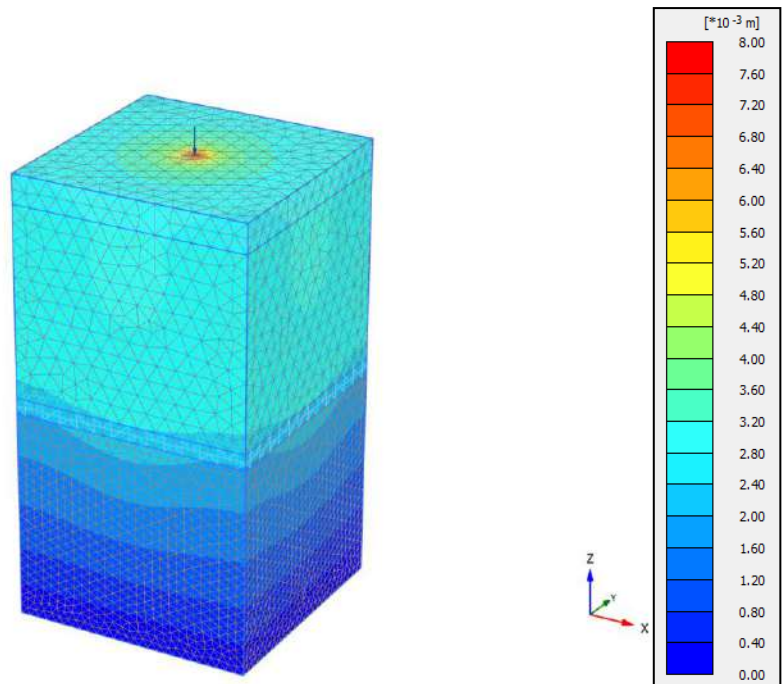
(b)

**Figure 4.8:** (a) Deformed mesh and (b) Total displacements at make ground condition



**Deformed mesh |u| (scaled up 200 times) (Time 0.5000 day)**  
 Maximum value =  $7.911 \times 10^{-3}$  m (at Node 26)

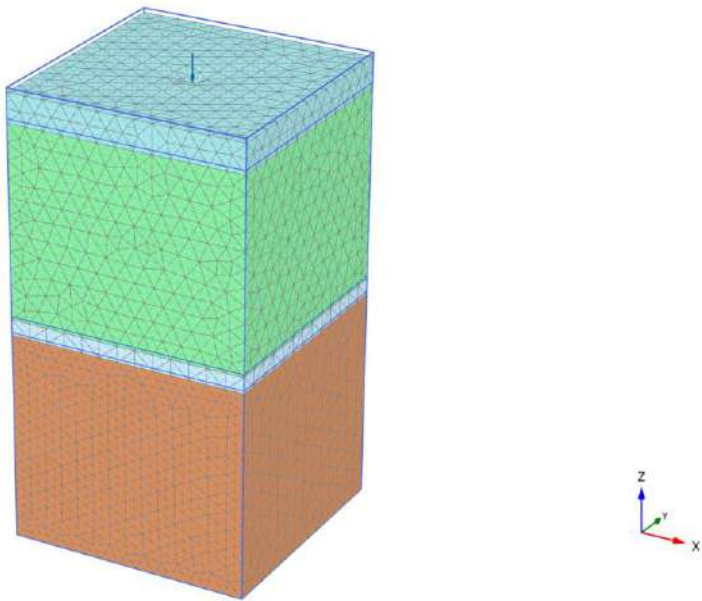
(a)



**Total displacements |u| (scaled up 200 times) (Time 0.5000 day)**  
 Maximum value =  $7.911 \times 10^{-3}$  m (Element 601 at Node 26)

(b)

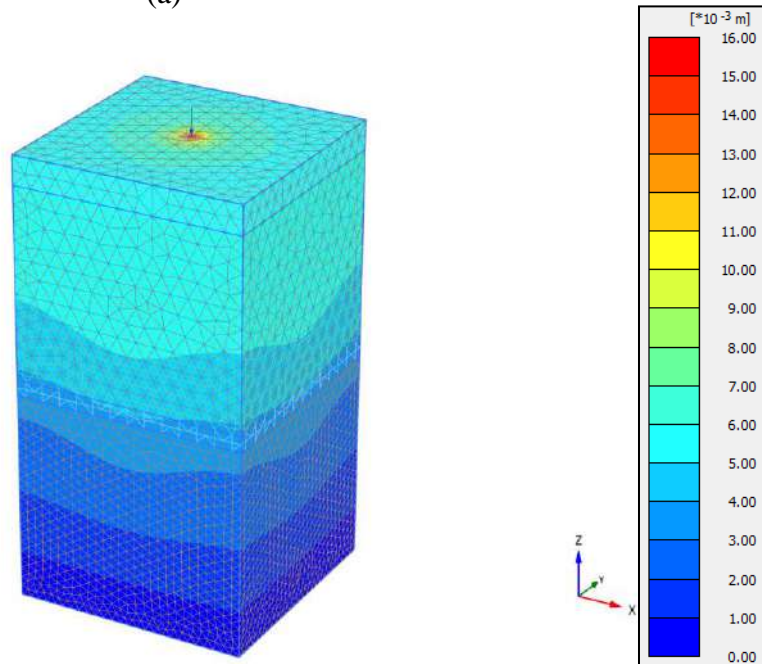
**Figure 4.9:** (a) Deformed mesh and (b) Total displacements at 100% design load



**Deformed mesh  $|u|$  (scaled up 100 times) (Time 1.750 day)**

Maximum value = 0.01554 m (at Node 26)

(a)



**Total displacements  $|u|$  (scaled up 100 times) (Time 1.750 day)**

Maximum value = 0.01554 m (Element 601 at Node 26)

(b)

**Figure 4.10:** (a) Deformed mesh and (b) Total displacements at 200% of design load

Following the ASTM D1143 guideline of loading-Unloading steps followed in the field, initially, the modeled pile was loaded till the 100% of design load with an increment of 25% for every loading steps. Next, it went through unloading phases with a decrement rate of same 25% till 0 kN of load. Then started the second loading phase with an initial increment of 50% for each steps till the 100% of design load. After reaching 100% of design load in the second loading phase, the loading rate was reduced to 25% and the pile was loaded with the maximum force of 5448 kN, which was precisely equal to 200% of the predicted capacity of the pile for the particular project that was chosen. The calculation results in an exceptional overall displacement of 15.54 mm. Further details are depicted in the deformed mesh model in Figure 4.10. Finally, the second loading phases were introduced and ultimately around 46% of the maximum settlement were noticed to get recovered with a permanent settlement of 7 mm (in Figure 4.11) at the end of the 2<sup>nd</sup> unloading phases.

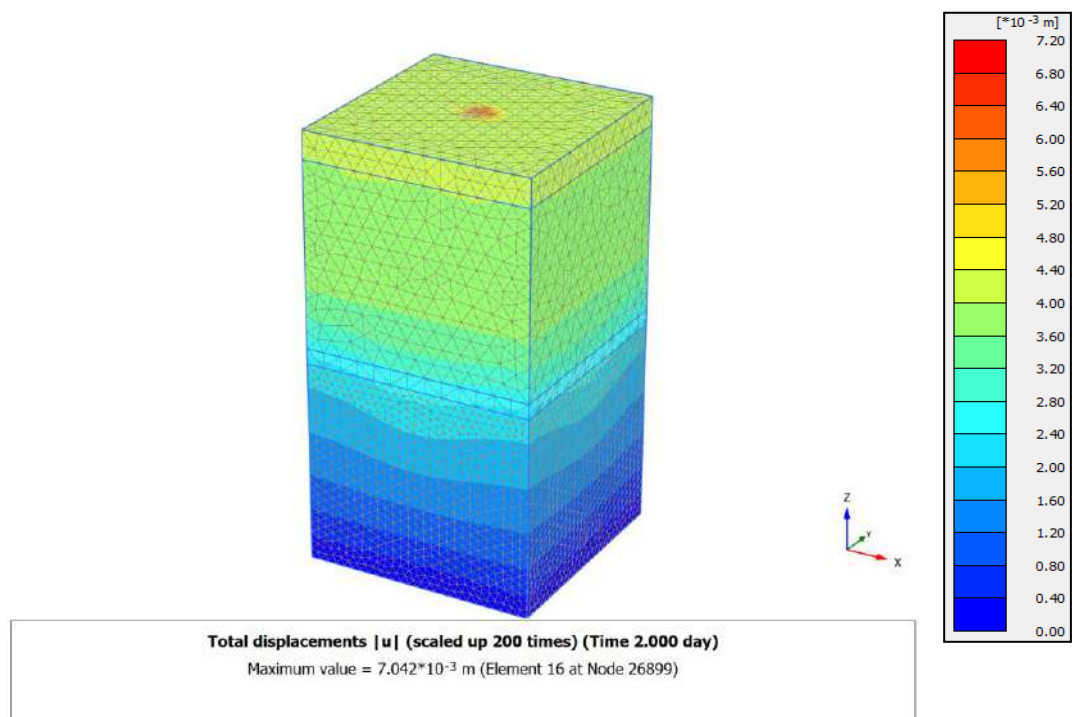
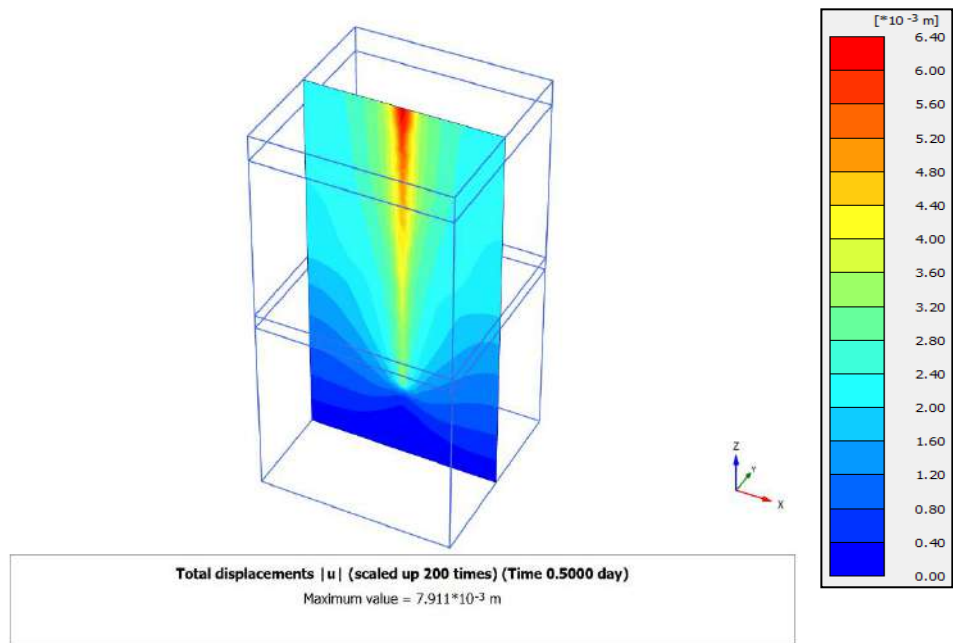


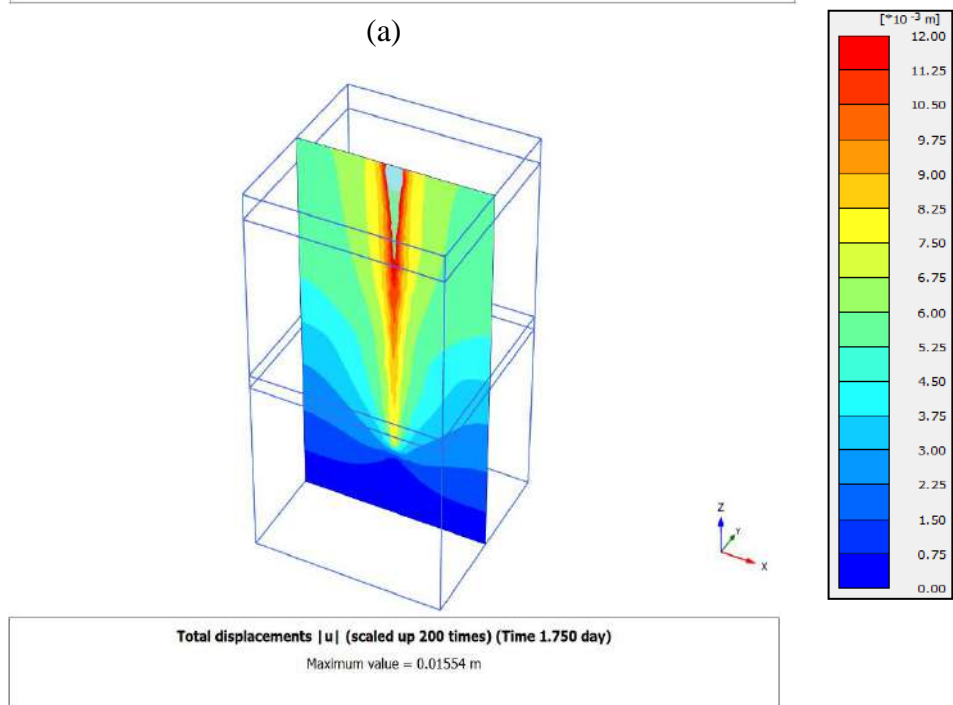
**Figure 4.11:** Total displacements at 0% of design load (end of final phase)

In order to have a Displacements and Cartesian effective stresses in the direction of movement are given from various viewpoints and cross sections are represented in the Figure 4.12 (a) and Figure 4.12 (b) respectively for 100% and 200% of the design load respectively. For further clarifications regarding soil structure (pile) interactions, however, one can also look into the details of the Displacement contours (in Figure

4.13), Stress Arrow Diagrams (Vector Diagrams) in Figure 4.14 (a) and Figure 4.14 (b) and 3D surface plots from Figure 4.15 (a) and Figure 4.15 (b).

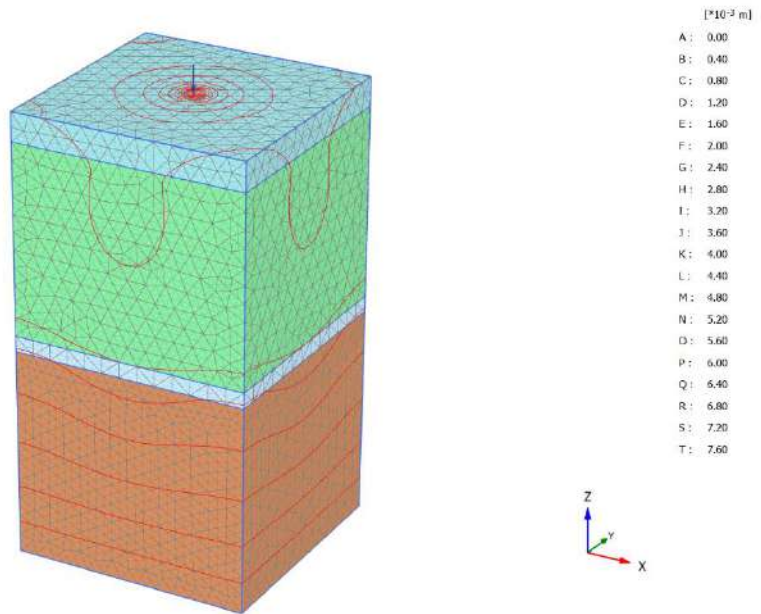


(a)



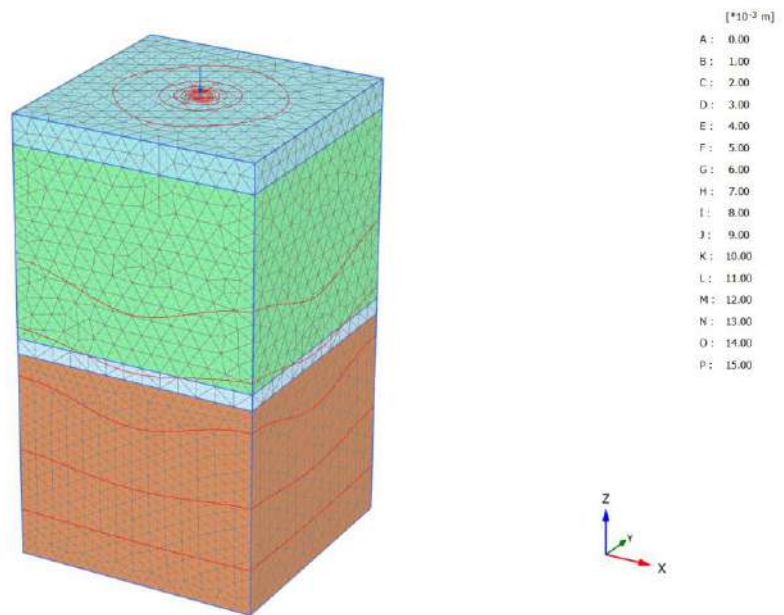
(b)

**Figure 4.12:** Total cross-sectional displacements at the pile center for (a) 100% and (b) 200% of design load



**Total displacements  $|u|$  (scaled up 200 times) (Time 0.5000 day)**  
 Maximum value =  $7.911 \cdot 10^{-3}$  m (Element 601 at Node 26)

(a)

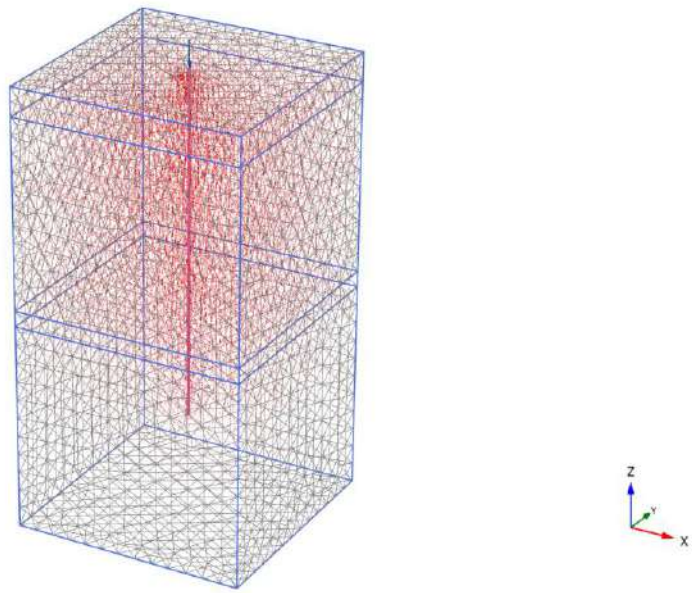


**Total displacements  $|u|$  (scaled up 100 times) (Time 1.750 day)**  
 Maximum value = 0.01554 m (Element 601 at Node 26)

(b)

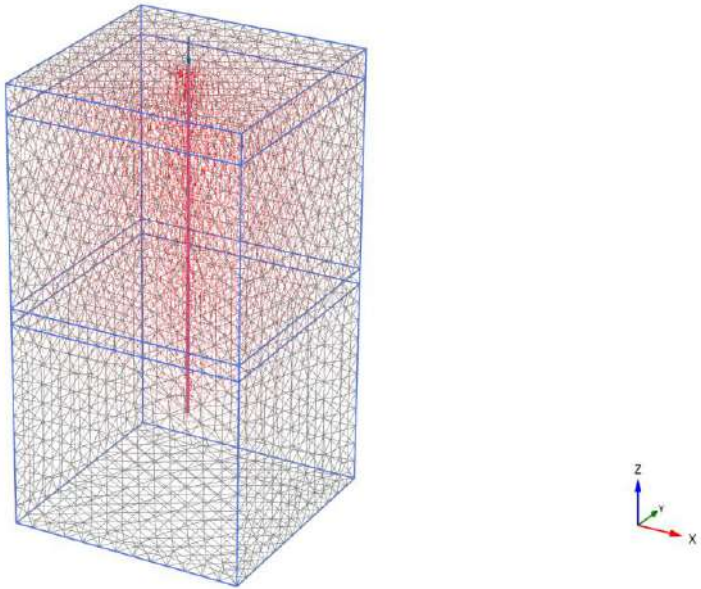
**Figure 4.13:** Displacement contours for (a) 100% and (b) 200% of design load





**Total displacements |u| (scaled up 200 times) (Time 0.5000 day)**  
 Maximum value =  $7.911 \cdot 10^{-3}$  m (Element 601 at Node 26)

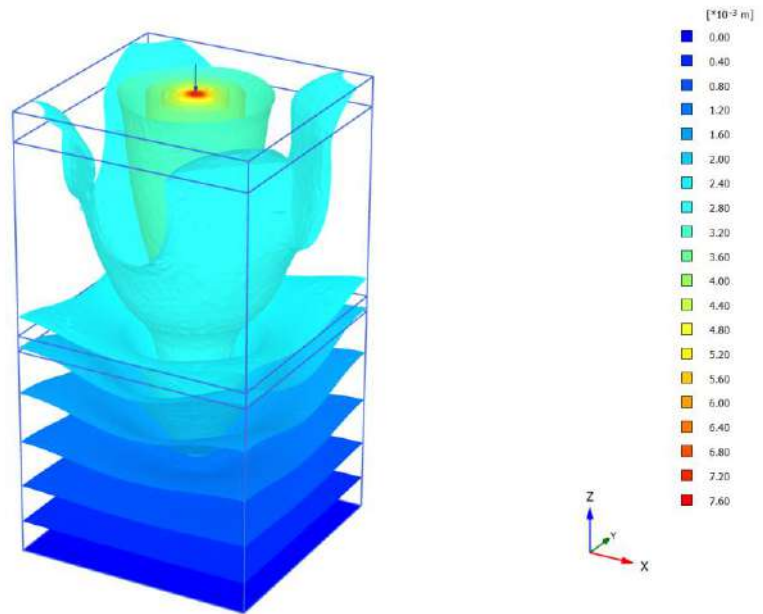
(a)



**Total displacements |u| (scaled up 100 times) (Time 1.750 day)**  
 Maximum value = 0.01554 m (Element 601 at Node 26)

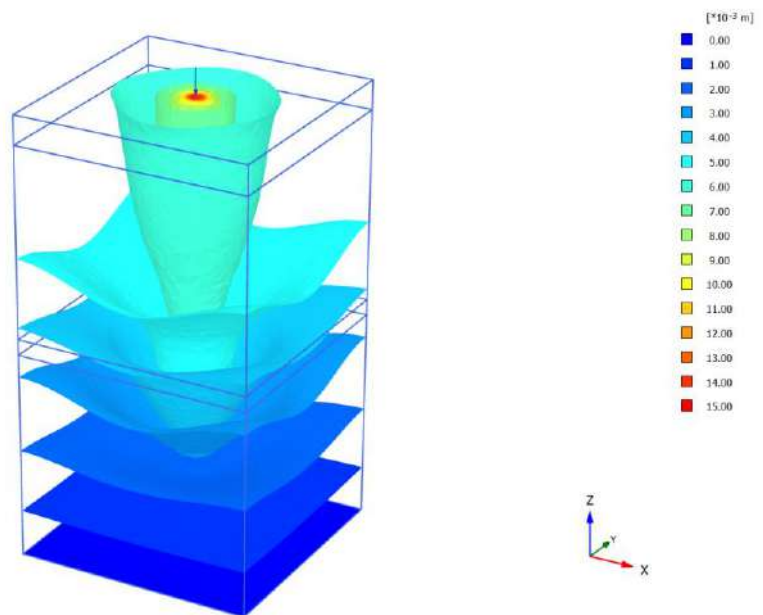
(b)

**Figure 4.14:** Stress-vector diagrams at loading condition of (a) 100% and (b) 200% design load



**Total displacements  $|u|$  (scaled up 200 times) (Time 0.5000 day)**  
 Maximum value =  $7.911 \times 10^{-3}$  m (Element 601 at Node 26)

(a)



**Total displacements  $|u|$  (scaled up 100 times) (Time 1.750 day)**  
 Maximum value = 0.01554 m (Element 601 at Node 26)

(b)

**Figure 4.15:** Surface plots at loading condition (a) 100% and (b) 200% of design load

## 4.7 Summary

Soil, structures, mesh, water levels, and construction stages are the five primary input programs that were set in the context. Boreholes are utilized to provide the soil stratigraphy. It also includes locating the water level in boreholes.

Finally, load-settlement graph of numerical analysis results using hardening soil model are compared with the respective actual pile load test. Comparison of field test and 3D analysis. From this model, the applicability and the efficiency of Plaxis-3D was clearly validated for the simulation of Static Load Test (SLT) of pile foundations.

Figure 4.16 illustrates how the FEM approach slightly over estimates the pile foundation's load-settlement behavior with the relevant material parameter sets. In fact, this result from the Plaxis 3D provides a reasonable match, adopting such an approach for the selection of soil parameter seems to be fair justification from an engineering point of view. Also, the co-efficient of determination value of 0.9162 observed in Figure 4.17 (a) and for normalized case in Figure 4.17 (b) are within a quite good range while comparing the Plaxis 3D result with insitu data. In light of this, it can be concluded that, when compared to other modeling approaches that have been looked into previous literatures, the Plaxis 3D finite element program coupled with the HS model approach efficiently forecasts the load-settlement behavior of pile foundations.

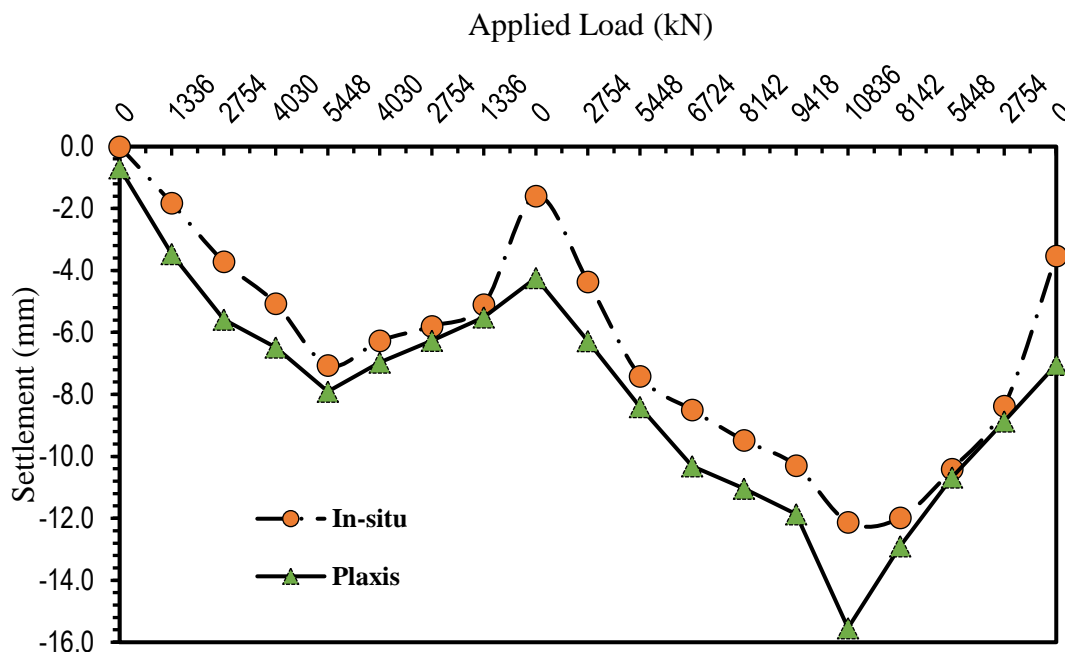
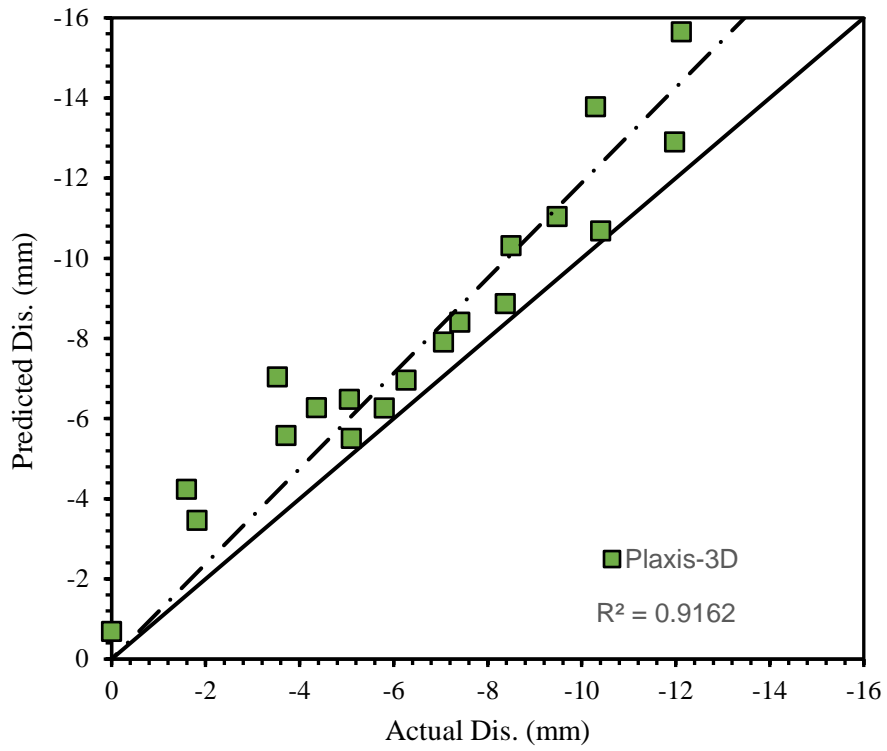
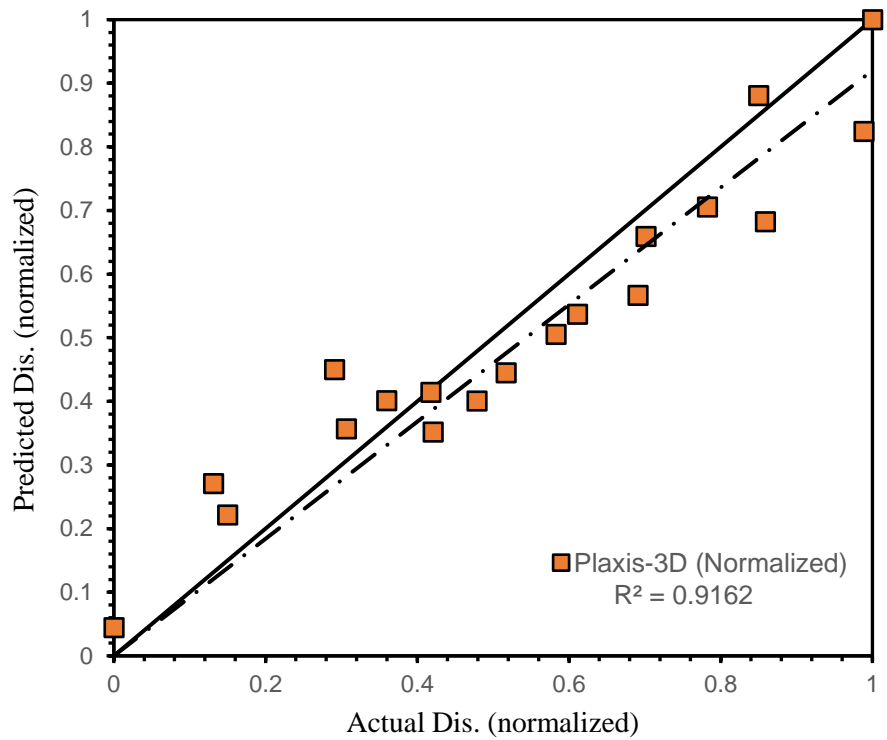


**Figure 4.16:** Comparison of Plaxis-3D result with insitu pile load test data.



(a)



(b)

**Figure 4.17:** Comparison of Plaxis 3D results with insitu pile load test data (a) General case and (b) Normalized case

## CHAPTER 5 DNN MODEL DEVELOPMENT

### 5.1 Introduction

In this chapter, the development procedures of the proposed Deep Neural network (DNN) models have been presented in details. DNN models were developed with the collected data. Google Colab notebooks which are Jupyter notebooks hosted by Colab, was used as the platform for the development of DNN models. Colab notebooks execute code on Google's cloud servers, meaning it is possible to leverage the power of Google hardware, including GPUs and TPUs, regardless of the power of your machine (Abid et al., 2019; Andrew, 2019). Description of the datasets and method of training or testing has also been discussed here.

Details of the analysis and performance comparison have been presented here. Validation was done for overall accuracy of the fitted full load-settlement curve. Model outcome for unknown characters have also been checked. At the end, performances of the models will be used to draw conclusions. Figure 5.1 demonstrates the overall methodology that has been adapted using MLP, LSTM, Bi-LSTM, CNN and TabNet architectures in this chapter. The total process has been diagrammed indicating all major steps in the models.

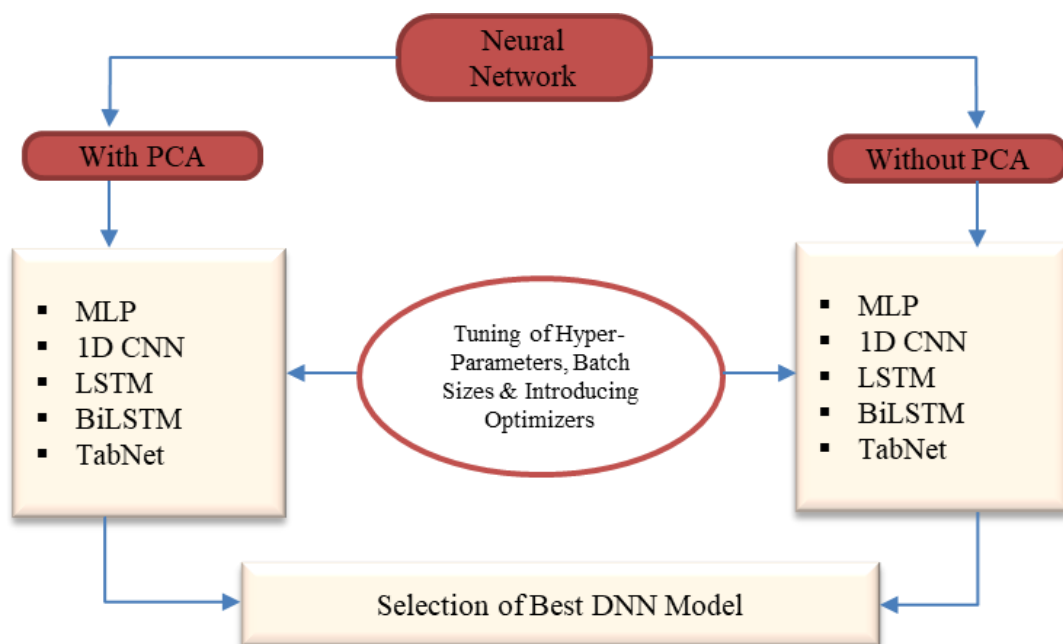


**Figure 5.1:** DNN model pipeline

## 5.2 Model inputs

Most traditional pile settlement methods include the following fundamental parameters: pile geometry, pile material properties, applied load and soil properties (All random literatures). Similarly, pile diameter ( $d$ ), embedded length ( $L_d$ ), Cross-sectional Area of pile bottom ( $A_b$ ), Surface Area of pile in contact with the soil ( $A_s$ ), Elastic Modulus in mega Pascal ( $E_s$ ), applied loads and corresponding settlement were among the input parameters for DNN model. However, there are some additional factors, such as the loading-unloading phase and load cycle considerations, layered soil profile, load test method and the depth to the water table. The depth of water table is not included in this study, as it is believed that its effect is already accounted for in the measured SPT blow count. However, the effect of these missing consideration from previous literatures were considered in this study.

The SPT ( $N$ ) throughout the embedded length of the pile is employed as a measure of soil compressibility for the purposes of this study because settlement is dependent on soil compressibility and the SPT is one of the most frequently used tests in practice for identifying the in-situ compressibility of soils. The embedded length of the pile is divided into several segments based on variability and corresponding depth of soil layers of equal thickness, with each segment being an average of  $N$  over that segment, in order to more accurately account for the variability of soil properties within different layers along the pile shaft. The average  $N$  count for each subdivision  $N_i$ , where "i" is determined using the recommendations from previous literatures (Hunt, 1984; Terzaghi and Peck, 1967). Also, the average of the SPT- $N$  value along the shaft and SPT- $N$  value where the pile bottom locates were also considered as ' $N_{avg}$ ' and ' $N_b$ ' respectively. Table 5.1 represents the layered soil profile considerations for proposed models.

**Table 5.1:** Criterion for layered soil profile considerations

| SPT- $N$ value | Soil Profile               | Annotation |
|----------------|----------------------------|------------|
| >50            | Very Dense Sand            | $N_1$      |
| 30-50          | Dense Sand                 | $N_2$      |
| 10-30          | Moderately Dense Sand/Silt | $N_3$      |
| 4-10           | Loose Sand/Medium Clay     | $N_4$      |
| <4             | Very loose Sand/Soft Clay  | $N_5$      |

Moreover, soil classification also has a greater effect on settlement (Moayedi et al., 2021; Elkateb et al., 2003; Coduto, 2001; McCarthy and McCarthy, 1977;). Hence, the percentages of Sand, Silt and Clay along the pile embedded length and toe were also within the list of input parameters for the proposed DNN models.

### **5.3 Data Preprocessing**

Preparation of raw data in a manner that the network can accept is a typical first step in the deep learning workflow. Preprocessing the collected data in order to fit the models was the first major issue. The shortage of data due to unavailability of large number of full-scale pile load test on same location was the most difficult challenge. However, the DNN models require a large amount of data to be able to fully capture the relationship. The raw data collected from field Static Load Test (SLT), pile geometry, materials and relevant soil profiles need to be pre-processed first to make it compatible with the deep neural network. This pre-processing stage consists of different operations. Each of them is described in detail below.

#### **5.3.1 Data Cleaning**

In total 712 Pile load-settlement data points, corresponding geometry, material properties and soil profile were used from 42 full load test data sets for training and testing purposes. As part of data preprocessing, data cleaning is done to clean the data by filling in missing values, smoothing out noisy data and outlier's removal.

- (i) **Missing Values:** The issues of missing values for a set or subset can be solved by ignoring those tuples when the data set is large in number. This can also be handled by filling the values by means of predicting the missing values using regression, arithmetic mean or other numerical tools.
- (ii) **Noisy Data:** It means getting rid of a random error or variation in an attribute that has been considered. It can be done with methods like Binning, Clustering, and so on. Binning is a way to smooth out any noise in data values that have already been put in order. The data is put into buckets that are all the same size, and each bucket is dealt with on its own. The segment's mean, median, or boundary values can be used to replace all of the data in the segment. On the other hand, clustering is the process of putting together groups or clusters of data with similar values. The

values that don't fit in the cluster can be thought of as noisy data and discarded for use.

- (iii) Removing Outliers: Clearing Outliers or inconsistent data means removing the data/pairs that don't fit into the cluster.

### 5.3.2 Data Scaling or Normalization

In this method, we limit our data attribute to a certain container in order to find a link between different data points. Scaling can be done in a number of ways. To improve convergence, the input parameters must be scaled (Alvarez et al., 2012). The numbers are scaled up or down so that they fit within a certain range.

Standardization was used to scale the input data because Garca et al. (2016) and Marquardt et al. Marquardt et al. (1980) found this to be the best way to do it for machine learning models. The standardization scaler was put on the training features, and it was used to change the testing features so that there wouldn't be any data leakage while the model was being tested (Anysz et al., 2016). The following equations are used to standardize the data:

Standardization,

$$z_i = \frac{x_i - \mu}{\sigma}$$

Here, mean

$$\mu = \frac{1}{N} \sum_{i=1}^N (x_i)$$

And standard deviation

$$\sigma = \sqrt{\frac{1}{N} \sum_{i=1}^N (x_i - \mu)^2}$$

Where,  $x_i$  is the  $i^{\text{th}}$  input value to the network and  $N$  is the total number of input values.

However, normalization can be performed using other methods like: Min-max normalization or even Decimal scaling normalization. In this research the standardization scalar was put on the training features, and it was used to change the testing features so that there wouldn't be any data leakage while testing.



## **5.4 Dimensionality Reduction and Feature Selection**

Dimensionality is the number of input variables or "features" in a dataset. Dimensionality reduction is a term for methods that cut down on the number of variables in a dataset (Murphy, 2018; Witten and Frank, 2002). When there are a lot of input features, the performance of machine learning algorithms may degrade. The curse of dimensionality is the idea that adding more features to a predictive modeling task makes it more difficult to predict. So, the trial keeps going with reducing the number of input features in order to better fit a predictive model. These methods can be used in applied machine learning to make a dataset for classification or regression easier to understand (Velliangiri and Alagumuthukrishnan, 2019; Xu et al., 2019). Feature selection, linear algebra methods, projection methods, and autoencoders are all ways to reduce the number of dimensions (Zebari et al., 2020; Huang et al., 2019; Thangavel and Pethalakshmi, 2009). In this research, "Feature Selection" method was introduced to reduce the dimension of input features. Initially, all the input features were annotated according to Table 5.2. Models were trained and tested selecting different batches of considered features.

## **5.5 Model Training and Validation**

In order to develop the DNN models, 80% of the data sets (34 pile-load test data sets) were used for training and rest 20% were used for testing and validation purposes. After completion of the training of each model, testing and validations were performed to assess the model performances. Models can be validated in variety of ways. The quickest and most straightforward method is to compare the accuracy of the data between the predicted result of the model and the actual result based on field data. It should be remembered that the data used for validation should be distinct from the data used for model development or calibration. Yet, as was previously noted, some studies had used the traditional goodness of fit method. Comparing the outcomes directly, it has the benefit of simplicity. While being straightforward, the method's lack of credibility contributes to its inability to anticipate long-term trends. Hence, in this research, after designing the DNN model, the next step was to compile it with a loss function and an optimizer. The loss function measured how well the model was doing, and the optimizer helped to minimize the loss function. After training, the model's performance was evaluated using the prepared validation data to ensure that the model

was not overfitted. The next step was to fine-tune the hyperparameters of the model, such as the learning rate, batch size, and number of epochs, to optimize its performance. Finally, once the model has been trained and optimized, it can be deployed to for validations and make predictions on unforeseen data.

**Table 5.2:** Feature selection and annotation

| Feature  | Annotation |
|--|------------|
| Pile diameter, $d$                                   | F1         |
| Area of pile bottom, $A_b$                           | F2         |
| Surface Area of pile in contact with the soil, $A_s$ | F3         |
| Load, $P$  | F4         |
| Pile length, $L_d$                                   | F5         |
| Elastic Modulus in mega Pascal, $E_s$                | F6         |
| Length-Diameter ratio, $L_d/D$                       | F7         |
| Dense Sand, $N_1$                                    | F8         |
| Corresponding Depth of Dense Sand, $L_1$             | F9         |
| Medium Dense, $N_2$                                  | F10        |
| Corresponding Depth of Medium Dense Sand, $L_1$      | F11        |
| Loose sand/Silt, $N_3$                               | F12        |
| Corresponding Depth of Loose sand/Silt, $L_1$        | F13        |
| Medium/Stiff Clay, $N_4$                             | F14        |
| Corresponding Depth of Medium/Stiff Clay, $L_1$      | F15        |
| Soft Clay, $N_5$                                     | F16        |
| Corresponding Depth of Soft Clay, $L_1$              | F17        |
| Average SPT, $N_{avg}$                               | F18        |
| SPT value at Pile Bottom, $N_b$                      | F19        |
| Percentage of Sand                                   | F20        |
| Percentage of Silt                                   | F21        |
| Percentage of Clay                                   | F22        |
| Loading/Unloading                                    | F23        |
| Loading Cycle  | F24        |
| Embedded Pile Length, $L$                            | F25        |
| Percentages of Applied Design Load                   | F26        |
| Settlement   | F27        |

Validation of a Deep Neural Network (DNN) model is a crucial step in the model development process. It involves evaluating the performance of the trained model on a separate dataset, called the validation set, that was not used during the training process. The goal of validation is to assess how well the model can generalize to new, unseen data. Here, during validation, the validation data set was used to assess the performance was measured using metrics, such as accuracy, precision, recall, or F1-score. The validation metrics are used to determine whether the model has overfitted or underfitted

to the training data. Overfitting occurs when the model has learned the training data too well and is unable to generalize to new data, while underfitting occurs when the model is too simple and cannot capture the patterns in the data. To prevent overfitting in this study, the regularization technique was used, such as dropout and weight decay, during training. Additionally, the use of an early stopping criterion based on the validation performance helped to prevent overfitting.

Both the actual and the predicted results were placed in the validation phase. The validation results can also be used to fine-tune the hyperparameters of the model, such as the learning rate, batch size, and number of epochs, to optimize its performance. Once the model has been validated and optimized, it was then deployed to make predictions on new, unseen data.

## 5.6 Performance Evaluation of the Models

Among various performance evaluation parameters, Root Mean Squared Error (RMSE) is the mostly used error measurement parameter and it has the benefit of drawing more attention to large errors than to minor ones (Hecht-Nielsen, 1989). RMSE is a common metric used to evaluate the performance of regression models. It measures the difference between the actual and predicted values of a model and is expressed in the same units as the target variable. The RMSE value represents the standard deviation of the residuals, where the residual is the difference between the actual and predicted values. The smaller the RMSE value, the better the model fits the data and the more accurate the predictions.

Here, the RMSE was calculated by first finding the difference between the actual and predicted values for each data point and then squaring these differences. The squared differences were then averaged over all data points and the square root of this average was taken to arrive at the RMSE value. Here,

$$\text{MSE} = \frac{1}{N} \sum_{i=1}^N (y_i - \hat{y}_i)^2$$
$$\text{RMSE} = \sqrt{\frac{1}{N} \sum_{i=1}^N (y_i - \hat{y}_i)^2}$$

Where,

$N$  = number of data points

$y_i$  = Actual observations

$\hat{y}_i$  = Predicted observations

The RMSE has been widely used in various domains such as finance, economics, engineering, and the environment. For example, in finance, the RMSE can be used to evaluate the accuracy of stock price predictions. In engineering, the RMSE can be used to evaluate the accuracy of predictions of physical quantities such as temperature and pressure. In the environment, the RMSE can be used to evaluate the accuracy of predictions of air pollution levels. There have been numerous studies that have applied the RMSE to evaluate the performance of machine learning models. For instance, in a study (Chai and Draxler, 2014) the RMSE was used to evaluate the performance of various machine learning models for predicting energy consumption in buildings. In another study (Chen et al., 2018), the RMSE was used to evaluate the performance of various deep learning models for predicting traffic flow in transportation networks. It provides a useful measure of the difference between the actual and predicted values and allows for the comparison of different models. The RMSE is the most popular error measure; it has the advantage that large errors receive much greater attention than small errors (Chai and Draxler, 2014).

However, as noted earlier (Cherkassky et al., 2006), there are instances where the RMSE cannot ensure that the model performance is optimal; as a result, the mean absolute error, MAE, was also used. When evaluating smooth or continuous data, as is the case in the current study, the MAE minimizes the focus placed on big errors and is a desirable metric. As indicated by Cherkassky et al., (2006), there are situations when the RMSE cannot guarantee that the model performance is optimal; thus, the mean absolute error, MAE, was also used.

$$MAE = \frac{1}{N} \sum_{i=1}^N |y_i - \hat{y}_i|$$

Again,

$N$  = number of data points

$y_i$  = Actual observations

$\hat{y}_i$  = Predicted observations

The MAE eliminates the emphasis given to large errors, and is a desirable measure when the data evaluations are smooth or continuous, which is in fact the case in the

current study. In metrics comparison the MSE, RMSE and MAE values of the 5 types of models were compared to demonstrate which model had the best performance. From Table 5.3, it was observed that the architecture that was proposed using TabNet outperforms the MLP, LSTM, Bi-LSTM and CNN architecture.

Several graphs were presented to display and discuss the projected settlement behavior that were observed at each load value in the independent testing for the suggested five models. They are the average error and residual plot, actual vs. projected displacement values displayed their linear relationship and correlation. Also, graphical representation of load vs. displacement values illustrated how they differ at each loading/unloading cycle's increment and decrement.

**Table 5.3:** Performance factors of DNN models

| Model   | MSE         | RMSE        | MAE         |
|---------|-------------|-------------|-------------|
| MLP     | 22.906217   | 4.786043983 | 3.517914951 |
| LSTM    | 51.31417096 | 7.163391024 | 6.321185042 |
| Bi-LSTM | 43.78197727 | 7.163391024 | 6.321185042 |
| 1D-CNN  | 181.0845358 | 13.45676543 | 9.368135376 |
| TabNet  | 10.42549191 | 3.228853033 | 2.972474709 |

### 5.6.1 MLP Model Development

Multilayer perceptron (MLP), the first neural network employed in this research, were trained using the back propagation approach (Rumelhart et al., 1986). To train a Multi-Layer Perceptron (MLP) model for the best fit, the following steps were maintained carefully:

- (i) Data preprocessing: The input data should be cleaned, normalized, and standardized to make it suitable for the model.
- (ii) Split the data into training and testing datasets: It is common to split the data into 80/20 or 70/30 ratios. Here, 80% of the data were used for training and 20% for testing.
- (iii) Determine the number of neurons and hidden layers: The performance of the MLP model can be significantly impacted by the quantity of hidden layers and neurons. Grid search and k-fold cross-validation were two methods used to figure out how many hidden layers and neurons were best.

- (iv) Train the model: Train the MLP model using a loss function like mean squared error (MSE) or binary cross-entropy, together with an optimization technique known as “Adam”.
- (v) Evaluate the model: Assess the model using the testing dataset to determine its accuracy, precision, MSE, RMSE, MAE and residuals.
- (vi) Fine-tune the model: In order to enhance the model's performance, the hyperparameters such as: the learning rate, the number of hidden layers and neurons were modified based on the previous findings.

An input layer, an output layer and one or more intermediate layers known as hidden layers make up the majority of processing components or nodes in a typical MLP. Weighted connections connect each processing element in one layer to the processing elements in the other layers. At each processing step, the weighted inputs are added up and a threshold value (or bias) is either added or subtracted. In this research, the output of the processing element was created by passing the combined input through a nonlinear transfer function (such as a sigmoidal or tanh function). The input for the processing elements in the following layer come from the output of the previous layer's processing element. The pattern of measured input data and associated measured outputs was supplied to the network at the input layer of MLPs, when information propagation begins. Errors mentioned in Table 5.4 were calculated by comparing the network's outputs to the outputs that were from actual field data. In order to decrease the prediction error, this error was combined with a learning rule to modify the connection weights and trials were given with different batch sizes. Up to a specific stopping requirement was satisfied, the aforementioned method kept on repeating with the display of the fresh input and output data. The network got a set of weights that creates input-output mapping with the least amount of error by following the approach described above. The performance of the trained model was then confirmed using an independent validation set (TP-07) after it has been successfully completed.

**Table 5.4:** Variation of MLP model results within different batch sizes

| Batch Size | MSE        | RMSE        | MAE        |
|------------|------------|-------------|------------|
| 8          | 16.7369118 | 4.091077095 | 3.84658259 |
| 16         | 22.9062178 | 4.786043983 | 3.51791496 |
| 32         | 20.0192820 | 4.474291232 | 4.29573456 |
| 64         | 16.7369117 | 4.091077095 | 3.84658259 |

In Figure 5.2, measurements from the pile load tests were contrasted with the predicted load-settlement curves. The outcomes demonstrate that the model's performance was below average and that the projected and observed values diverge significantly. The observed value of co-efficient of determination  $R^2$  was 0.65 in this instance also justifies the comparatively lower prediction accuracy of this proposed MLP model.

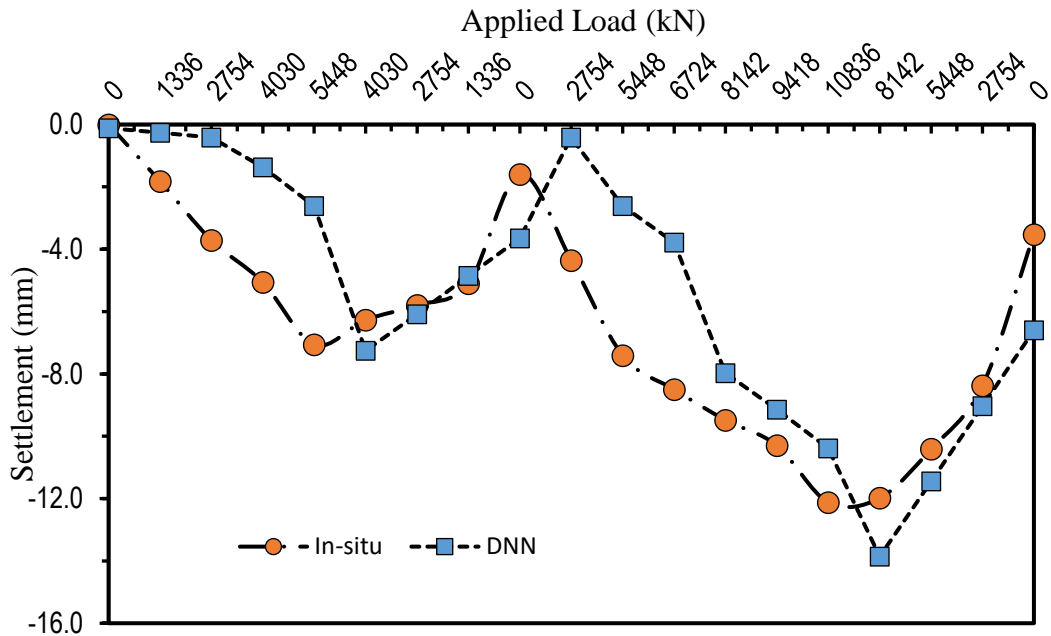
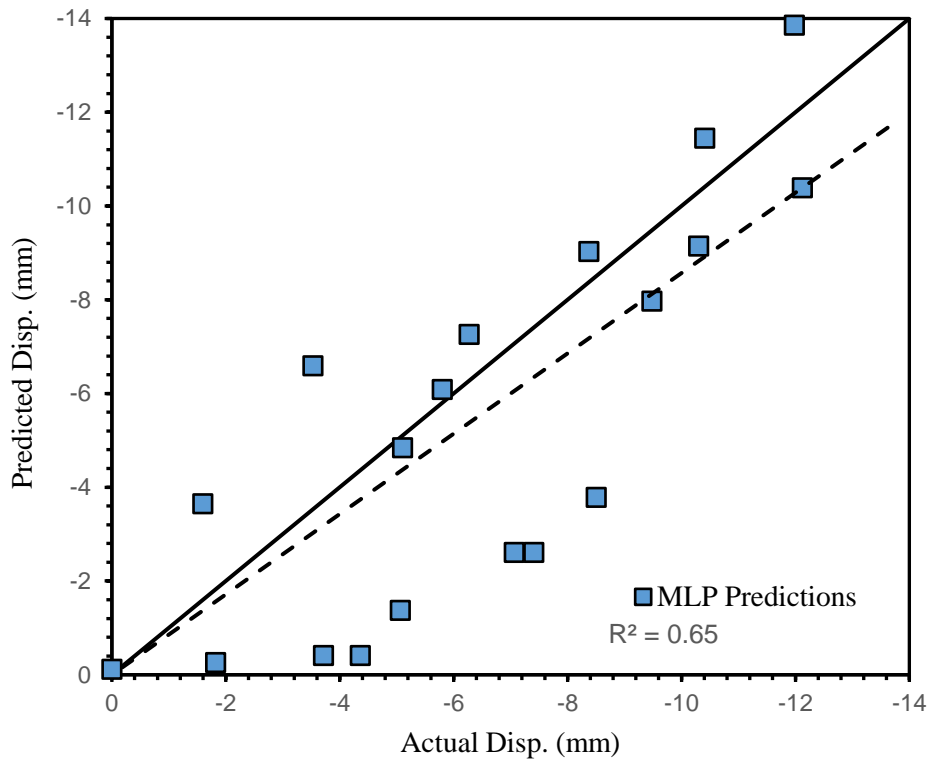


**Figure 5.2:** Performance of MLP model with respect field data



(a)

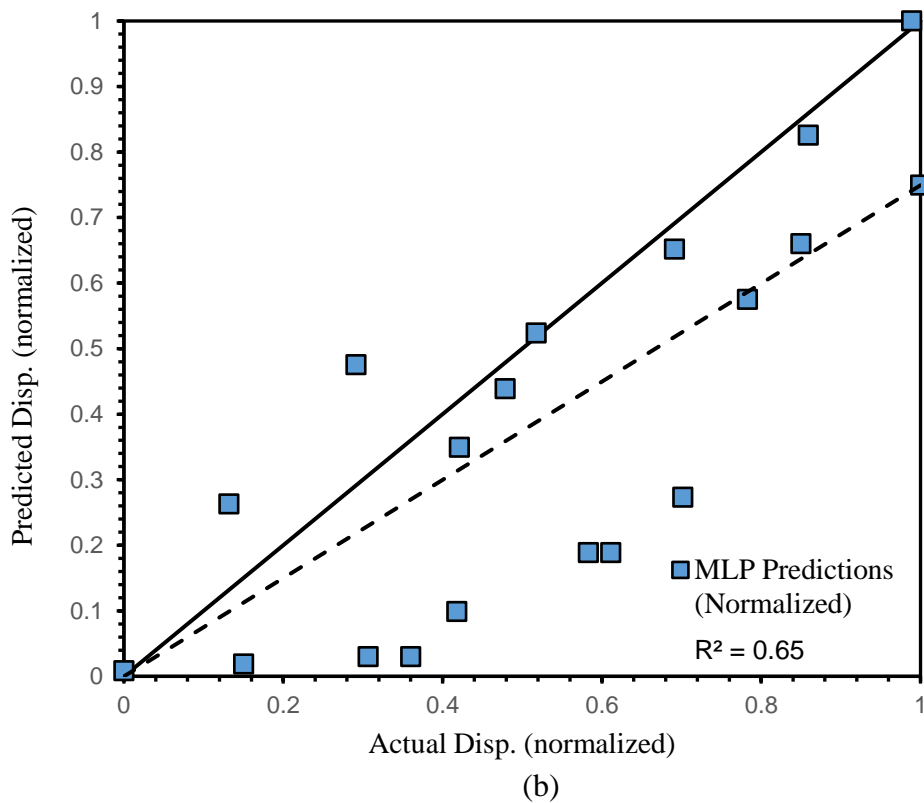


**Figure 5.3:** Regression plot for MLP model (a) Generalized and (b) Normalized

### 5.6.2 RNN Model Development

- (i) LSTM: The fundamental concept behind LSTM is that its architecture is made up of two states: a hidden state and a cell state. The output of the LSTM is stored in the hidden state and the data from the previous step is stored in the cell state. An LSTM node updates or modifies the cell state, which is managed by the forget gate, at each step.
- (ii) Bi-LSTM: As a more robust successor to the standard LSTM, the Bi-LSTM network has many advantages. Bi-LSTM employs two independent hidden layers, one for forward and one for reverse processing. Since the Bi-LSTM network can learn and use information from the past and the future simultaneously, this structure has the potential to boost the model's performance (Shen et al., 2021).

One hidden layer network in the Bi-LSTM operates in the forward direction, while the other operates in the reverse direction. The LSTM and Bi-LSTM (Graves et al., 2005) network structures in this work were used the same as shown in Figure 5.4.



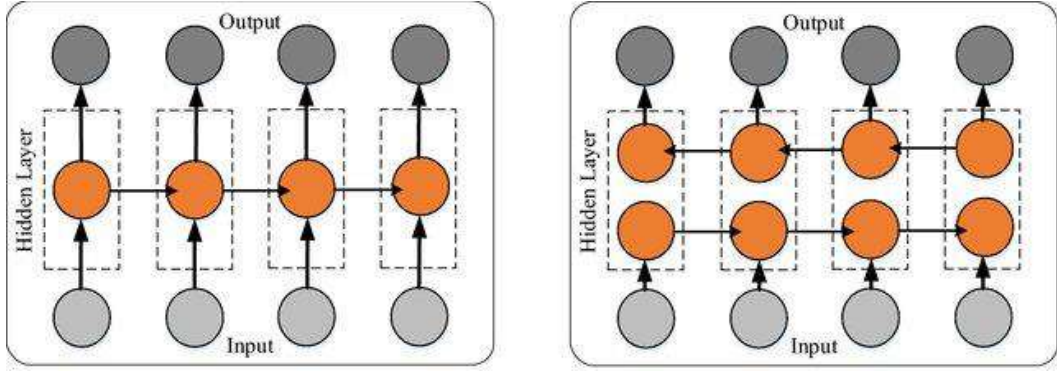


**Figure 5.4:** Adopted (a) LSTM (Hochreiter and Schmidhuber, 1997) and (b) Bi-LSTM (Graves and Schmidhuber, 1997) architectures

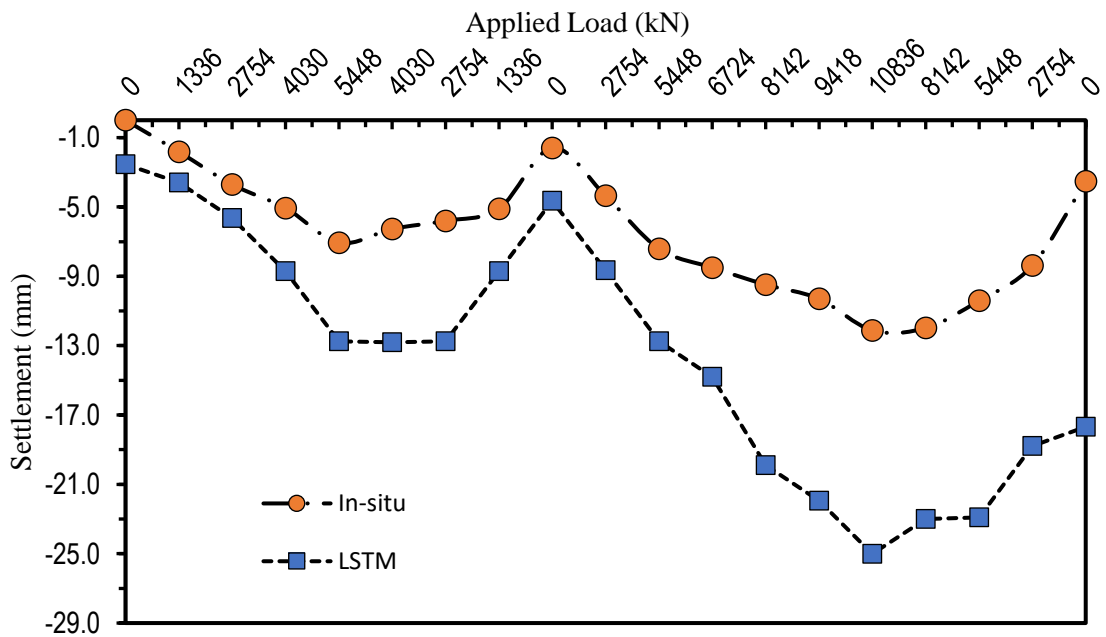
Like regular feedforward and back-propagation networks, these forward and backward propagations unfolded the concealed states at every time step (Graves et al., 2013). In this research, LSTMs and BI-LSTMs were trained using the following procedures:

- (i) Data pre-processing: Clean and format the input data, usually transforming it into sequences of fixed length.
- (ii) Model definition: Define the architecture of the RNN model using appropriate TensorFlow library.
- (iii) Hyperparameter tuning: Appropriate values for hyperparameters were chosen such as the number of hidden units, learning rate, and batch size. Initially, batch size was considered 16 in every case. With an initial learning rate of 0.01, it was chosen to employ the Adam optimizer and the SoftMax function. An L2 regularization term was added to an RNN-based model to prevent overfitting.
- (iv) Model training: Train the model on the pre-processed data using an optimizer, such as Adam or SGD, and a loss function, such as mean squared error or categorical cross-entropy.
- (v) Model evaluation: The performance of the model on a held-out validation set were evaluated using performance metrics such as MSE, RMSE and MAE. Detailed performances are mentioned in Table 5.5.

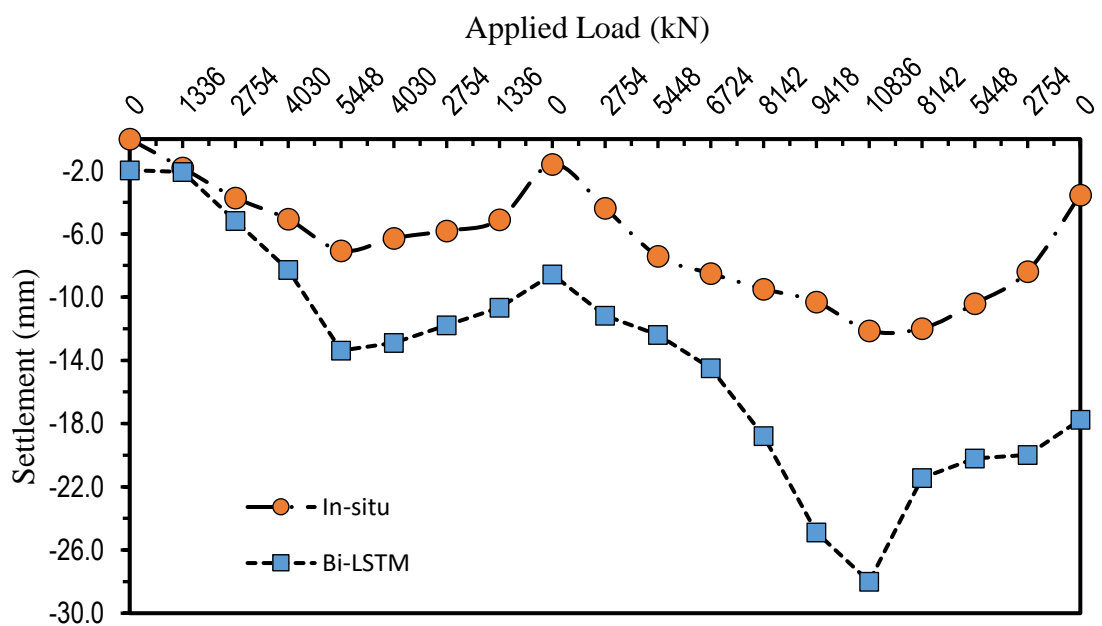
**Table 5.5:** Performances of RNN models

| Model   | MSE        | RMSE        | MAE        |
|---------|------------|-------------|------------|
| LSTM    | 51.3141709 | 7.163391023 | 6.32118504 |
| Bi-LSTM | 43.7819772 | 6.616795090 | 5.81786446 |

Figure 5.5 (a) and (b) represents the prediction results of RNN models comparing with the actual load test results. It was observed that the RNN results were significantly deviated from the actual ones. Further demonstration of the RNN model performances were represented with the coefficient of determination depicted in Figure 5.6 (a) and (b) where, the coefficient of determinations ( $R^2$ ) was noticed to be 0.843 and 0.784 for LSTM and Bi-LSTM models respectively.

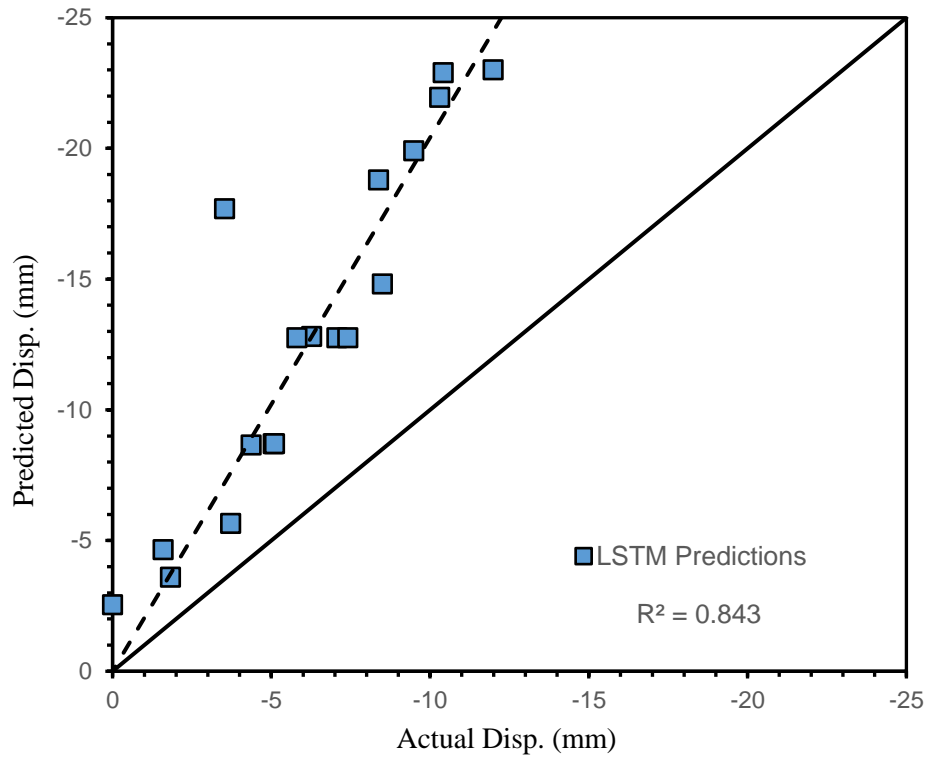


(a)

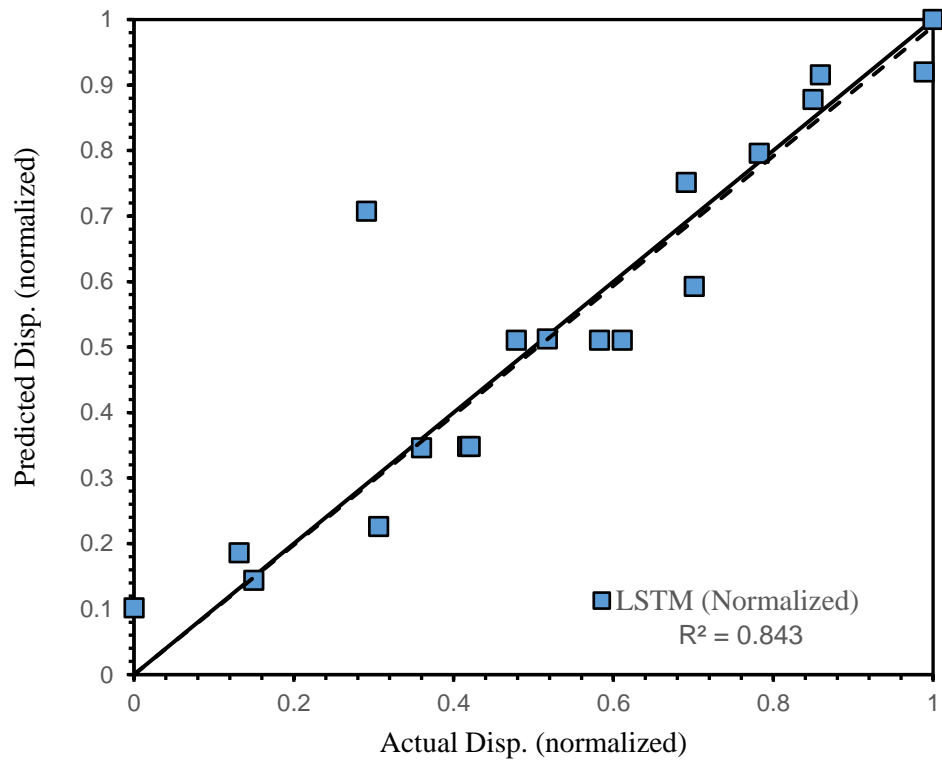


(b)

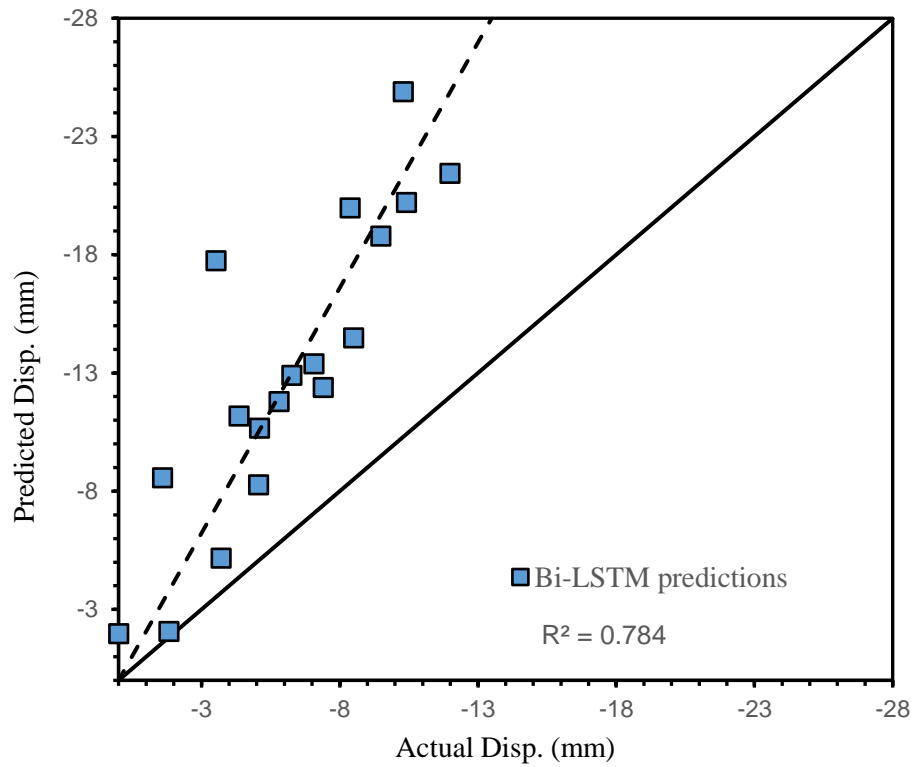
**Figure 5.5:** Prediction results of (a) LSTM model (b) Bi-LSTM model



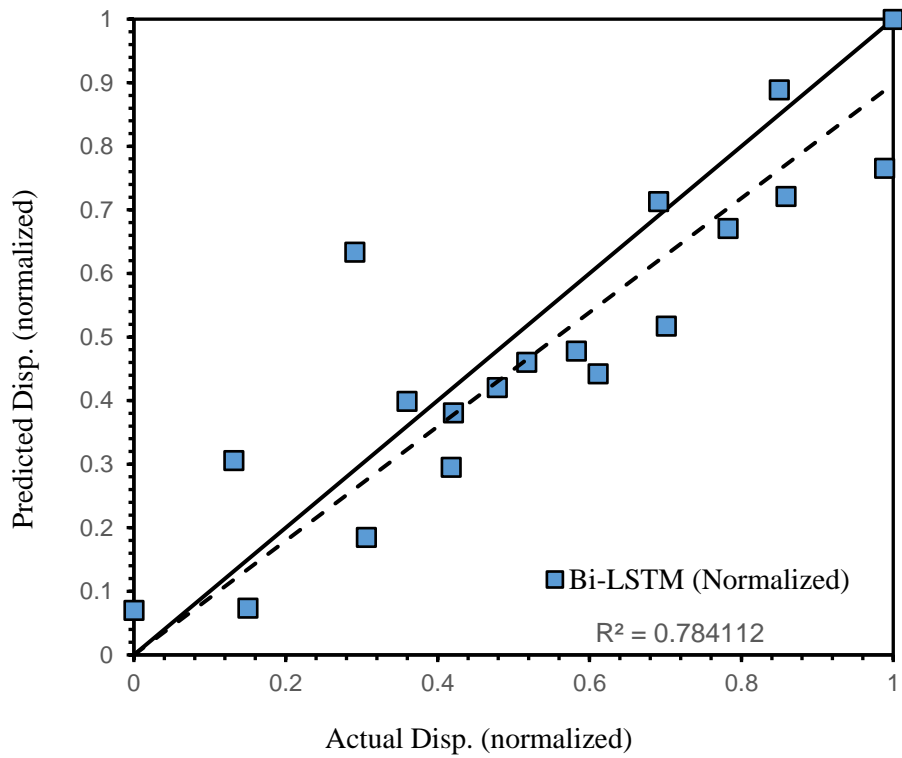
(a)



(b)



(c)



(d)

**Figure 5.6:** Performances of different RNN models (a) LSTM, (b) LSTM (Normalized), (c) Bi-LSTM and (d) Bi-LSTM (Normalized)

### 5.6.3 1D-CNN Model Development

Exploring if it is possible to get close to some important values with a machine learning (ML) model instead of doing tedious numerical simulations; an additional method that can help automate the process more effectively (Wolf et al., 2020) is the 1D Convolutional Neural Network (1D CNN). Using CNNs it is possible to optimize numerical simulations in geotechnical engineering. Hence, an attempt was made in this study. Here, 1D CNN was applied to predict pile settlements. By using one-dimensional time series data, CNN, which primarily employed two-dimensional data, used for data feature extraction and data prediction analysis (Wolf et al., 2020; Erdeljan et al., 2017). CNN has the benefit of making training simpler by requiring fewer parameters and data preprocessing. The output of a CNN corresponding to one-dimensional input data is described by equation (5.1) below.

$$s(t) = (x * w)(t) = \sum x(a)w(t - a) \dots \dots \dots (5.1)$$

where  $s(t)$  is the feature map, which is the output layer,  $w$  is the kernel map, and  $x$  is the input data. The four steps of the CNN algorithm are as follows.

- (i) In the first phase, a weighted function used as input data is traversed by the kernel in a certain flow, and many convolution products are produced concurrently.
- (ii) The features of the input data are recognized and output to the feature map in the second stage, where the values computed in parallel pass through the activation function.
- (iii) The pooling function in the pooling layer is utilized in the third phase to decrease the feature data found in the feature map. According to what was previously said, the CNN algorithm extracts the data's features through repetitions of the CNN and pooling layers. In order to extract the periodic and non-periodic aspects of the time-series data, this method was performed three times. As a result, the data size was substantially smaller than it had been initially.
- (iv) The data created in an array are transformed into a column vector array through the fully connected layer in the final step for the dataset collected from the CNN and pooling layers, and the features of the data are categorized and relations between the inputs and outputs are established. On the basis of this established relation, future data were forecasted.
- (v) 1D Convolutional Neural Network (1D CNN) implemented using the Keras API in Python using Google Colab. The code consists of a series of operations that are

performed on the input 'inp' to build the layers of the network. The operations include batch normalization, dropout, weight normalization, and reshaping, which are commonly used techniques for improving the training stability and accuracy of neural networks.

- (a) Batch Normalization: This layer applies batch normalization to the activations of the previous layer. Batch normalization helps to reduce the internal covariate shift and stabilize the training process, leading to faster convergence and improved accuracy. The normalization is performed across the batch dimension of 16. Also, weight normalization was applied to a dense (fully connected) layer with 128 output units. Weight normalization is a type of normalization that helps to improve the training stability of neural networks.
- (b) Dropout (0.3): This layer applies dropout regularization to the activations of the previous layer. During training, dropout randomly sets a fraction of the activations to zero, helping to prevent overfitting. The argument 0.3 specifies the fraction of activations that will be set to zero.
- (c) Reshape ((8, 16)): This layer reshapes the activations of the previous layer into a tensor with shape (8, 16). The Reshape layer is used to change the shape of the activation tensor, which is useful when transitioning from dense layers to convolutional layers in a 1D CNN.

A full pile load test was analyzed using the suggested CNN model (i.e. with batch size 16) and the predictions were compared with the measured settlements in order to offer a further evaluation of the 1D-CNN model's accuracy. It should be emphasized that none of the information related to this pile load tests had been sent to the CNN model and was therefore only being used for supplemental validation.

The projected load-settlement curves were compared to the measurements from the pile load tests in Figure 5.7. The results showed that the model's performance was below average. It had a high error level and the predicted values were highly deviated from the measured ones presented in Table 5.6. Here,  $R^2$  is equal to 0.77, RMSE is 13.457 and MAE is 9.368. The maximum predicted settlement was observed to be 36.58 mm which is very high compared to the actual settlement obtained during in-situ load test results.

**Table 5.6:** Performance on settlement behavior prediction with 1D-CNN model

| Model  | MSE     | RMSE   | MAE   |
|--------|---------|--------|-------|
| 1D-CNN | 181.085 | 13.457 | 9.368 |

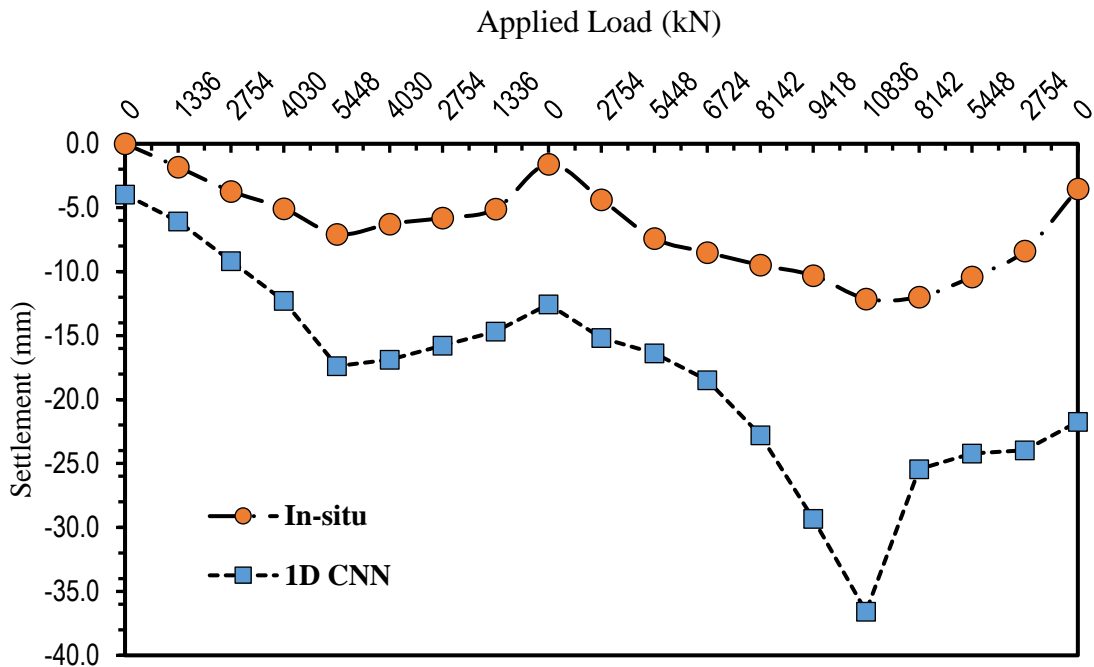
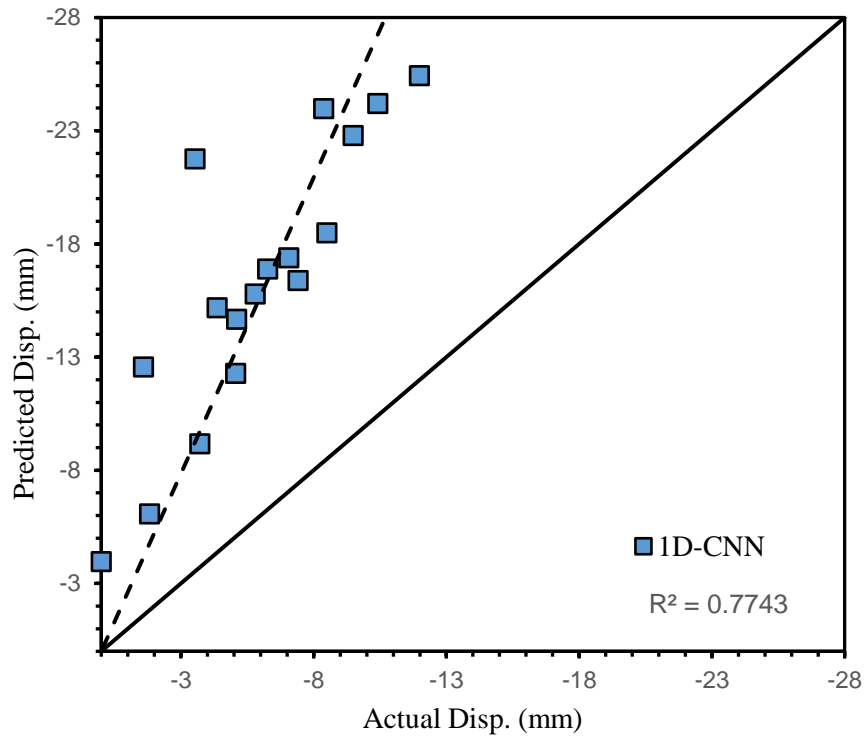
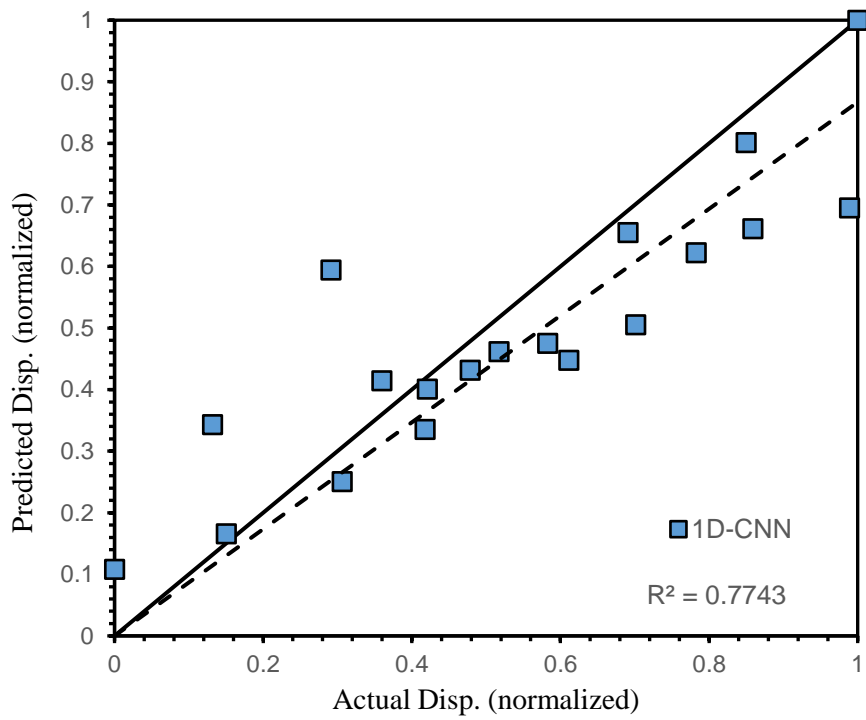


**Figure 5.7:** 1D-CNN prediction results

Even in case of 1D-CNN model it was observed that the statistical tests such as coefficient of determination ( $R^2$ ) from Figure 5.8 shows very low accuracy with a value of. On the other hand, in the context of proposed 1D-Convolutional Neural Network (CNN) model, residuals were plotted as the difference between the predicted values and the actual values of settlement. Visualizing the distribution of residuals can provide insights into the performance of this model. If the residuals were randomly distributed around zero, this suggests that the model is making accurate predictions, while a systematic pattern in the residuals may indicate that the model is not capturing some important aspect of the data. From the residual plot in Figure 5.9 it was also clear that the 1D-CNN model was very insignificant in predicting the load-settlement behavior of pile.



(a)



(b)

**Figure 5.8:** Comparison between field test data and 1D-CNN prediction results  
 (a) General case and (b) Normalized case



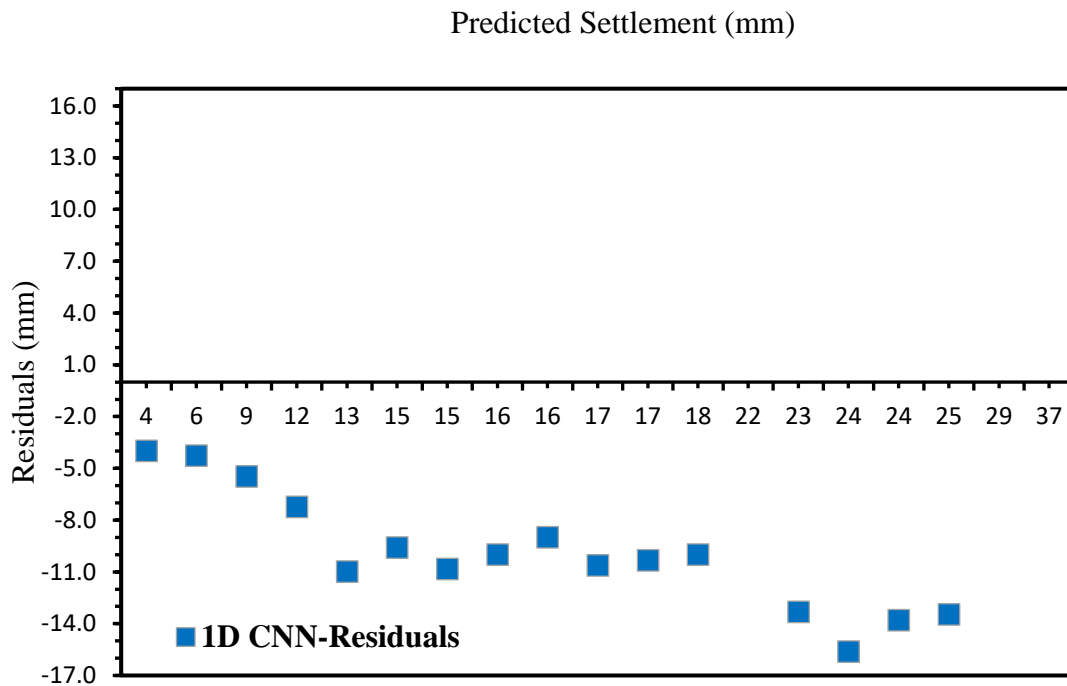


**Figure 5.9:** Residual plot for 1D-CNN prediction

#### 5.6.4 TabNet Model Development

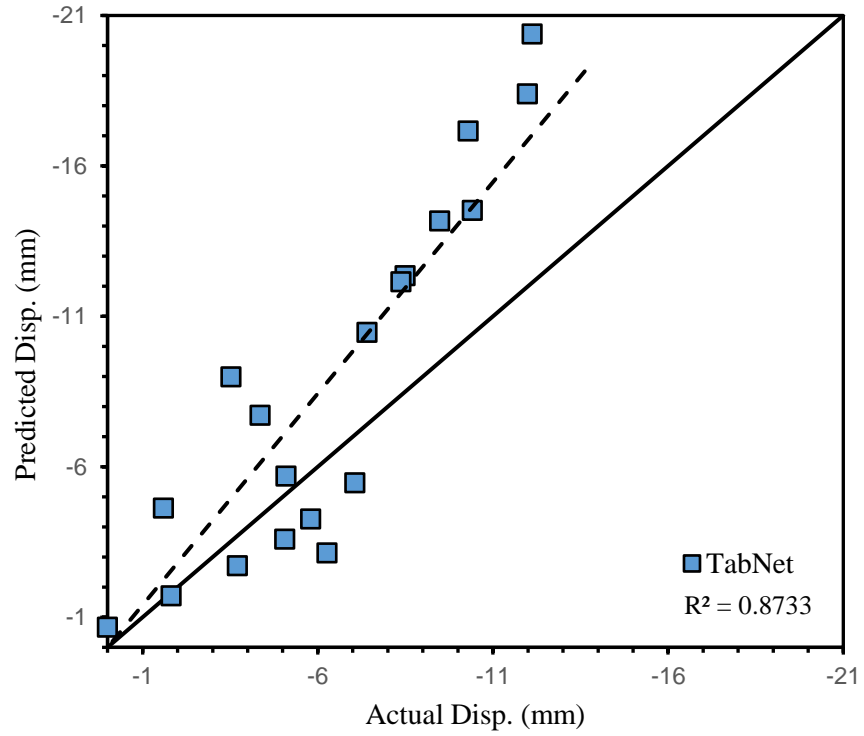
The latest addition in deep neural network which is in fact is a neural network architecture that combines the strengths of convolutional neural networks (CNNs), recurrent neural networks (RNNs), and attention mechanisms to handle structured data, such as tables and time series data. TabNet has shown promising results in a variety of tasks, such as classification, regression, and anomaly detection, and has demonstrated strong performance on benchmark datasets. The proposed TabNet model included several key features that contribute to its performance, including:

- (i) Attention mechanism: TabNet uses an attention mechanism to dynamically weight the importance of each feature in the input data. This allows the model to focus on the most important features, improving its ability to learn complex relationships in the data.
- (ii) End-to-end training: TabNet is an end-to-end model, meaning that it can be trained from raw data to predictions, without the need for preprocessing or feature engineering.
- (iii) Regularization: TabNet uses a combination of dropout, L1 and L2 regularization to reduce overfitting and improve generalization.

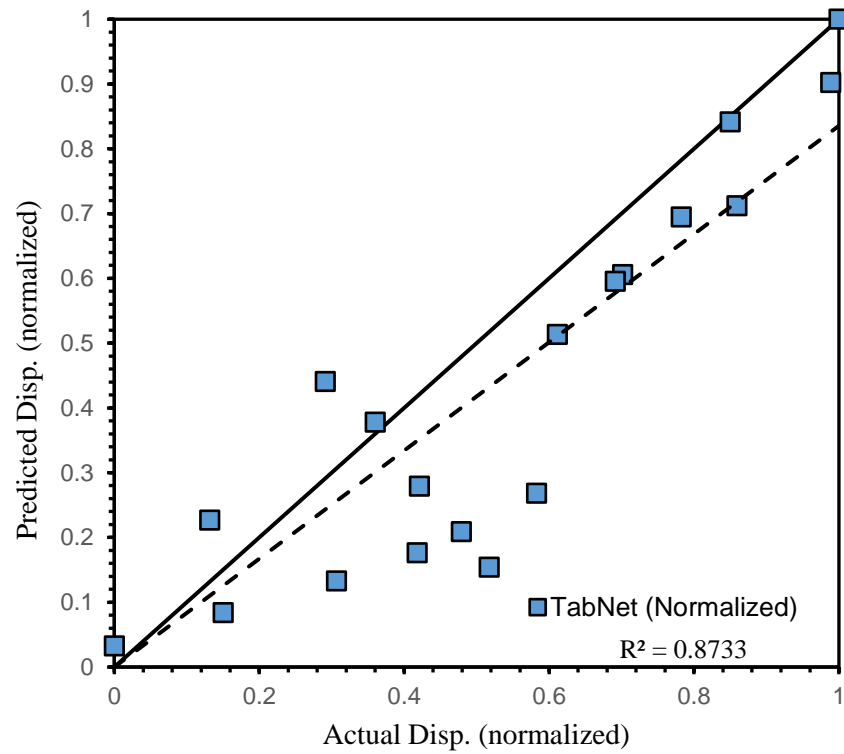
(iv) Scalability: TabNet is designed to be scalable, making it well suited for large datasets and high-dimensional data.

Overall, the performance of TabNet was depended on the specific problem and dataset, but it had shown to be a strong performer in a variety of tasks and is a promising deep learning architecture for structured data. TabNet was a deep learning architecture that had shown strong performance in a variety of tasks involving structured data. However, as with any machine learning model, its performance also depended on the specific problem and dataset it was being applied to. Nonetheless, TabNet's success in various tasks indicates that it has the potential to be a powerful tool for data analysis and prediction in many different fields. Hence, in predicting load-settlement behavior of pile this model was incorporated in the scope of this research and was implemented successfully following the modeling steps of TabNet, (Arik & Pfister, 2021). This is a tutorial that provides an implementation of TabNet in TensorFlow, including a detailed explanation of the code and a discussion of the results. It provides a good understanding of the modeling steps of TabNet, including its architecture, training process, and performance evaluation. Understanding the architecture and its capabilities is an important step in deciding whether or not it is appropriate for a particular problem. Additionally, the discussion of its performance and limitations is also important, as it helps to set realistic expectations and highlights areas where TabNet may not be the best solution. This type of information can be helpful for researchers and practitioners alike, as it can inform decision-making and help to ensure that the best tools are being used for the task at hand.

These resources should provide a good understanding of the modeling steps of TabNet, including its architecture, training process, and performance evaluation. The TabNet model performed significantly better than all other previous Neural Network models (Batch size=16) in terms of the training phase, producing a correlation of  $R^2 = 0.8733$  demonstrated in Figure 5.10. Also, the values  $MSE = 22.906$ ,  $RMSE = 4.786$  and  $MAE = 3.518$  validated the model to be the best one for prediction of load-settlement behavior of pile foundation in the scope of this research.



(a)



(b)

**Figure 5.10:** Comparison between field test data and TabNet prediction results without PCA (a) General case and (b) Normalized case

### 5.6.5 TabNet with PCA

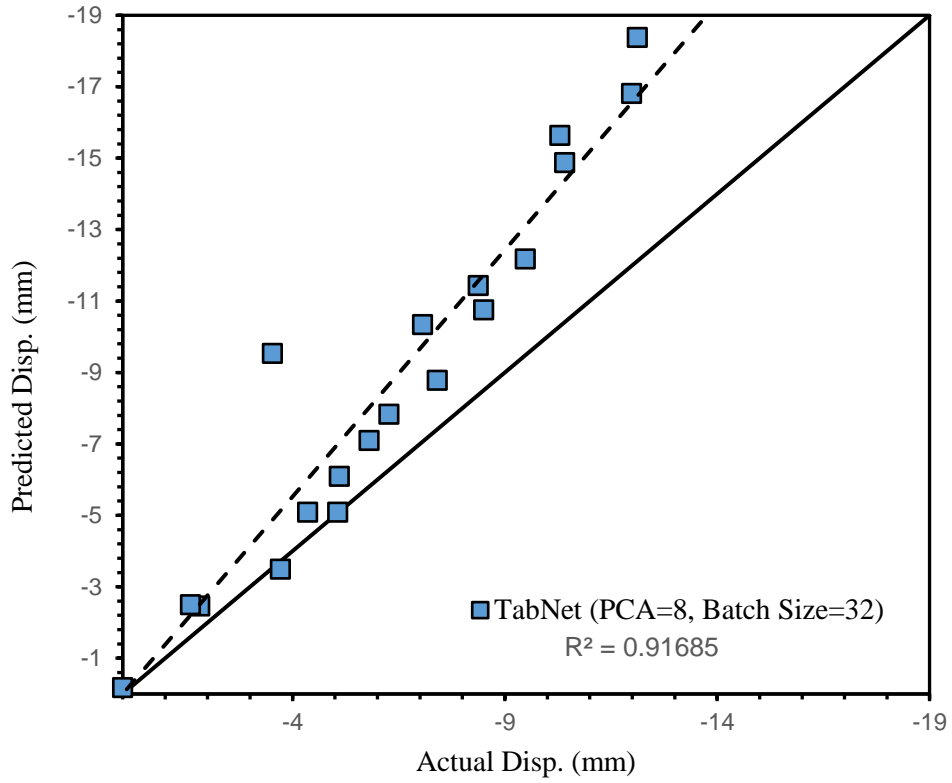
Inaccurate interpretations could result from the datasets' inclusion of noise and outliers (Chu et al., 2016). Therefore, in this research the goal of principal component analysis (PCA) was used to eliminate unnecessary dimensions.

Following the higher accuracy of TabNet model, as discussed during the development of validation model, initially, the network was trained with a set of random initial weights, a fixed learning rate of 0.001, a “tanh” transfer function in the hidden layer nodes, and a sigmoidal transfer function in the output layer nodes. Also, Dropout layers (Maizir & Kassim, 2013) were additionally introduced to lessen the effects of overfitting. "RMSprop" optimizer was used to update the neural network weights. It is a gradient descent algorithm that modifies the learning rate for each weight using a moving average of the squared gradients. This promotes faster convergence and improved generalization performance by reducing the vanishing or exploding gradient problem. As was previously noted, the cross-validation strategy was employed in this study since it is believed to be the most effective method for preventing overfitting and that there is enough data to produce training, testing, and validation sets.

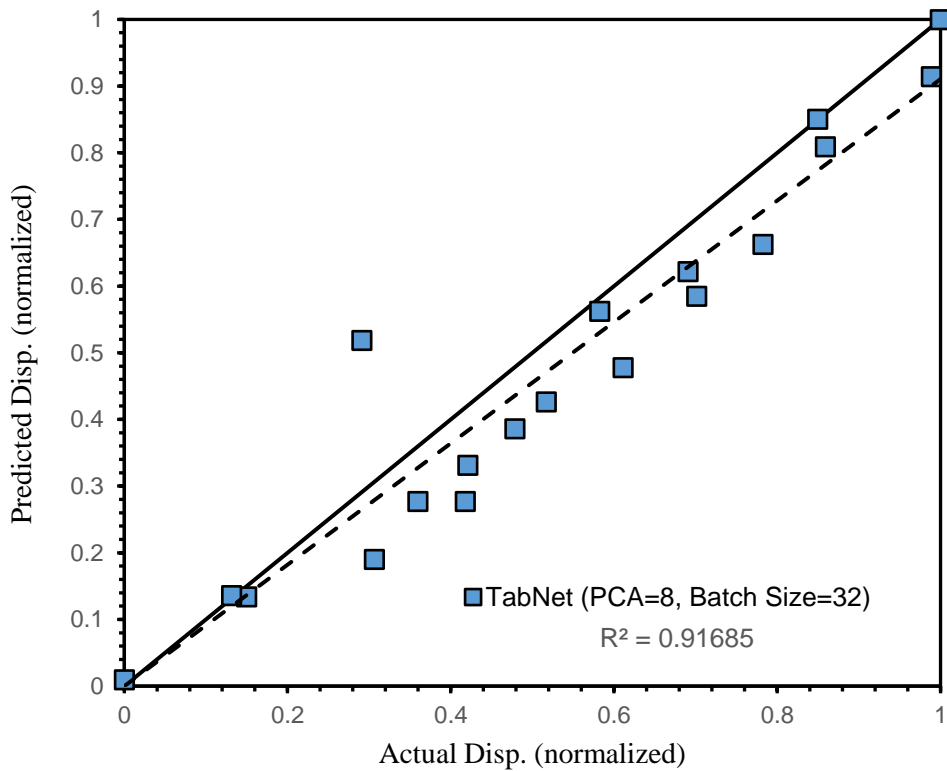
Now, trial was given by training and testing the TabNet model for Batch sizes of 8,16,32,64 and with varying PCA of 6,7,8 and 10 respectively. It was done in order to determine the optimal and most appropriate DNN model in terms of coefficient of determination ( $R^2$ ), MSE, RMSE and MAE presented.

From the comparison of performances of different models displayed in Figure 5.12, it was clear that the TabNet model with PCA=8 and Batch size = 32 was identified to be the most appropriate and best performing DNN model in terms of predicting the load-settlement behavior of pile one because it displays the highest accuracy. Also, significant improvement was further justified by the higher coefficient of determination of 0.91685 mentioned in Figure 5.11.

Figure 5.13 displays the result of importance analysis with ranking of features in descending order. It is obvious that the pile geometry, applied load (P) and the soil characteristics have the most impacts on the expected settlement, which is what the PCA has ultimately predicted. Further, a complete pile load test was analyzed using the optimal DNN model (with PCA=8 and Batch size=32), and the DNN predictions are compared with the measured settlements, in order to offer a further assessment of the DNN model's accuracy.

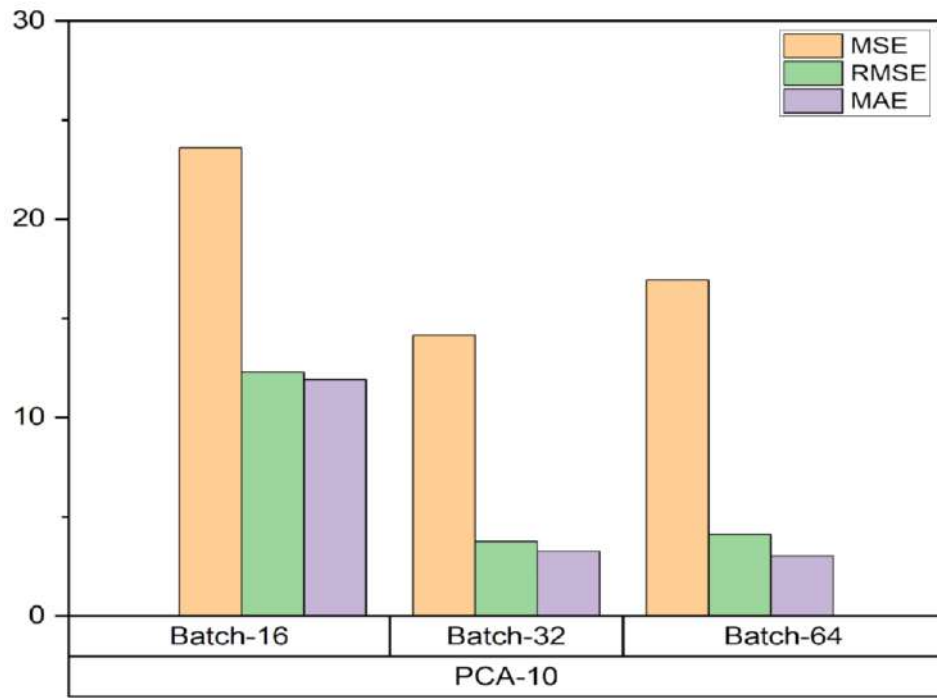


(a)

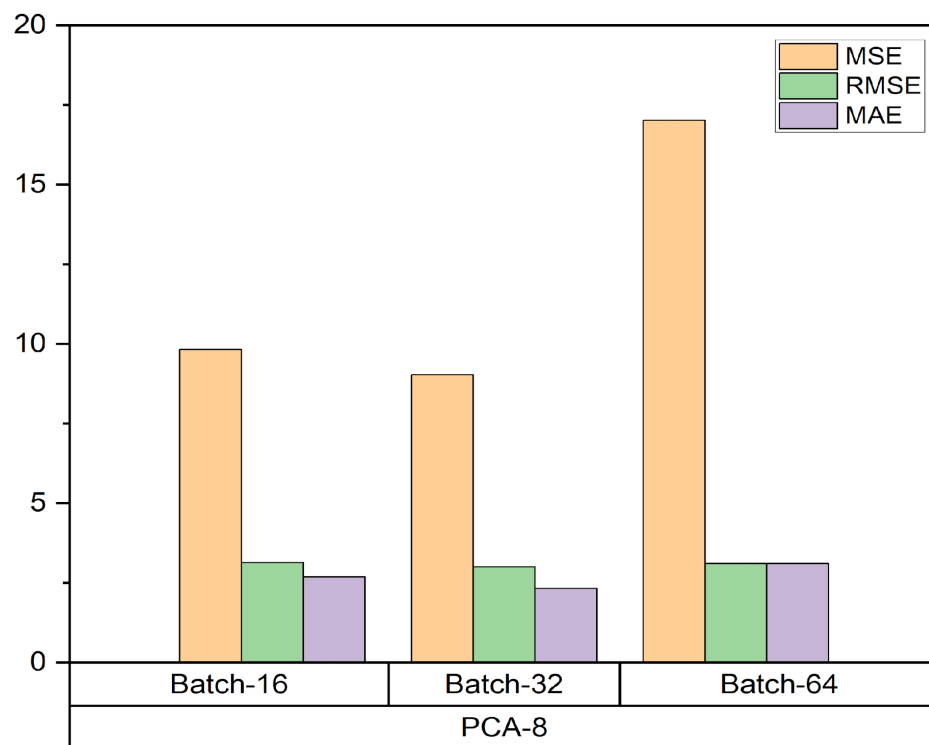


(b)

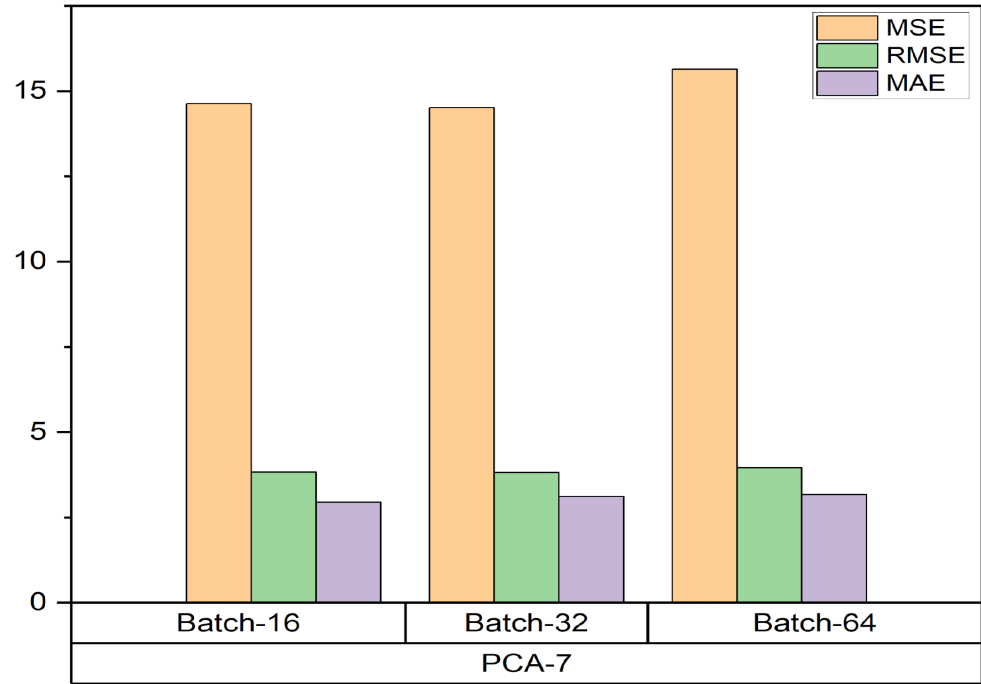
**Figure 5.11:** Comparison between field test data and TabNet prediction results with PCA (a) General case and (b) Normalized case



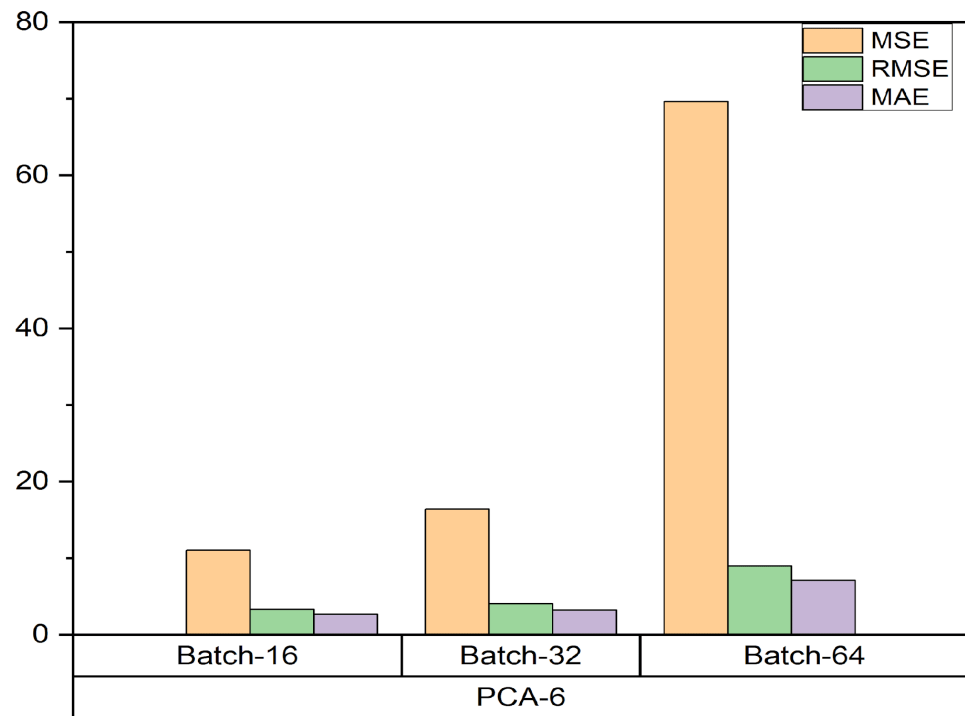
(a)



(b)



(c)



(d)

**Figure 5.12:** Performance comparison of TabNet model with different PCA and batch size

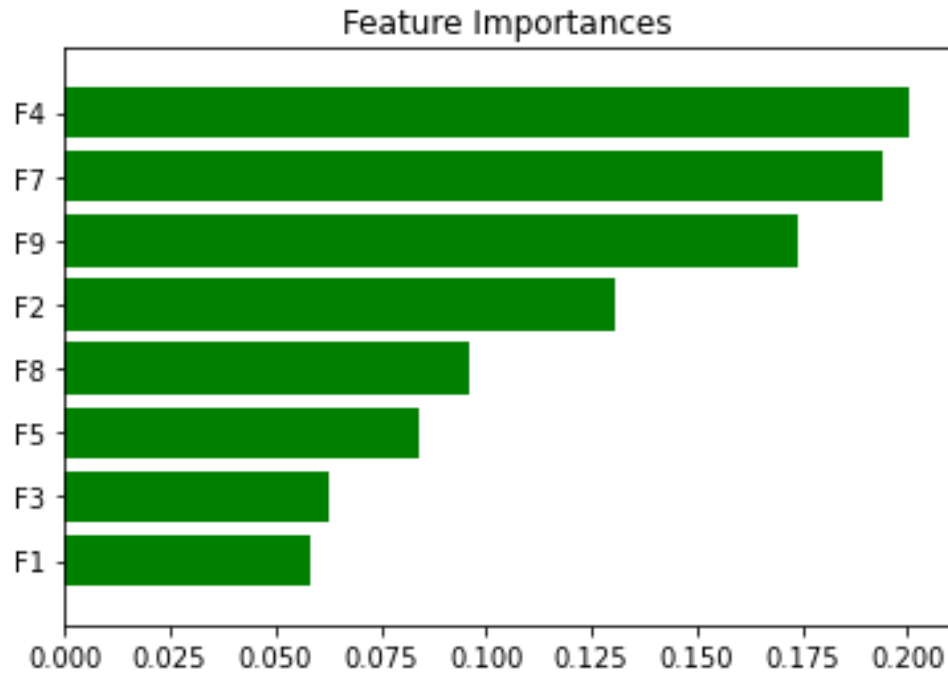
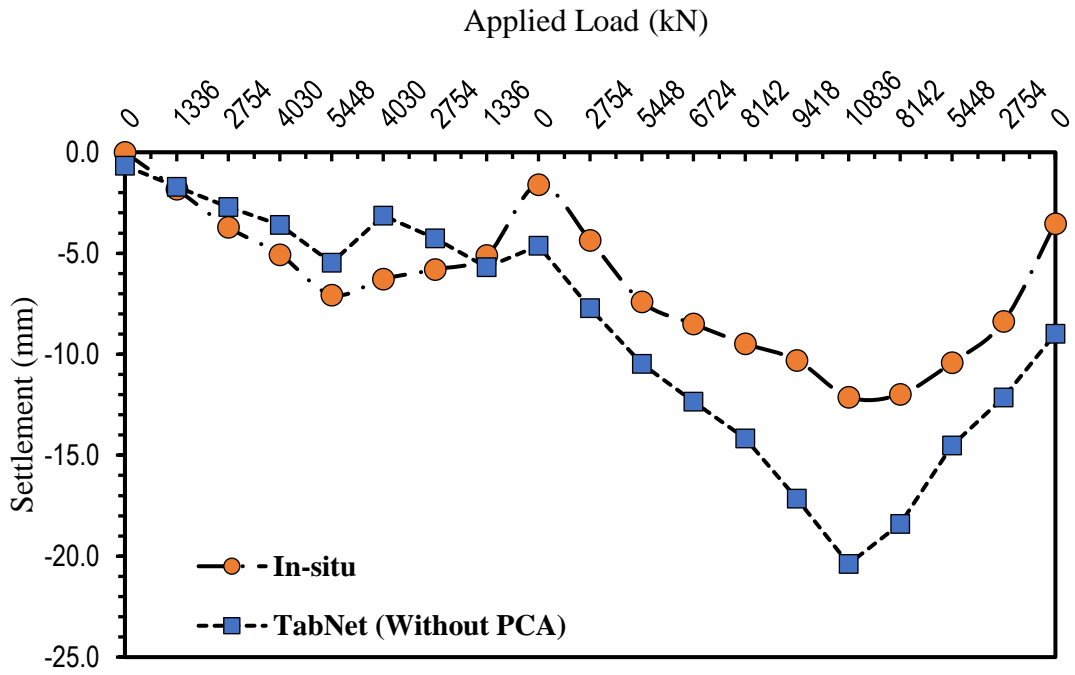


**Figure 5.13:** Importance analysis of components

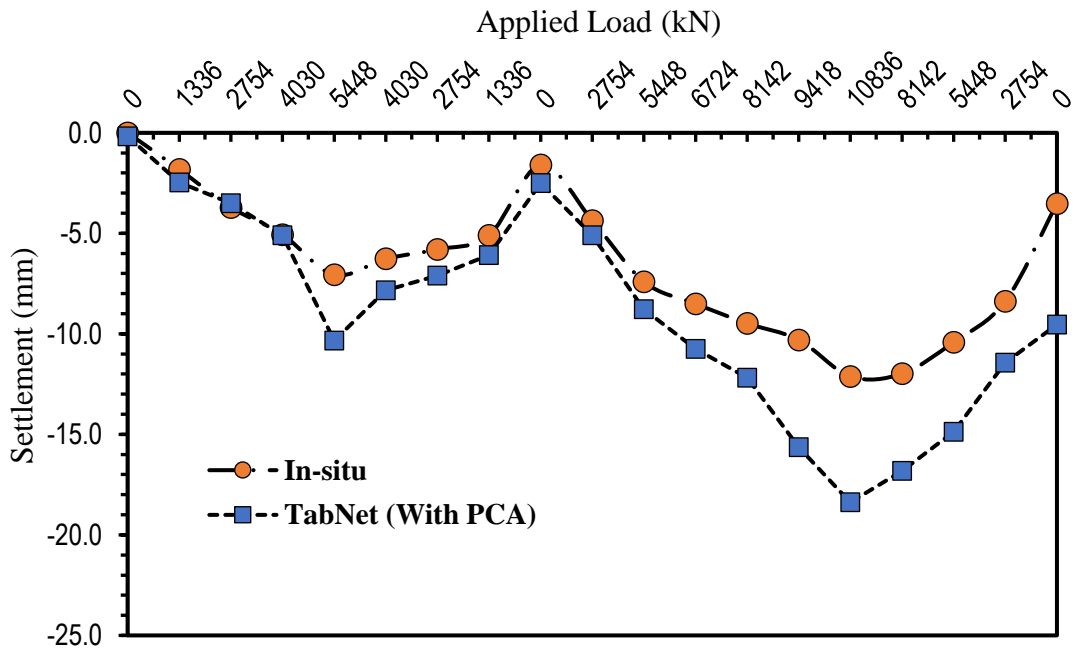
Figure 5.14 displays the graphs of the measured versus predicted settlement for the testing and validation set. Here, it was noted that the differences between the actual settlement and the settlement predicted by the TabNet model with PCA decreased within a reasonable range. For this case, a maximum settlement of mm was noted to be around 18 mm.

Visualizing the distribution of residuals can further illustrate the performance of models. The residuals being closely distributed around zero suggests the model to be performing better, while a systematic pattern in the residuals may indicate that the model is not capturing some important aspect of the data. From the residual plot in Figure 5.15 it is also clear that the after PCA the TabNet model performs in a very significant manner in predicting the load-settlement behavior of pile.



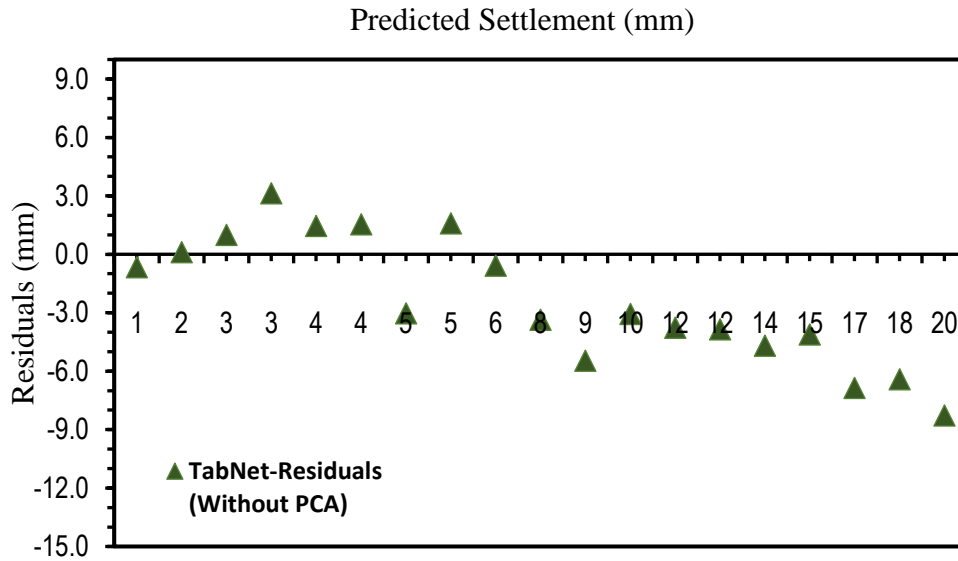


(a)

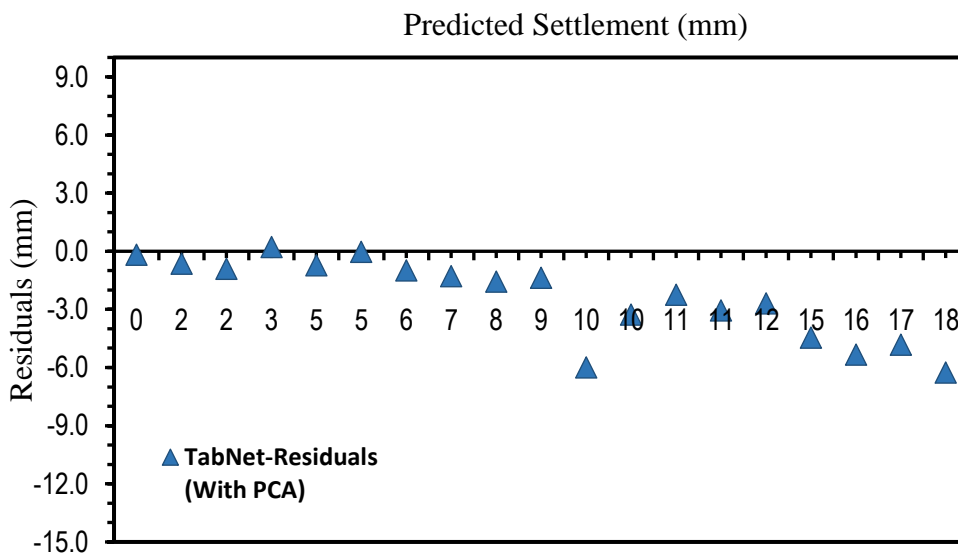


(b)

**Figure 5.14:** TabNet prediction results (a) Without PCA and (b) With PCA



(a)



(b)

**Figure 5.15:** Residual plot for TabNet models (a) Without PCA (b) With PCA

### 5.7 Summary

Starting from the beginning of the chapter, validation criteria and methodology was discussed. Based on the methodology, analyses for different machine learning techniques had been taken into account. Also, the predefined data set for validation from the collected data was utilized. As the best model was represented by a prediction value near to 1. From the initial performance comparisons of different models represented in Table 5.7, it was clear that the TabNet model was identified to be

performing best for pile load-settlement behavior prediction. To get a more substantiated view of the best-suited model for the prediction of the load-settlement behavior, the component analysis was taken into account. Consequently, several observations with different batch sizes and Principal Component Analysis (PCA) displayed substantial reduction in error and improvements in the model were noticed. The comparative study's findings showed that the DNN model we proposed (with Batch size=32 and PCA=8) is the one that performs the best and has the highest level of accuracy (0.9795 for all data). Hence, it was clear that the TabNet model with PCA was the best performing Deep Neural Network (DNN) model to be acknowledged.

**Table 5.7:** Comparative experiment results

| Model                | MSE         | RMSE        | MAE         |
|----------------------|-------------|-------------|-------------|
| MLP                  | 22.906217   | 4.786043983 | 3.517914951 |
| LSTM                 | 51.31417096 | 7.163391024 | 6.321185042 |
| Bi-LSTM              | 43.78197727 | 7.163391024 | 6.321185042 |
| 1D-CNN               | 181.0845358 | 13.45676543 | 9.368135376 |
| TabNet               | 10.42549191 | 3.228853033 | 2.972474709 |
| TabNet<br>(With PCA) | 9.025502108 | 3.004847345 | 2.320185963 |

## CHAPTER 6 COMPARISON OF MODEL PERFORMANCES

### 6.1 Introduction

Performances of DNN models vary based on the dataset, model architecture and other factors. Overview of the performances of used deep neural network (DNN) models has been illustrated in this chapter. Moreover, results from FEM model were also taken into account comparing with the field static load test data sets.

### 6.2 Performance Comparison

Based on the methodology, analyses for different machine learning techniques have been taken into account. Also, the predefined data set for validation from the collected data has been utilized. As the best model is represented by a prediction value near to 1, it goes without saying that the correlation coefficient is a crucial indicator when evaluating the prediction precision. From the initial performance comparisons of different models represented in Table 6.1, it was clear that the TabNet model was identified to be performing best for pile load-settlement behavior prediction. To get a more substantiated view of the best-suited model for the prediction of the load-settlement behavior, the component analysis was taken into account. Consequently, several observations with different batch sizes and Principal Component Analysis (PCA) displayed substantial reduction in error and improvements in the model were noticed. The overall changes in between loading and unloading phases for both cycles of the pile-load test simulation model in Plaxis-3D and best fitted DNN model comparing with field load test has been clearly demonstrated in Figure 6.1. Also, Figure. 6.2 depicted the clear performances of several DNN models and Figure. 6.3 for Plaxis-3D model, where, once again TabNet with PCA 8 and batch size of 32 performed almost closer to the Plaxis-3D results in terms of the correlation coefficient  $R^2$ . The comparative study's findings showed that the DNN model we proposed (with Batch size=32 and PCA=8) is the one that performs the best and has the highest level of accuracy (0.9795 for all data). On the other hand, the observed value of co-efficient of determination  $R^2$  shows very low accuracy with a value of 0.65 for the proposed MLP model. In the context of 1D-CNN model it was observed that the  $R^2$  value is 0.7743. Even in case of proposed LSTM and Bi-LSTM models  $R^2$  were noticed to be 0.843 and 0.784 respectively. In fact, at the end of the second loading phases the maximum

settlement was noticed to get recovered around 46% of the total settlement, offering a permanent settlement of 7 mm (in Figure 6.1) ultimately. These justifies the comparatively lower prediction accuracy. Hence, it was clear that the TabNet model with PCA was the best performing Deep Neural Network (DNN) model to be acknowledged.

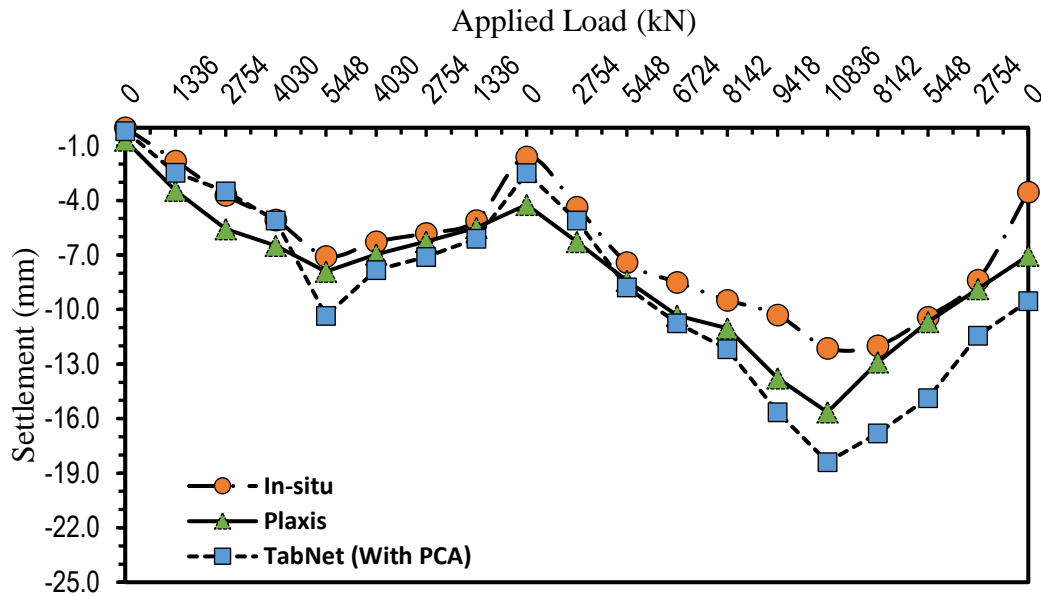
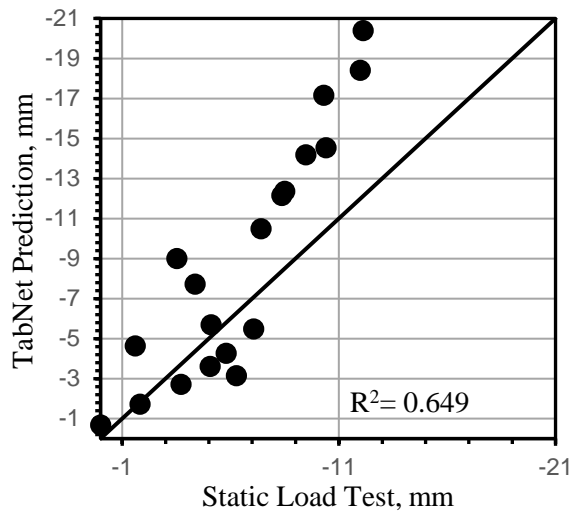


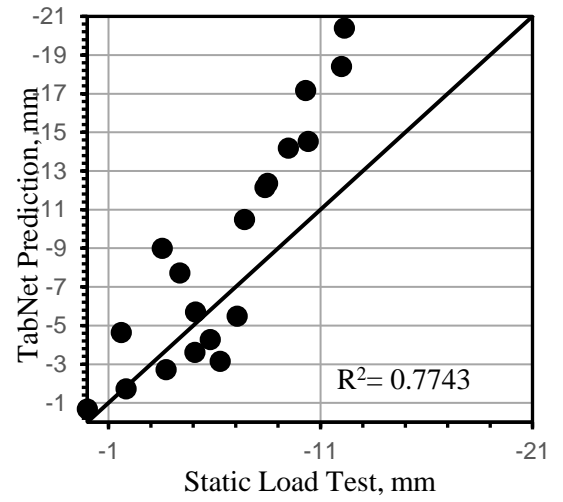
**Figure 6.1:** Prediction results of different models

**Table 6.1:** Comparison of performances of different models

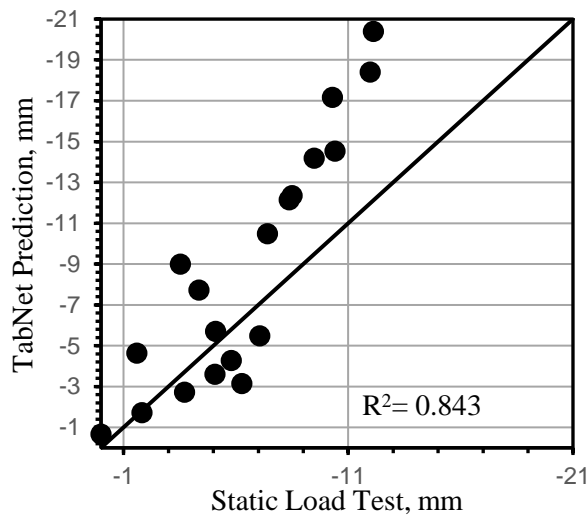
| Model             | $R^2$   | MSE         | RMSE        | MAE         |
|-------------------|---------|-------------|-------------|-------------|
| MLP               | 0.649   | 22.906217   | 4.786043983 | 3.517914951 |
| LSTM              | 0.843   | 51.31417096 | 7.163391024 | 6.321185042 |
| Bi-LSTM           | 0.7841  | 43.78197727 | 7.163391024 | 6.321185042 |
| 1DCNN             | 0.7743  | 181.0845358 | 13.45676543 | 9.368135376 |
| TabNet            | 0.8733  | 10.42549191 | 3.228853033 | 2.972474709 |
| TabNet (With PCA) | 0.91685 | 9.025502108 | 3.004847345 | 2.320185963 |
| Plaxis-3D         | 0.9162  | -           | -           | -           |



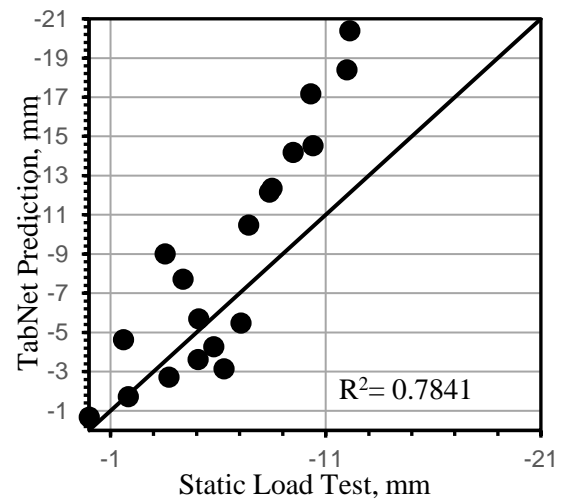
(a) MLP model



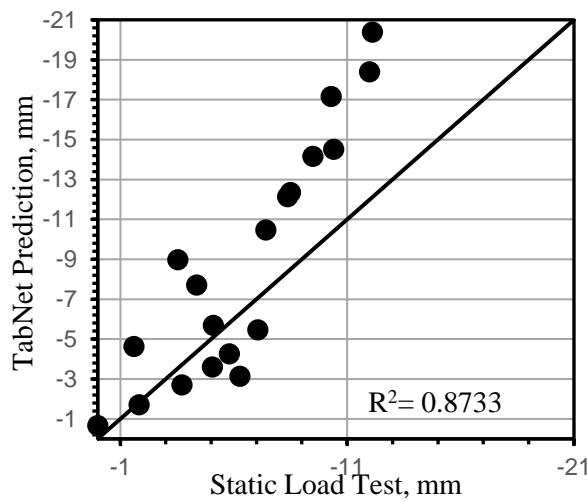
(b) 1D-CNN



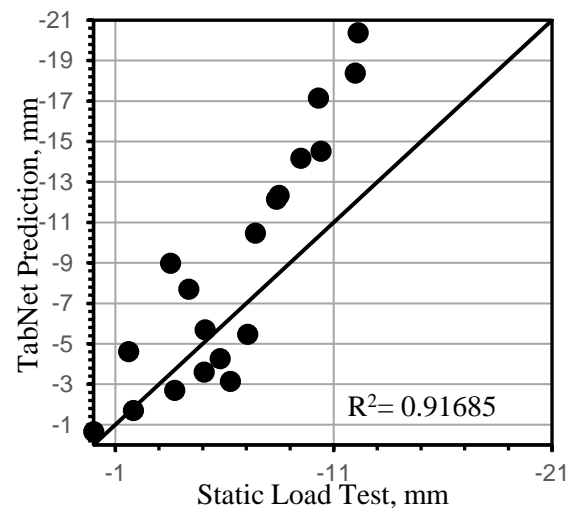
(c)



(d)



(e) TabNet (Without PCA)



(f) TabNet (With PCA)

**Figure 6.2:** Performances of different DNN models (a) MLP model, (b) 1D-CNN, (c) LSTM, (d) Bi-LSTM model, (e) TabNet (Without PCA) and (f) TabNet (With PCA)

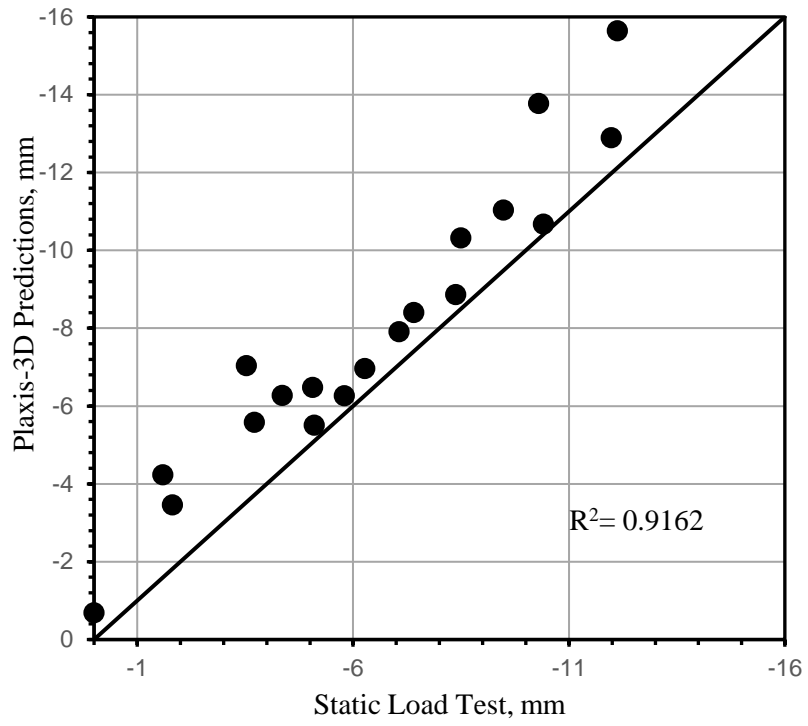


**Figure 6.3:** Performance of Plaxis 3D model

## **CHAPTER 7**

### **CONCLUSIONS AND RECOMMENDATIONS**

#### **7.1 Introduction**

The main goal of this study was to create models that can predict how pile foundations will behave under different loads. To achieve this, a load test simulation was conducted on a project with a varied soil profile using the FEM program Plaxis-3D. Popular DNN models, including MLP, RNN, 1D-CNN, and TabNet, were used to develop load test behavior prediction models. Statistical errors, coefficient of determination, and residual plots were generated after training the models to evaluate their performances. In addition, a DNN model was developed using data from 42 load-test data sets of nominated projects and their basic soil profiles. Approximately 712 load-test data points were used to predict the load-settlement behavior of pile foundations. After training the models, validation was done by checking statistical correlation parameters and assessing errors, and the best-fitted DNN model was identified. The findings of the investigation have been summarized in this chapter.

#### **7.2 Conclusions**

As we can see from the project under discussion, different findings were obtained with various approaches employed to compute the pile foundation settlement under varying loading. Using results from construction work, it is possible to generate a valid conclusion using a non-linear model in a straightforward manner using both FEM model and DNN model. The main features of the study developed can be listed as follows:

- (i) Prior to the modeling of the static load test in Plaxis-3D, the HS model for silty clay was calibrated and was observed to show higher accuracy in simulating the soil behavior using triaxial test results. It clearly signifies the justification of preferring the HS model in predicting the load-settlement behavior of pile foundations with FEM techniques.
- (ii) (ii)The FEM model with the HS model accurately demonstrated the differences between the loading and unloading phases for both cycles during the pile-load test simulation in Plaxis-3D. It should be noted that the maximum settlement observed after the second loading phase recovered by approximately 46% of the total settlement. Despite a slight deviation in the curve of Plaxis-3D for the maximum



settlement case compared to the static load test field data using ASTM D1143 guidelines, this exception does not affect the research findings as comparisons were made between the in situ SLT outcomes and Plaxis 3D prediction. From an engineering perspective, the obtained coefficient of determination ( $R^2$ ) value of 0.9162 suggests that using this strategy for the selection of soil parameters is a reasonable approach due to Plaxis 3D's accurate match.

- (iii) While performing the DNN operations, focus was initially given to all 26 input features for predicting the settlement. In response to the model performances, TabNet model was noticed to be significant in terms of errors with a batch size of 16 being the best-fitted one.
- (iv) For further better prediction modeling, PCA was introduced for the best fitted TabNet model with varying PCA and batch sizes. It concluded that the TabNet with PCA of 8 and batch size of 32 was the model with higher accuracy comparing to the all-other models.
- (v) TabNet with PCA 8 and batch size of 32 performed almost similarly to the Plaxis-3D results in terms of the correlation coefficient  $R^2$ . Hence, the validation model can be applied at any time for additional data to vindicate the consistency of the DNN model. It is expected that every time it would give the similar accuracy for RCC piles as obtained.
- (vi) From the overall research, it can also be concluded that the current study will be useful for predicting the pile load settlement behavior using simple parameters like soil profile, SPT-N value, pile geometry, pile material properties and applied load which will ultimately ensure optimization of test plans in a cost effective and compatible way.

Despite achieving a better accuracy range, the study has certain limitations. Improving the precision of the DNN model and increasing its accuracy would require a larger number of datasets. Additionally, the accuracy of the FEM model could be enhanced if triaxial tests were conducted for all layers.

One of the specific limitations of the numerical study is that it only considered the HS soil model. Other relevant models, such as the soft-soil model and subloading- $t_{ij}$  model in Plaxis-3D, were skipped in the load-settlement assessment. Furthermore, it's worth noting that this study focused solely on the load-settlement behavior of prefabricated and cast in situ RCC piles. As a result, the DNN models developed were specific to RCC piles and did not account for the load-settlement behavior of steel piles. This

aspect creates limitations for the study, as it neglects the behavior of an essential type of pile used in construction.

Overall, while the study made advancements in prediction accuracy, these limitations highlight the need for further research and consideration of different soil models and pile types to develop more comprehensive and precise models for load-settlement assessment in various construction scenarios.

### **7.3 Recommendations for Future Research**

Due to time and resource constraints, we were unable to explore all of the potential avenues of inquiry that this model suggests. Together with the model's analysis and validation came the discovery of a few schemes. What follows is a list of suggestions about where to go from here in terms of future research.

- (i) For both the FEM and DNN models, it is recommended in future study to incorporate instrumented pile-load test data with an aim to increase the accuracy level of the models. Instrumented pile enables to interpret the micro level load-settlement behavior of pile and to assess their behavioral changes with respect to soil conditions.
- (ii) The model developed in this study should be trained with a large number of datasets and tested accordingly. Variation in accuracy level may also be assessed tuning the activation functions and including ensemble techniques to achieve higher accuracy in future. A detailed study can be conducted considering the variations in pile types and materials. Specifically, steel piles and pre-stressed piles may also be taken into considerations while developing the models.
- (iii) Detailed numerical study may be conducted using soft-soil model and subloading  $t_{ij}$  model to further assess the accuracy level with respect to the changes in soil models. Triaxial tests will also be conducted for all soil layers to enhance the accuracy level of used numerical modeling soil parameters. Constraints in collecting undisturbed sand sample may be counteract by using relative density to simulate the infield condition of sand sample.
- (iv) This study recommends the development of DNN model using ensemble techniques to assess the pile load-settlement behavior with probable higher accuracy of prediction results.

## REFERENCES

- Abid, A., Abdalla, A., Abid, A., Khan, D., Alfozan, A., and Zou, J. (2019). Gradio: Hassle-free sharing and testing of ml models in the wild. *arXiv preprint arXiv:1906.02569*.
- Abu Sadeque, M. (1989). Performance of bored piles alluvial soils of Bangladesh. MSc. Engg Thesis, Department of Civil Engineering, Bangladesh University of Engineering and Technology, 2015.
- Acharya, U. R., Oh, S. L., Hagiwara, Y., Tan, J. H., Adam, M., Gertych, A., and San Tan, R. (2017). A deep convolutional neural network model to classify heartbeats. *Computers in biology and medicine*, 89, 389-396.
- Ahmed, A. J. M. M. U. (2021). Bangla license plate recognition using image processing and adaptive neuro-fuzzy inference technique. MSc. Engg Thesis, Department of Civil Engineering, Bangladesh University of Engineering and Technology.
- Ahmed, M.Y., and Neelima, S. D. (2009). Numerical analysis of a pile subjected to lateral loads. *IGC*, 2009.
- Al-Homoud, A. S., Fouad, T., and Mokhtar, A. (2004). Evaluating accuracy for two empirical methods in predicting settlement of drilled shafts. *Geotechnical & Geological Engineering*, 22, 245-267.
- Albusoda, B. S., Mohammed, S., and Abbas, M. F. (2020). Comparison among Different Methods to Estimate Ultimate Capacity of Bored Pile. *IOP Conference Series: Materials Science and Engineering*.
- AlKhafaji, H., and Imani, M. (2022). Numerical Simulation of Driven Piles Under Static Axial Compressive Load Testing Using Finite Element Model. In *Geotechnical Engineering and Sustainable Construction: Sustainable Geotechnical Engineering* (pp. 305-314). Springer.
- Alvarez, J. M., LeCun, Y., Gevers, T., and Lopez, A. M. (2012). Semantic road segmentation via multi-scale ensembles of learned features. *Computer Vision—ECCV 2012. Workshops and Demonstrations: Florence, Italy, October 7-13, 2012, Proceedings, Part II* 12.
- Alzo'Ubi, A., and Ibrahim, F. (2021). Predicting the pile static load test using backpropagation neural network and generalized regression neural network—a comparative study. *International Journal of Geotechnical Engineering*, 15(7), 810-821.
- Andrew, M. (2019). Collaborating online with four different google apps: Benefits to learning and usefulness for future work. *Journal of Asia TEFL*, 16(4), 1268.
- Ansary, M., Siddiquee, M. A., Siddique, A., and Safiullah, A. M. (2001). Status of static pile load tests in Bangladesh. *Soil mechanics and geotechnical engineering. Eleventh Asian Regional Conference*. (pp. 241-244).
- Anysz, H., Zbiciak, A., and Ibadov, N. (2016). The influence of input data standardization method on prediction accuracy of artificial neural networks. *Procedia Engineering*, 153, 66-70.
- Arik, S. Ö., and Pfister, T. (2021). Tabnet: Attentive interpretable tabular learning. *Proceedings of the AAAI Conference on Artificial Intelligence*. (Vol. 35, No. 8, pp. 6679-6687).
- Banerjee, P., and Davies, T. (1978). The behaviour of axially and laterally loaded single piles embedded in nonhomogeneous soils. *Geotechnique*, 28(3), 309-326.
- Benali, A., and Nechnech, A. (2011). Prediction of the pile capacity in purely coherent soils using the approach of the artificial neural networks. *International Seminar*,

- Innovation & Valorization in Civil Engineering & Construction Materials*. (No. 50-239).
- Boscardin, M. D., and Cording, E. J. (1989). Building response to excavation-induced settlement. *Journal of geotechnical engineering*, 115(1), 1-21.
- Brinkgreve, R., and Engin, E. (2013). Validation of geotechnical finite element analysis. *Proceedings of the 18th International Conference on Soil Mechanics and Geotechnical Engineering*. (Vol. 2, pp. 677-682).
- Cardoso Bernardes, H., Martines Sales, M., Rodrigues Machado, R., José da Cruz Junior, A., Pinto da Cunha, R., Resende Angelim, R., and Félix Rodríguez Rebolledo, J. (2022). Coupling hardening soil model and Ménard pressuremeter tests to predict pile behavior. *European Journal of Environmental and Civil Engineering*, 26(11), 5221-5240.
- Chai, T., and Draxler, R. R. (2014). Root mean square error (RMSE) or mean absolute error (MAE)?—Arguments against avoiding RMSE in the literature. *Geoscientific model development*, 7(3), 1247-1250.
- Chan, W., Chow, Y., and Liu, L. (1995). Neural network: an alternative to pile driving formulas. *Computers and geotechnics*, 17(2), 135-156.
- Chen, X., Huang, L., Xie, D., and Zhao, Q. (2018). EGBMMDA: extreme gradient boosting machine for MiRNA-disease association prediction. *Cell death & disease*, 9(1), 3.
- Cherkassky, V., Krasnopolsky, V., Solomatine, D. P., and Valdes, J. (2006). Computational intelligence in earth sciences and environmental applications: Issues and challenges. *Neural Networks*, 19(2), 113-121.
- Chu, X., Ilyas, I. F., Krishnan, S., and Wang, J. (2016). Data cleaning: Overview and emerging challenges. *Proceedings of the 2016 international conference on management of data*. (pp. 2201-2206).
- Chung, S.H., and Yang, S.R. (2017). Numerical analysis of small-scale model pile in unsaturated clayey soil. *International Journal of Civil Engineering*, 15, 877-886.
- Coduto, D. P. (2001). Foundation design. *Pomona, California State Polytechnic University*.
- Coduto, D. P. (2014). *Foundation design: principles and practices*. Pearson Education Limited.
- Computation, N. (2016). Long short-term memory. *Neural Comput*, 9, 1735-1780.
- Dao, T. (2011). Validation of PLAXIS embedded piles for lateral loading. MSc. Engg Thesis, Department of Civil Engineering, Delft University of Technology.
- Das, S. K. (2013). 10 Artificial neural networks in geotechnical engineering: modeling and application issues. *Metaheuristics in Water Geotech Transp Eng*, 45, 231-267.
- Desai, C. S., Johnson, L. D., and Hargett, C. M. (1974). Analysis of pile-supported gravity lock. *Journal of the geotechnical engineering division*, 100(9), 1009-1029.
- Duncan, O. D., and Duncan, B. (1955). A methodological analysis of segregation indexes. *American sociological review*, 20(2), 210-217.
- El-Mossallamy, Y. (2020). Load settlement behavior of large diameter bored piles in over-consolidated clay. In *Numerical Models in Geomechanics* (pp. 443-450). CRC Press.
- Elkateb, T., Chalaturnyk, R., and Robertson, P. K. (2003). An overview of soil heterogeneity: quantification and implications on geotechnical field problems. *Canadian Geotechnical Journal*, 40(1), 1-15.

- Elsherbiny, Z. H., and El Naggar, M. H. (2013). Axial compressive capacity of helical piles from field tests and numerical study. *Canadian Geotechnical Journal*, 50(12), 1191-1203.
- Erdeljan, A., Vukobratović, B., and Struharik, R. (2017). IP core for efficient zero-run length compression of CNN feature maps. In *2017 25th Telecommunication Forum (TELFOR)* (pp. 1-4). IEEE.
- Esfe, M. H., Wongwises, S., Naderi, A., Asadi, A., Safaei, M. R., Rostamian, H., Dahari, M., and Karimipour, A. (2015). Thermal conductivity of Cu/TiO<sub>2</sub>-water/EG hybrid nanofluid: Experimental data and modeling using artificial neural network and correlation. *International communications in heat and mass transfer*, 66, 100-104.
- Fakharian, K., Meskar, M., and Mohammadlou, A. S. (2014). Effect of surcharge pressure on pile static axial load test results. *International Journal of Geomechanics*, 14(6), 04014024.
- Farquhar, G. (1990). Pile load tests at an Auckland industrial facility. In *Proc of the 8th ANZ conference on geomechanics, Hobart* (Vol. 1, pp. 383-7).
- Fath, A. H., Madanifar, F., and Abbasi, M. (2020). Implementation of multilayer perceptron (MLP) and radial basis function (RBF) neural networks to predict solution gas-oil ratio of crude oil systems. *Petroleum*, 6(1), 80-91.
- Fellenius, B. H. (1980). The analysis of results from routine pile load tests. *Ground Engineering*, 13(6), 19-31.
- Fellenius, B. H., Harris, D. E., and Anderson, D. G. (2004). Static loading test on a 45 m long pipe pile in Sandpoint, Idaho. *Canadian Geotechnical Journal*, 41(4), 613-628.
- Franke, E., Lutz, B., and El-Mossallamy, Y. (1994). Measurements and numerical modelling of high rise building foundations on Frankfurt Clay. In *Vertical and horizontal deformations of foundations and embankments* (pp. 1325-1336). ASCE.
- Franzius, J., and Potts, D. (2005). Influence of mesh geometry on three-dimensional finite-element analysis of tunnel excavation. *International Journal of Geomechanics*, 5(3), 256-266.
- García, J., Salmerón, R., García, C., and López Martín, M. d. M. (2016). Standardization of variables and collinearity diagnostic in ridge regression. *International Statistical Review*, 84(2), 245-266.
- Gers, F. A., Schmidhuber, J., and Cummins, F. (2000). Learning to forget: Continual prediction with LSTM. *Neural computation*, 12(10), 2451-2471.
- Goh, A. (1995). Empirical design in geotechnics using neural networks. *Geotechnique*, 45(4), 709-714.
- Goodfellow, I., Bengio, Y., and Courville, A. (2016). *Deep learning*. MIT press.
- Gouda, A., Gomaa, S., Attia, A., Emara, R., Desouky, S., and El-hoshoudy, A. (2022). Development of an artificial neural network model for predicting the dew point pressure of retrograde gas condensate. *Journal of Petroleum Science and Engineering*, 208, 109284.
- Gowthaman, S., and Nasvi, M. (2017). 2D and 3D numerical simulation of load-settlement behaviour of axially loaded pile foundations. *American Journal of Civil Engineering and Architecture*, 5(5), 187-195.
- Graves, A., Fernández, S., and Schmidhuber, J. (2005). Bidirectional LSTM networks for improved phoneme classification and recognition. In *International conference on artificial neural networks* (pp. 799-804). Berlin, Heidelberg: Springer Berlin Heidelberg.

- Graves, A., Jaitly, N., and Mohamed, A.R. (2013). Hybrid speech recognition with deep bidirectional LSTM. *In 2013 IEEE workshop on automatic speech recognition and understanding* (pp. 273-278). IEEE.
- Griffiths, D., and Fenton, G. A. (2004). Probabilistic slope stability analysis by finite elements. *Journal of Geotechnical and Geoenvironmental Engineering*, 130(5), 507-518.
- Halder, A. K. (2016). Pile Load Capacity using Static and Dynamic Load test. MSc. Engg. Thesis, Department of Civil Engineering, Bangladesh University of Engineering and Technology
- Hanna, A. M., Ural, D., and Saygili, G. (2007). Neural network model for liquefaction potential in soil deposits using Turkey and Taiwan earthquake data. *Soil Dynamics and Earthquake Engineering*, 27(6), 521-540.
- Hannun, A. Y., Rajpurkar, P., Haghpanahi, M., Tison, G. H., Bourn, C., Turakhia, M. P., and Ng, A.Y. (2019). Cardiologist-level arrhythmia detection and classification in ambulatory electrocardiograms using a deep neural network. *Nature medicine*, 25(1), 65-69.
- Hazewinkel, A. (2022). Driveability predictions in vibratory pile driving: A comparison of various machine learning approaches and the traditional model. MSc. Engg Thesis, Department of Civil Engineering, Delft University of Technology.
- Hecht-Nielsen, R. (1989). Neurocomputing. Addison-Wesley Longman Publishing Co., Inc.
- Hejazi, Y., Dias, D., and Kastner, R. (2008). Impact of constitutive models on the numerical analysis of underground constructions. *Acta Geotechnica*, 3, 251-258.
- Hochreiter, S., and Schmidhuber, J. (1997). Long short-term memory. *Neural computation*, 9(8), 1735-1780.
- Huang, X., Li, Q., Tai, Y., Chen, Z., Liu, J., Shi, J., and Liu, W. (2022). Time series forecasting for hourly photovoltaic power using conditional generative adversarial network and Bi-LSTM. *Energy*, 246, 123403.
- Huang, X., Wu, L., and Ye, Y. (2019). A review on dimensionality reduction techniques. *International Journal of Pattern Recognition and Artificial Intelligence*, 33(10), 1950017.
- Hunt, R. (1984). Geotechnical Engineering Investigation Manual. McGraw-Hill Book Company. New York.
- Ihsanto, E., Ramli, K., Sudiana, D., and Gunawan, T. S. (2020). An efficient algorithm for cardiac arrhythmia classification using ensemble of depthwise separable convolutional neural networks. *Applied Sciences*, 10(2), 483.
- Islam, M. S., Shahin, H. M., Banik, S., and Azam, F. (2013). Elasto-plastic constitutive model parameters and their application to bearing capacity estimation for Dhaka sub-soil. *Journal of Civil Engineering, The Institution of Engineers, Bangladesh, Vo. CE, 42*, 171-188.
- Islam, T. I., Mohammad. (2018). Estimation of pile bearing capacity using different methods. *4<sup>th</sup> International Conference on Advances in Civil Engineering 2018*.
- Javadi, A., and Rezaia, M. (2009). Applications of artificial intelligence and data mining techniques in soil modeling. *Geomechanics and Engineering*, 1(1), 53-74.
- Jebur, A. A., Atherton, W., and Al Khaddar, R. M. (2018). Feasibility of an evolutionary artificial intelligence (AI) scheme for modelling of load settlement response of concrete piles embedded in cohesionless soil. *Ships and Offshore Structures*, 13(7), 705-718.

- Jiang, Q., Zhu, L., Shu, C., and Sekar, V. (2022). An efficient multilayer RBF neural network and its application to regression problems. *Neural Computing and Applications*, 1-18.
- Jimenez, R., and Sitar, N. (2009). The importance of distribution types on finite element analyses of foundation settlement. *Computers and geotechnics*, 36(3), 474-483.
- Johnson, K., Lemcke, P., Karunasena, W., and Sivakugan, N. (2006). Modelling the load–deformation response of deep foundations under oblique loading. *Environmental Modelling & Software*, 21(9), 1375-1380.
- Kabir, M. U., Hossain, S. A., Alam, M., and Azim, M. (2017). *Numerical Analyses of the Karnaphuli River Tunnel*. BSc. Engg Thesis, Department of Civil and Environment Engineering, Islamic University of Technology.
- Karthigeyan, S., Ramakrishna, V., and Rajagopal, K. (2006). Influence of vertical load on the lateral response of piles in sand. *Computers and geotechnics*, 33(2), 121-131.
- Kardani, N., Zhou, A., Nazem, M., and Shen, S.L. (2020). Estimation of bearing capacity of piles in cohesionless soil using optimised machine learning approaches. *Geotechnical and Geological Engineering*, 38, 2271-229.
- Karthigeyan, S., Ramakrishna, V., and Rajagopal, K. (2007). Numerical investigation of the effect of vertical load on the lateral response of piles. *Journal of Geotechnical and Geoenvironmental Engineering*, 133(5), 512-521.
- Kee, C. F. (1978). Diagnosis of pile condition. *Geotechnical Engineering*, 9, 85-104.
- Kiefa, M. A. (1998). General regression neural networks for driven piles in cohesionless soils. *Journal of Geotechnical and Geoenvironmental Engineering*, 124(12), 1177-1185.
- Kimura, M., and Zhang, F. (2000). Seismic evaluations of pile foundations with three different methods based on three-dimensional elasto-plastic finite element analysis. *Soils and foundations*, 40(5), 113-132.
- Kiranyaz, S., Ince, T., and Gabbouj, M. (2015). Real-time patient-specific ECG classification by 1-D convolutional neural networks. *IEEE Transactions on Biomedical Engineering*, 63(3), 664-675.
- Kondner, R. L. (1963). Hyperbolic stress-strain response: cohesive soils. *Journal of the Soil Mechanics and Foundations Division*, 89(1), 115-143.
- Krasinśkin, A. (2014). Numerical simulation of screw displacement pile interaction with non-cohesive soil. *Archives of Civil and Mechanical Engineering*, 14, 122-133.
- Krasinśki, A., and Wiszniewski, M. (2017). Static load test on instrumented pile–field data and numerical simulations. *Studia Geotechnica et Mechanica*, 39(3), 17-25.
- Kumar, P., Sihag, P., Sharma, A., Pathania, A., Singh, R., Chaturvedi, P., Mali, N., Uday, K., and Dutt, V. (2021). Prediction of real-world slope movements via recurrent and non-recurrent neural network algorithms: a case study of the tangni landslide. *Indian Geotechnical Journal*, 51(4), 788-810.
- Lee, C. (1993). Settlement of pile groups—Practical approach. *Journal of geotechnical engineering*, 119(9), 1449-1461.
- Lee, I.M., and Lee, J.H. (1996). Prediction of pile bearing capacity using artificial neural networks. *Computers and geotechnics*, 18(3), 189-200.
- Li, S., Lai, Y., Zhang, S., and Liu, D. (2009). An improved statistical damage constitutive model for warm frozen clay based on Mohr–Coulomb criterion. *Cold Regions Science and Technology*, 57(2-3), 154-159.

- Likitlersuang, S., Surarak, C., Balasubramania, A., Oh, E., Syeung, R., and Wanatowski, D. (2013). Duncan-chang-parameters for hyperbolic stress strain behaviour of soft Bangkok clay. In *Proceedings of the 18th International Conference on Soil Mechanics and Geotechnical Engineering (ICSMGE'13)*.
- Liu, M., Liao, S., Yang, Y., Men, Y., He, J., and Huang, Y. (2021). Tunnel boring machine vibration-based deep learning for the ground identification of working faces. *Journal of Rock Mechanics and Geotechnical Engineering*, 13(6), 1340-1357.
- Lundberg, S. M., Erion, G. G., and Lee, S.I. (2018). Consistent individualized feature attribution for tree ensembles. *arXiv preprint arXiv:1802.03888*.
- Maizir, H., and Kassim, K. A. (2013). Neural network application in prediction of axial bearing capacity of driven piles. In *Proceedings of the international multiconference of engineers and computer scientists* (Vol. 1, pp. 13-15).
- Marquardt, D. W. (1980). Comment: You should standardize the predictor variables in your regression models. *Journal of the American Statistical Association*, 75(369), 87-91.
- Mazzoni, S., McKenna, F., and Fenves, G. L. (2006). Open system for earthquake engineering simulation user manual. Pacific Earthquake Engineering Research Center. *University of California, Berkeley*.
- McCarthy, D. F., and McCarthy, D. F. (1977). *Essentials of soil mechanics and foundations* (p. 505). Reston Publishing Company Virginia.
- Middendrop, P., Bermingham, P., and Kuiper, B. (2022). Statnamic load testing of foundation piles. In *Application of stress-wave theory to piles* (pp. 581-588). Routledge.
- Moayedi, H., Gör, M., Foong, L. K., and Bahiraei, M. (2021). Imperialist competitive algorithm hybridized with multilayer perceptron to predict the load-settlement of square footing on layered soils. *Measurement*, 172, 108837.
- Mohanty, R., Suman, S., and Das, S. K. (2018). Prediction of vertical pile capacity of driven pile in cohesionless soil using artificial intelligence techniques. *International Journal of Geotechnical Engineering*, 12(2), 209-216.
- Momeni, E., Nazir, R., Armaghani, D. J., and Maizir, H. (2014). Prediction of pile bearing capacity using a hybrid genetic algorithm-based ANN. *Measurement*, 57, 122-131.
- Momeni, E., Nazir, R., Armaghani, D. J., and Maizir, H. (2015). Application of artificial neural network for predicting shaft and tip resistances of concrete piles. *Earth Sciences Research Journal*, 19(1), 85-93.
- Montazer, G. A., Giveki, D., Karami, M., and Rastegar, H. (2018). Radial basis function neural networks: A review. *Comput. Rev. J*, 1(1), 52-74.
- Morshed, J. (1991). Prediction of load deformation behaviour of axially loaded piles in sand. MSc. Engg Thesis, Department of Civil Engineering, Bangladesh University of Engineering and Technology.
- Mousavi, S., and Afghah, F. (2019). Inter-and intra-patient ecg heartbeat classification for arrhythmia detection: a sequence to sequence deep learning approach. In *ICASSP 2019-2019 IEEE international conference on acoustics, speech and signal processing (ICASSP)* (pp. 1308-1312). IEEE.
- Muqtadir, A., and Desai, C. S. (1986). Three-dimensional analysis of a pile-group foundation. *International journal for numerical and analytical methods in geomechanics*, 10(1), 41-58.
- Murphy, K. P. (2018). Machine learning: A probabilistic perspective (adaptive computation and machine learning series). *The MIT Press: London, UK*.



- Naveen, B., Parthasarathy, C., and Sitharam, T. (2014). Numerical modeling of pile load test. *Proc., 4th China Int. Piling and Deep Foundations Summit*, 156-161.
- Naveen, B., Sitharam, T., and Vishruth, S. (2011). Numerical simulation of vertically loaded piles. *Young*, 21(22.00), 25.00.
- Nejad, F. P., and Jaksa, M. B. (2017). Load-settlement behavior modeling of single piles using artificial neural networks and CPT data. *Computers and geotechnics*, 89, 9-21.
- Nejad, F. P., Jaksa, M. B., Kakhi, M., and McCabe, B. A. (2009). Prediction of pile settlement using artificial neural networks based on standard penetration test data. *Computers and geotechnics*, 36(7), 1125-1133.
- Nishida, K., Sadamitsu, K., Higashinaka, R., and Matsuo, Y. (2017). Understanding the semantic structures of tables with a hybrid deep neural network architecture. In *Proceedings of the AAAI Conference on Artificial Intelligence* (Vol. 31, No. 1).
- Nour, A., Slimani, A., and Laouami, N. (2002). Foundation settlement statistics via finite element analysis. *Computers and geotechnics*, 29(8), 641-672.
- Obrzud, R. F. (2010). On the use of the Hardening Soil Small Strain model in geotechnical practice. *Numerics in geotechnics and structures*, 16, 1-17.
- Ofrikhter, I., and Ponomarev, A. (2021). Estimation of load-set behavior of driven concrete piles using artificial neural network and cone penetration test. In *Journal of Physics: Conference Series* (Vol. 1928, No. 1, p. 012055). IOP Publishing.
- Ottaviani, M. (1975). Three-dimensional finite element analysis of vertically loaded pile groups. *Geotechnique*, 25(2), 159-174.
- Pascanu, R., Gulcehre, C., Cho, K., and Bengio, Y. (2013). How to construct deep recurrent neural networks. *arXiv preprint arXiv:1312.6026*.
- Pascanu, R., Mikolov, T., and Bengio, Y. (2013). On the difficulty of training recurrent neural networks. *International conference on machine learning*. (pp. 1310-1318). Pmlr.
- Pham, T. A., Ly, H. B., Tran, V. Q., Giap, L. V., Vu, H. L. T., and Duong, H. A. T. (2020). Prediction of pile axial bearing capacity using artificial neural network and random forest. *Applied Sciences*, 10(5), 1871.
- Potts, D. M., Zdravković, L., Addenbrooke, T. I., Higgins, K. G., and Kovačević, N. (2001). *Finite element analysis in geotechnical engineering: application* (Vol. 2). Thomas Telford London.
- Poulos, H. (1968). Analysis of the settlement of pile groups. *Geotechnique*, 18(4), 449-471.
- Pressley, J., and Poulos, H. G. (1986). Finite element analysis of mechanisms of pile group behaviour. *International journal for numerical and analytical methods in geomechanics*, 10(2), 213-221.
- Rahaman, S. (2008). Axial load capacity of cast-in-situ bored piles in stiff Dhaka clay. MSc. Engg Thesis, Department of Civil Engineering, Bangladesh University of Engineering and Technology.
- Rahman, H. (2016). Experimental and analytical investigations on skin friction and end bearing resistance of single pile. MSc. Engg Thesis, Department of Civil Engineering, Bangladesh University of Engineering and Technology
- Rajagopal, C., Solanki, C., and Tandel, Y. (2012). Comparison of static and dynamic load test of pile. *Electron. J. Geotech. Eng*, 17, 1905-1914.
- Randolph, M. F., and Wroth, C. P. (1978). Analysis of deformation of vertically loaded piles. *Journal of the geotechnical engineering division*, 104(12), 1465-1488.

- Reul, O. (2004). Numerical study of the bearing behavior of piled rafts. *International Journal of Geomechanics*, 4(2), 59-68.
- Rumelhart, D. E., Hinton, G. E., and Williams, R. J. (1986). Learning representations by back-propagating errors. *nature*, 323(6088), 533-536.
- Rybak, J., & Król, M. (2018). Limitations and risk related to static capacity testing of piles—"unfortunate case" studies. *MATEC Web of Conferences*. (Vol. 146, p. 02006). EDP Sciences.
- Said, I. d., De Gennaro, V., and Frank, R. (2009). Axisymmetric finite element analysis of pile loading tests. *Computers and geotechnics*, 36(1-2), 6-19.
- Sarkar, G., Siddiqua, S., Banik, R., and Rokonzaman, M. (2015). Prediction of soil type and standard penetration test (SPT) value in Khulna City, Bangladesh using general regression neural network. *Quarterly Journal of Engineering Geology and Hydrogeology*, 48(3-4), 190-203.
- Schanz, T., Vermeer, P., and Bonnier, P. G. (2019). The hardening soil model: formulation and verification. In *Beyond 2000 in computational geotechnics* (pp. 281-296). Routledge.
- Schmüdderich, C., Shahrabi, M. M., Taiebat, M., and Lavasan, A. A. (2020). Strategies for numerical simulation of cast-in-place piles under axial loading. *Computers and geotechnics*, 125, 103656.
- Schweiger, H., Thurner, R., and Pöttler, R. (2001). Reliability analysis in geotechnics with deterministic finite elements: theoretical concepts and practical application. *International Journal of Geomechanics*, 1(4), 389-413.
- Sellountou, E., and Roberts, T. (2007). The Cost-Effectiveness of Dynamic Pile Installation Monitoring: A Case Study. In *7th FMGM 2007: Field Measurements in Geomechanics* (pp. 1-12).
- Shahin, M. A. (2014). Load–settlement modeling of axially loaded steel driven piles using CPT-based recurrent neural networks. *Soils and foundations*, 54(3), 515-522.
- Shahin, M. A. (2016). State-of-the-art review of some artificial intelligence applications in pile foundations. *Geoscience Frontiers*, 7(1), 33-44.
- Shahin, M. A., Maier, H. R., and Jaksa, M. B. (2002). Predicting settlement of shallow foundations using neural networks. *Journal of Geotechnical and Geoenvironmental Engineering*, 128(9), 785-793.
- Shahjahan Khan, M. (1997). Performance of axially loaded small size prestressed concrete piles. MSc. Engg Thesis, Department of Civil Engineering, Bangladesh University of Engineering and Technology.
- Shehab Uddin, M. (2015). Evaluation of dynamic properties of Dhaka sub-soil for ground shaking assessment. MSc. Engg Thesis, Department of Civil Engineering, Bangladesh University of Engineering and Technology.
- Shavitt, I., and Segal, E. (2018). Regularization learning networks: deep learning for tabular datasets. *Advances in Neural Information Processing Systems*, 31.
- Shen, S.-L., Atangana Njock, P. G., Zhou, A., and Lyu, H.-M. (2021). Dynamic prediction of jet grouted column diameter in soft soil using Bi-LSTM deep learning. *Acta Geotechnica*, 16(1), 303-315.
- Smith, E. (1960). Pile-driving analysis by the wave equation. *Journal of the Soil Mechanics and Foundations Division*, 86(4), 35-61.
- Terzaghi, K., and Peck, R. B. (1967). *Soil mechanics in engineering practice* (No. 624.151 T47 1967).
- Thangavel, K., and Pethalakshmi, A. (2009). Dimensionality reduction based on rough set theory: A review. *Applied soft computing*, 9(1), 1-12.

- Ti, K. S., Huat, B. B., Noorzaei, J., Jaafar, M. S., and Sew, G. S. (2009). A review of basic soil constitutive models for geotechnical application. *Electronic Journal of Geotechnical Engineering*, 14, 1-18.
- Tourille, J., Ferret, O., Neveol, A., and Tannier, X. (2017). Neural architecture for temporal relation extraction: A Bi-LSTM approach for detecting narrative containers. In *Proceedings of the 55th Annual Meeting of the Association for Computational Linguistics (Volume 2: Short Papers)* (pp. 224-230).
- Übeyli, E. D. (2009). Combining recurrent neural networks with eigenvector methods for classification of ECG beats. *Digital Signal Processing*, 19(2), 320-329.
- Unsever, Y., Matsumoto, T., and Özkan, M. Y. (2015). Numerical analyses of load tests on model foundations in dry sand. *Computers and geotechnics*, 63, 255-266.
- Unsever, Y., Matsumoto, T., and Özkan, M. Y. (2014). Static cyclic load tests on model foundations in dry sand. *Geotech. Eng. Journal of SEAGS AGSSEA*, 45(2).
- Velliangiri, S., and Alagumuthukrishnan, S. (2019). A review of dimensionality reduction techniques for efficient computation. *Procedia Computer Science*, 165, 104-111.
- Vesic, A. S. (1977). Design of pile foundations. *NCHRP synthesis of highway practice* (42).
- Viggiani, C., Mandolini, A., and Russo, G. (2014). *Piles and pile foundations*. CRC Press.
- Vilhar, G., Laera, A., Foria, F., Gupta, A., and Brinkgreve, R. B. (2018). Implementation, validation, and application of PM4 Sand model in PLAXIS. In *Geotechnical Earthquake Engineering and Soil Dynamics V: Numerical Modeling and Soil Structure Interaction* (pp. 200-211). American Society of Civil Engineers Reston, VA.
- Wehnert, M., and Vermeer, P. (2004). Numerical analyses of load tests on bored piles. *Numerical methods in geomechanics—NUMOG IX*, 505-511.
- Witten, I. H., and Frank, E. (2002). Data mining: practical machine learning tools and techniques with Java implementations. *Acm Sigmod Record*, 31(1), 76-77.
- Wolf, B., Donzallaz, J., Jost, C., Hayoz, A., Commend, S., Hennebert, J., and Kuonen, P. (2020). Using CNNs to optimize numerical simulations in geotechnical engineering. *APR Workshop on Artificial Neural Networks in Pattern Recognition* (pp. 247-256). Cham: Springer International Publishing.
- Wu, J. T., Pham, T. Q., and Adams, M. T. (2013). *Composite behavior of geosynthetic reinforced soil mass* (No. FHWA-HRT-10-077). United States. Federal Highway Administration
- Wu, J. T., Tung, C.-Y., Adams, M. T., and Nicks, J. E. (2018). Analysis of stress-deformation behavior of soil-geosynthetic composites in plane strain condition. *Transportation Infrastructure Geotechnology*, 5, 210-230.
- Wu, Y., Yamamoto, H., and Yao, Y. (2013). Numerical study on bearing behavior of pile considering sand particle crushing. *Geomech. Eng*, 5(3), 241-261.
- Xu, L., Skoularidou, M., Cuesta-Infante, A., and Veeramachaneni, K. (2019). Modeling tabular data using conditional gan. *Advances in Neural Information Processing Systems*, 32.
- Xu, X., Liang, T., Zhu, J., Zheng, D., and Sun, T. (2019). Review of classical dimensionality reduction and sample selection methods for large-scale data processing. *Neurocomputing*, 328, 5-15.
- Yamashita, K. (2012). Field measurements on piled raft foundations in Japan. *Proceedings of IS-Kanazawa*, 79-96.

- Yamashita, K., Yamada, T., and Hamada, J. (2011). Investigation of settlement and load sharing on piled rafts by monitoring full-scale structures. *Soils and foundations*, 51(3), 513-532.
- Yan, J., Xu, T., Yu, Y., and Xu, H. (2021). Rainfall forecast model based on the tabnet model. *Water*, 13(9), 1272.
- Yasin, S., Alam, M., Islam, M., and Siddique, A. (2009). Static load capacity of RCC piles in soft clay-A case study. In *Proc., 17th Int. Conf. on Soil Mechanics and Geotechnical Engineering, Bibliotheca Alexandrina, Alexandria, Egypt* (pp. 1325-1328).
- Ye, H., Cao, B., Peng, Z., Chen, T., Wen, Y., and Liu, J. (2019). Web services classification based on wide & Bi-LSTM model. *IEEE Access*, 7, 43697-43706.
- Yuan, X., Li, L., and Wang, Y. (2019). Nonlinear dynamic soft sensor modeling with supervised long short-term memory network. *IEEE transactions on industrial informatics*, 16(5), 3168-3176.
- Zebari, R., Abdulazeez, A., Zeebaree, D., Zebari, D., and Saeed, J. (2020). A comprehensive review of dimensionality reduction techniques for feature selection and feature extraction. *Journal of Applied Science and Technology Trends*, 1(2), 56-70.
- Zhang, K., Zhang, K., Cai, C., Liu, W., and Xie, J. (2021). Displacement prediction of step-like landslides based on feature optimization and VMD-Bi-LSTM: a case study of the Bazimen and Baishuihe landslides in the Three Gorges, China. *Bulletin of Engineering Geology and the Environment*, 80, 8481-8502.
- Zheng, H., Liu, D., and Li, C. G. (2005). Slope stability analysis based on elasto-plastic finite element method. *International Journal for Numerical Methods in Engineering*, 64(14), 1871-1888.
- Zhu, J.-H., Zaman, M. M., and Anderson, S. A. (1998). Modeling of soil behavior with a recurrent neural network. *Canadian Geotechnical Journal*, 35(5), 858-872.

## APPENDIX-A

.ipynb file in Google Colab

```
import pandas as pd
import numpy as np
import os
from sklearn import preprocessing
import scipy
import tensorflow
import tensorflow as tf
from tensorflow.keras import Model
# import theano
# import theano.tensor as T
import keras
from keras.models import Sequential, load_model
from keras.layers import Dense, Activation, Bidirectional, InputLayer, BatchNormali
zation, Reshape, AveragePooling1D, MaxPool1D, Multiply, Input
from keras.preprocessing import image
from __future__ import print_function
import numpy as np
import matplotlib.pyplot as plt

from keras.callbacks import EarlyStopping, ModelCheckpoint, ReduceLROnPlateau
from keras.models import Sequential
from keras.layers import Dense, Dropout, Activation, Flatten
from keras.layers import Convolution2D, MaxPooling2D
from keras.utils import np_utils
from keras.preprocessing import sequence
from tensorflow.keras.layers import Embedding
from tensorflow.keras.layers import LSTM, GRU, SimpleRNN
from sklearn.preprocessing import LabelEncoder
from sklearn.preprocessing import StandardScaler
from sklearn.model_selection import train_test_split
from keras.callbacks import EarlyStopping, ModelCheckpoint
from tensorflow.keras.utils import to_categorical
from tensorflow_addons.layers import WeightNormalization
from keras.layers.convolutional import Conv1D
from keras.layers.normalization.batch_normalization import BatchNormalization
import matplotlib.pyplot as plt

from sklearn import svm, metrics
from sklearn.tree import DecisionTreeClassifier
from xgboost import XGBClassifier
from sklearn.metrics import matthews_corrcoef
```

```

import torch
import torch.nn as nn
from pytorch_tabnet.tab_model import TabNetClassifier, TabNetRegressor
from sklearn.preprocessing import LabelEncoder
from sklearn.metrics import roc_auc_score, accuracy_score, confusion_matrix, roc_curve
from sklearn.linear_model import LinearRegression
from sklearn.metrics import mean_squared_error, mean_absolute_error, matthews_corrcoef
from sklearn.decomposition import PCA
from sklearn.metrics import matthews_corrcoef

```

```

# Data Loading

```

```

# !gdown 1M9a5drTvpK3EYXrzarkmaTOWI9-Eksrp
!gdown 1JXOYaZJzD6ByvJ1bPZfr0t9ImHth0qar
df = pd.read_excel('/content/ANN Dataset_Last.xlsx')

```

```

% unnecessary rows eliminated first

```

```

M(Msz+1:end,:) = [];

```

```

% mean of M is determined as funtion return

```

```

rt1 = mean(M);

```

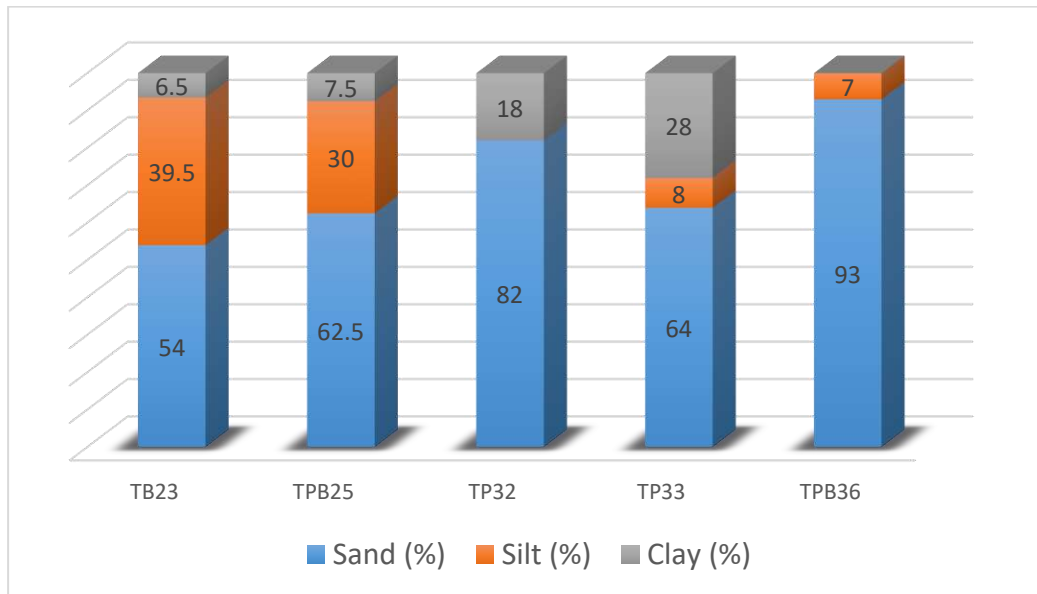
```

end

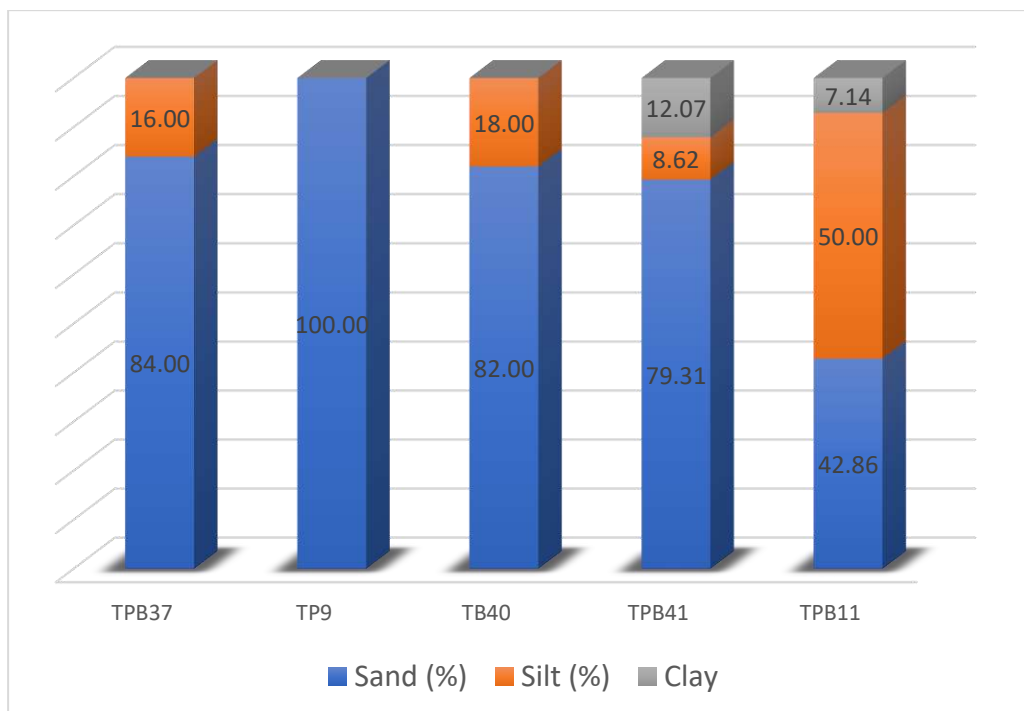
```

## APPENDIX-B

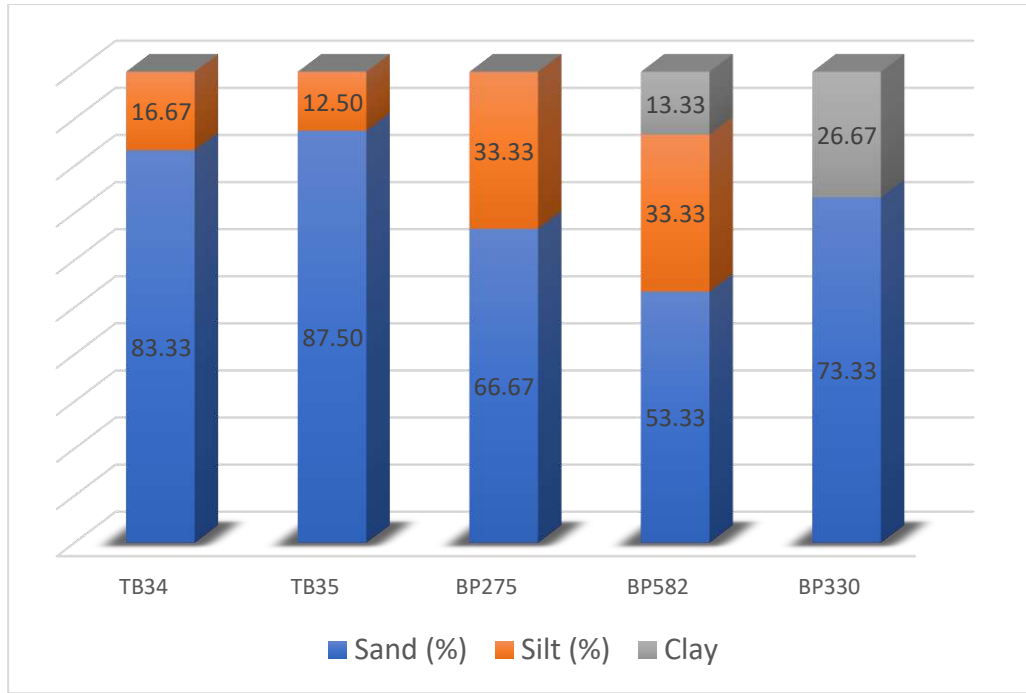
### SOIL PROFILE FROM COLLECTED SOIL REPORTS OF DIFFERENT LOCATIONS



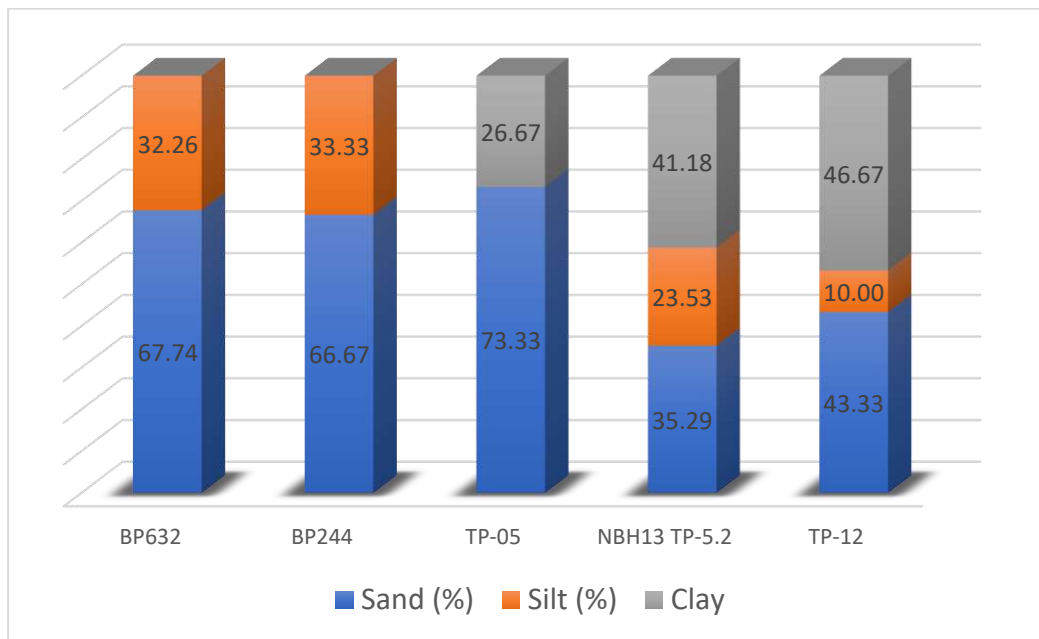
(a)



(b)

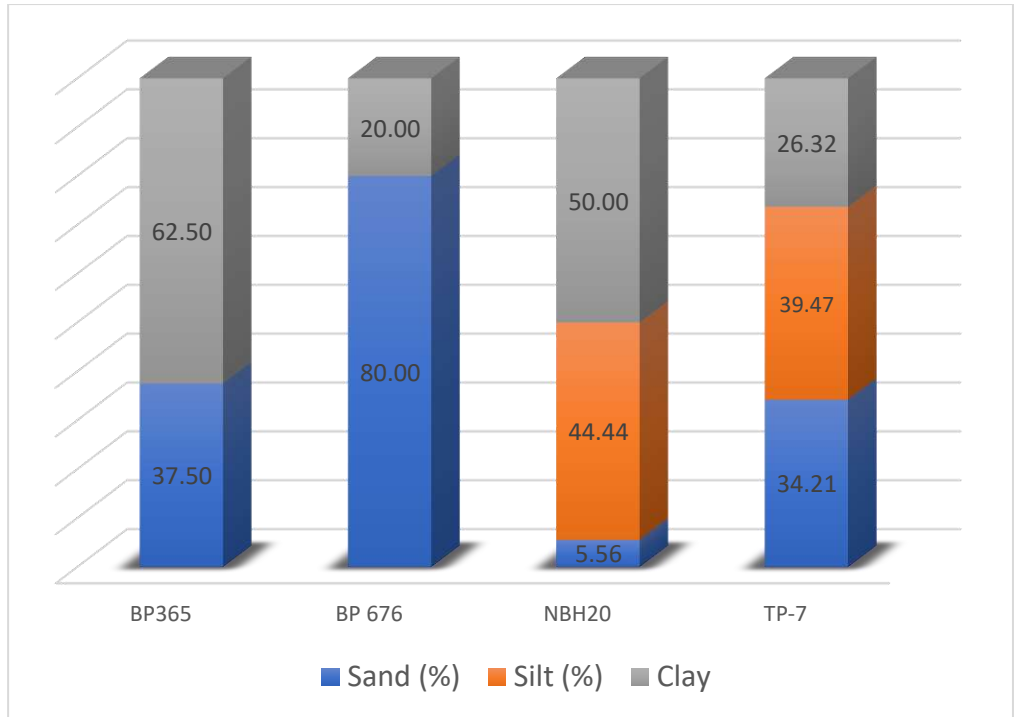


(c)



(d)





(e)

**APPENDIX-C**  
SAMPLE LOAD TESTS

